Technische Universität München

Lehrstuhl für Anorganische Chemie

Transformation of Carbon Dioxide to Esters and Cyclic Carbonates by Molecular Catalysts

Amylia Binte Abdul Ghani

Vorsitzender: Univ.- Prof. Dr. Thomas Brück

Prüfer der Dissertation:

1. Univ.- Prof. Dr. Fritz E. Kühn
2. Jun.-Prof. Dr. Konrad Tiefenbacher

Die vorliegende Arbeit entstand in der Zeit von Mai 2011 bis Dezember 2013 an der Fakultät für Chemie, Lehrstuhl für Anorganische Chemie der Technischen Universität München und der King Abdullah University of Science and Technology Catalysis Centre.

"O you who believe! Seek help with patient perseverance and prayer, for God is with those who patiently persevere"

The Holy Quran, *2:153*

"There is no happiness except in the realization that we have accomplished something."

Henry Ford

Acknowledgements

Alhamdulillah - all praises to God

One of the joys of completing this thesis is the ability to look back and remember everyone who has helped and supported me throughout this long and fulfilling journey.

To Professor Kühn, for giving me this opportunity to work in his group, the ability to work in KAUST, the academic freedom and his valuable input throughout this PhD journey. My academic advisor, Dr Cokoja for always making time for chemistry despite his extremely busy schedule. Thank you for the encouragement and motivation when the going got tough. I truly value all the scientific discussions we had. Professor Basset for hosting me in his laboratories during my stay at KAUST. The laboratories were second to none and I am honoured to have been able to conduct a large portion of this work there. Thank you for your scientific input to this work as well. Professor Emsley is also acknowledged for his input on the bidimensional NMR spectra.

Dr Valerio D'Elia, my supervisor in KAUST, who taught me a lot about chemistry and also a lot about life. I will always remember preparing many sumbles and your random yet insightful analogies and ancient Italian quotes, some more nonsensical than others. Also I will miss having someone addressing me by "*cappuccetto* (insert colour)" in the morning. Thank you for the encouragements and thank you for the laughs.

Thanks also go to Geta and Jürgen in TUM for doing all the special NMR measurements for me. I enjoyed all our little chats in my broken german while waiting for the low temperature experiments to run their course. Dr Guo, Dr Emwas and Khalid in KAUST for your input to this work and patiently teaching me how to programme the NMR machines for all the "*multizg*" experiments with fancy parameters. I have learnt plenty from all of you. I also acknowledge the efforts from Dr Li in KAUST for XRD measurements of all my crystal samples.

The secretarial staff in TUM - Frau Hifinger, Frau Grötsch, Frau Schuhbauer-Gerl and Frau Kaufmann: Thank you for arranging my flights and visas and making my transitions to KAUST seamless. Thanks also go to Nathalie in KAUST for always being there to help me when I have visa troubles or any kind of trouble really (they seem to find me) even on weekends and holidays (!). You are a rockstar and one of the kindest most efficient people I know.

The original TUM-KAUST team: Tina and Antoine. We were pioneers! Thank you both for being supportive team and lab mates. Lab life in both TUM and KAUST would be so monotonous without the both of you. All the fun and squabbles will remain dear to me. Not forgetting co-workers in the Rieger group: Abdussalam, Khalifah and Carly thank you for the friendship. The other TUM folk from the Heiz, Kühn and Köhler group who jumped on the KAUST bandwagon

later: Florian S., Claron, Andrew, Markus, Costas, Florian B. and Oliver (the diva), thank you for the brotherly advice and pep talks while I was preparing this thesis and of course for being wonderful company in both KAUST and TUM. I hope yall never forget that day I owned all of yall in bowling - 4 strikes in a row say whaaat :p

My co-workers in AK Kühn, Thomas, Nidhi, Bo, Su, Typhene, Mei, Bill, Sara, Valentina, Christina, Claudia, Barnali and Sophie. I will always remember sighing over failed experiments, lunch escapades in the mensa, cookie breaks at the Greek's, driving to Weihenstephan for praktikum, unnecessarily excessive chinese lunch buffets... thank you for the fond memories.

The lovely people I've met along the way in Munich and KAUST, the folks from the *other* university in Munich, Christoph, Teresa, and my long time WG buddies Nunna and Gina. Thank you for all the memories. Also to Jun Heui - thank you for helping me translate that korean journal article. (I didn't forget!) Your translation helped get part of this work published and I am grateful. Also my Singaporean bros in munich: Jeffrey and Jafnie thanks for the laughs, cafe hunting and ketchup stains. Jaf also I hope you remember that *mohn* is poppy seeds and not a large carrot!

I also fondly acknowledge the craziest bunch of postdocs I've ever met, my colleagues in the TUM-KAUST lab: Serena, Manuel and Julien aka "The Beast". The three of you will forever have a special place in my heart. Thank you for making everyday a joy to be in the lab. I will always remember being called out for being the only one in the lab without a PhD and always being blamed when the oxygen in the glovebox skyrockets to 400 ppm. Please. We all know it is Julien's fault because he's... (two acceptable answers) Jokes aside, I thoroughly enjoyed all the time we spent in and outside the lab, snorkelling and diving the Red Sea, dinner gatherings, trips to Jeddah, coffee breaks at the donut shop. Thank you for all your advice, encouragement and suggestions along the way and also proofreading this thesis.

And to everyone else who made my stay in KAUST the most memorable and delightful 18 months: My KCC family Ali, Umesh, Bilal, Gabriel, Alex, Fred, Elodie and little Loulan. I will always remember our highly entertaining lunch breaks, potluck dinners and movie nights. My Singaporean *makan* crew Roslinda and Shwen - food hunting in Jeddah was awesome with you guys! Mohannad for all the Baik deliveries from Jeddah, scumhunting and for being a great friend. My Coastline diving family for making me fall in love with the sport. Also to Quan, even though you were not physically in KAUST with me, you kept me company through the toughest days by giving me lels. This unexpected, most random godfather tier friendship that blossomed during my PhD will always be dear to me.

Not forgetting my friends back home Shahreena, Rafiq, Aizat, Jasmine, Muthiah, Sandy, Jia Yi, Mary, Diatch and a whole bunch of others (there are just too many of you sweethearts!)- thank

you for the emotional support and for being a constant reminder of what awaits at home. Dazril and Irwan my fellow PhD candidates, the both of you have been my companions throughout this journey for no one would ever understand our strife and struggle. Thank you for also being the source of all disgustingly lame chemistry jokes, I've got one - What do you call a clown who is in jail? A silicon. Laugh please.

Finally, my loved ones. Hieu for bringing so much joy to my life. Thank you for believing in me and thank you for being my tech support when LaTeX drove me nuts writing this. My extended family and close family friends for their emotional support and being most encouraging. Thank you for posting pictures of yummy local food while I am away with intense cravings (you all know who you are!).

And of course, my dearest parents for their unwavering support and love for the past 27 years. Back then when they had little for themselves, they still selflessly managed to give me the best of everything. No amount of gratitude could ever amount to all the sacrifice you both have made for me and I will remain eternally indebted. My sister, best friend, confidante and soon-to-be Dr Amelina Abdul Ghani (M.B.B.S), you are an amazing girl and you inspire me more than you will ever know.

Abstract

The synthesis of palladalactones from various palladium complexes, ethylene and carbon dioxide was attempted and monitored by *in situ* IR and NMR techniques. $Pd(PCy_3)_2$ was found to undergo oxidative CO_2 addition, forming a palladium-peroxocarbonate complex, structurally characterised by XRD.

β-hydride elimination was induced in "bench"-synthesized palladalactones with methyl iodide and methyl triflate to form esters. Methyl triflate proved to be the better methylating agent with faster reaction rates and better selectivity.

A mechanistic study of the $NbCl_5$/DMAP and $NbCl_5$/TBAB catalysed reaction between propylene oxide and CO_2 was performed by kinetic analysis, monitored by a series of *in situ* IR and NMR measurements. The co-catalyst was found to have a bifunctional role in the catalytic cycle.

Contents

Abbreviations

acac	acetylacetonate
ARS	Asymmetric ring stretching
ATR	Attenuated total reflection
bipy	2,2'-bipyridine
CCS	Carbon Capture and Storage
cdt	trans, trans-1,5,9-cyclododecatriene
CF	Fluorocarbon
CFC	Chlorofluorocarbon
COD	cis, cis-1,5-cyclooctadiene
COSY	Correlation Spectroscopy
dba	dibenzylideneacetone
dbu	diazabicyclo-undec-7-ene
dcpe	1,2-bis(dicyclohexylphosphino)ethane
DFT	Density Field Theory
diars	1,2-bis(diphenylarsino)benzene
DMAP	4-dimethylaminopyridine
dmpe	1,2-bis(dimethylphosphino)ethane
DMSO	dimethyl sulfoxide
dppb	1,4-bis(diphenylphosphino)butane
dppe	1,2-bis(diphenylphosphino)ethane
dppf	1,1'-bis(diphenylphosphino)ferrocene
dppp	1,3-bis(diphenylphosphino)propane
dtbpe	1,2-bis(di-tert-butylphosphino)ethane
EC	ethylene carbonate
Et	ethyl
HMBC	Heteronuclear Multiple-Bond Correlation

HOMO	Highest Occupied Molecular Orbital
HSQC	Heteronuclear Single Quantum Correlation
IMes	1,3-bis(2,4,6-trimethylphenyl) imidazol-2-ylidene
IR	Infra-Red
LUMO	Lowest Unoccupied Molecular Orbital
Me	methyl
MeI	methyl iodide
MeOH	methanol
MeOTf	methyl triflate
Mes	1,3,5-trimethylbenzene
mol. equiv.	Mole Equivalent
NHC	N-Heterocyclic carbene
NMR	Nuclear Magnetic Resonance
ORTEP	Oak Ridge Thermal Ellipsoid Plot
PC	propylene carbonate
PCy$_3$	tricyclohexylphosphine
Ph	phenyl
P($o-$tolyl)$_3$	tri(o-tolyl)phosphine
PPh$_3$	triphenylphosphine
ppm	parts per million
SOHIO	Standard Oil of Ohio
TBAB	tetra-n-butylammonium bromide
TEAB	tetraethylammonium bromide
THF	tetrahydrofuran
tmeda	N, N, N', N'-tetramethylethylenediamine
TOF	Turnover Frequency
TON	Turnover Number
XPhos	2-Dicyclohexylphosphino-2,4,6-triisopropylbiphenyl
XRD	X-Ray Diffraction

For MZ, DZ and NM.

♥

Chapter 1

Carbon Dioxide: An Introduction

1.1 Carbon Dioxide and Climate Change

Climate change represents one of the greatest environmental threats today.[1] Most climate scientists agree that it is caused by the greenhouse effect, which is the warming of the surface of the earth by gases that trap heat in the atmosphere. These gases, aptly called "greenhouse gases" include nitrous oxide (N_2O), methane (CH_4), fluorocarbons (CFs), chlorofluorocarbons (CFCs) and carbon dioxide (CO_2).

While CO_2 is the least effective greenhouse gas per kilogram emitted, it is the main contributor to global warming due to copious amounts being released to the atmosphere through human activities.[2] The emissions are so high that there is currently an excess of 3.9% with respect to the carbon cycle,[3] meaning that the increase in CO_2 levels is not balanced by its fixation in nature. This imbalance is also exacerbated by deforestation, resulting in an increase in atmospheric CO_2 levels from approximately 280 ppm in pre-industrial times to 390 ppm today. At present, the largest sources of CO_2 emission come from power generation, public electricity and heat production by the combustion of fossil fuels.

There are three possible strategies to slow the increase of CO_2 concentration in the atmosphere:

- Reducing emissions

- CO_2 capture-storage

- CO_2 utilization

Reducing CO_2 emissions could be addressed by replacing a carbon-rich energy carrier like coal by a less carbon rich source like oil or natural gas.[1] While this would mildly alleviate the amount of CO_2 produced, a greater reduction could be gained by switching to non fossil fuel energy sources

like hydrogen or renewable energy. Carbon capture and storage (CCS), a potential method to allow the continued use of fossil fuels has also been actively developed with leading technologies, available in the short and long run.[4,5] CCS, however is also known to be expensive.[6] CO_2 utilization, on the other hand, is a more viable option over storage especially if the transformation to value-added products is economical and in demand.

1.1.1 Applications of Carbon Dioxide

CO_2 is used for its physical and chemical properties. Some areas where it is used for its physical properties include refrigerants,[7] fire extinguishers, use in the beverage industry,[8] enhanced oil recovery,[9] and use as supercritical solvents[10] and extraction media.[11]

CO_2 is also a chemical reactant. In the organic chemical industry, it is used to synthesize urea, salicylic acid, methanol and cyclic organic carbonates. In the inorganic chemical industry, the Solvay process uses it to form $NaHCO_3$ and Na_2CO_3. CO_2 is also consumed in the production of biomass and also in greenhouses to stimulate plant growth. For water purification, it is used as an acid. Despite its many uses, only 1% of the CO_2 produced is being consumed again.[6]

1.2 Understanding the Carbon Dioxide Molecule

CO_2 is a colourless gas that is also odourless at low concentrations. At higher concentrations, it has a sharp acidic odour. It is a solid at temperatures below -78.5°C and sublimes directly into the gaseous state below 5.1 bar.

CO_2 is linear in its ground state and consequently apolar despite having two polar C=O bonds. The carbon atom of CO_2 is *sp* hybridized and has a C−O bond length of 1.16 Å, which is shorter than a C=O with an sp^2 hybridised carbon centre. It is also a bifunctional moleucle as it has two different reaction sites. The carbon atom is an electrophile and is weakly Lewis acidic. The oxygen atoms, on the other hand, are nucleophiles and are weakly Lewis basic. Overall, CO_2 is a weak electrophile.

1.2.1 The Intrinsic Stability of Carbon Dioxide

Even though CO_2 is abundant and cost effective as a carbon source, very few industrial processes make use of it as a raw material. The carbon atom in CO_2 is in its most oxidised form resulting in a thermodynamically stable molecule. As a direct consequence, CO_2 is not very reactive and a large amount of energy is required to transform CO_2 into other chemicals. This, however, can be altered in four ways:[1,12]

- Using energy intensive starting materials like hydrogen, organometallics or unsaturated compounds

- Having low energy synthetic targets

- Having processes designed such that by-products are removed, forcing equilibrium towards the products

- Supplying physical energy like light or electricity

It is therefore crucial to select the appropriate method for a particular transformation to afford an overall exergonic process ($\Delta G < 0$).

1.3 Coordination Chemistry of Carbon Dioxide

Due to the stability of CO_2, catalysis plays an important role in its conversion. CO_2 activation may proceed through binding to a transition metal centre, lowering the activation energy required for its transformation, consequently increasing the reaction rate.

This activation is due to the bending of the CO_2 molecule as it coordinates to a metal centre (see Section 1.3.1). The bent molecule then interacts with nucleophillic or electrophillic substrates through its frontier orbitals. The LUMO has a strongly localised wave function probability which enhances interaction with nucleophiles by facilitating electron density transfer. The HOMO has a strongly localised electron density due to the electron lone pairs on both the oxygen atoms, allowing the activated molecule to interact with electrophiles. With suitable substrates, the coordination of CO_2 to a metal makes it possible to convert this relatively inert molecule into value added products that will be discussed in greater detail later on.

There are three possible routes for the reaction of CO_2 and a substrate ($R-X$) at a transition metal (Scheme 1.1, from left to right).[13]

1. The coordination of the substrate to the metal, forming a substrate-metal complex R-M-X, which then reacts with CO_2. A subsequent reduction elimination step would give the desired product R-CO_2-X, reforming the starting metal complex.

2. The coordination of the substrate and CO_2 to the metal is simultaneous and elimination takes place to give the desired product, while reforming the starting metal complex.

3. CO_2 first coordinates to the metal, forming a M$-CO_2$ complex, which then reacts with the substrate and undergoes reductive elimination to form the desired product. The metal complex is then reformed.
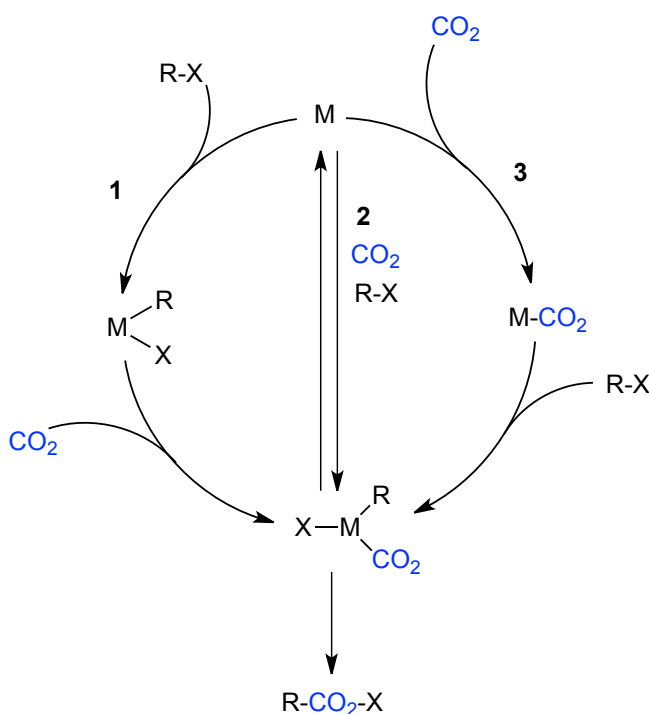
SCHEME 1.1: Routes of interaction between CO_2 and a substrate (R-X) on a transition metal complex (M).

In all cases, the formation of the (R)(CO_2)-M-X complex is the most crucial step in catalytic reactions of CO_2.

1.3.1 Interaction of Carbon Dioxide with Transition Metal Centres

As discussed in Section 1.2, the CO_2 molecule has two different coordination sites due to the different electronic properties of the C and O atoms. It is also a weak electrophile that requires a Lewis basic metal centre for coordination. Therefore, there are several ways that CO_2 could coordinate to a metal centre. Figure 1.1 summarises the properties of CO_2 as a ligand and possible coordination modes to a metal centre.

CO_2 may coordinate to a metal centre in three general ways (η^n indicates the number of bonds, n, between CO_2 and the metal): A $\eta^1(\sigma$-C) side on coordination (Figure 1.1, **1**), a $\eta^2(\sigma$-C,O) side on coordination (Figure 1.1, **2**), and a $\eta^1(\sigma$-O) coordination (Figure 1.1, **3**). While **1** and **2** are common in catalysis, **3** is usually more difficult to obtain as the CO_2 molecule is forced to coordinate end-on at the metal, dictated by the ligands. [14]

Figure 1.1 (top), shows that the coordination of CO_2 to a metal via the double bond or the carbon atom results in a transfer of electron density from the metal to the LUMO of the CO_2 molecule. The LUMO of CO_2 is an antibonding orbital and this electron transfer would result in a weakened C−O interaction. This, coupled with Walsh's rules, [15] suggest that the CO_2 molecule should have a bent geometry, similar to the formate radical anion $\cdot CO_2^-$ that is produced by a one
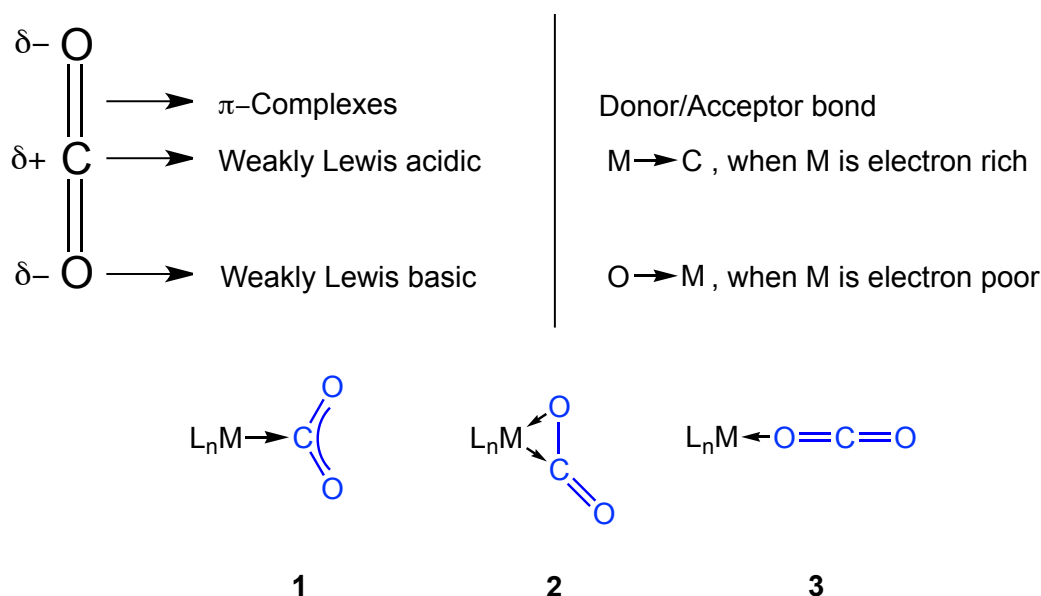
FIGURE 1.1: Properties of CO_2 as a ligand (top) and possible coordination modes of CO_2 to a transition metal (bottom).

electron reduction of CO_2. The bent configuration of CO_2 was indeed observed in the first few metal-CO_2 complexes that were structurally elucidated.[16–19] On the other hand, coordination of CO_2 to the metal by the lone pairs on oxygen (in the case of **3**) would leave the LUMO empty, keeping the linearity of the CO_2 molecule.

It is also useful to dichotomise the η^1 and η^2 bonding modes to gain a better understanding of the metal-CO_2 bond. The η^1-CO_2 bonding involves a strong charge transfer between the d_{z^2} orbital of the metal and the π^* orbital of CO_2 (Figure 1.2, left). The η^1 mode is favoured when the metal has a doubly occupied d orbital for σ bonding that is high in energy. This is usually the case with metals in low oxidation states. d_8 metal complexes with square planar, square pyramidal or trigonal bipyramidal geometries usually bind with CO_2 in this manner.
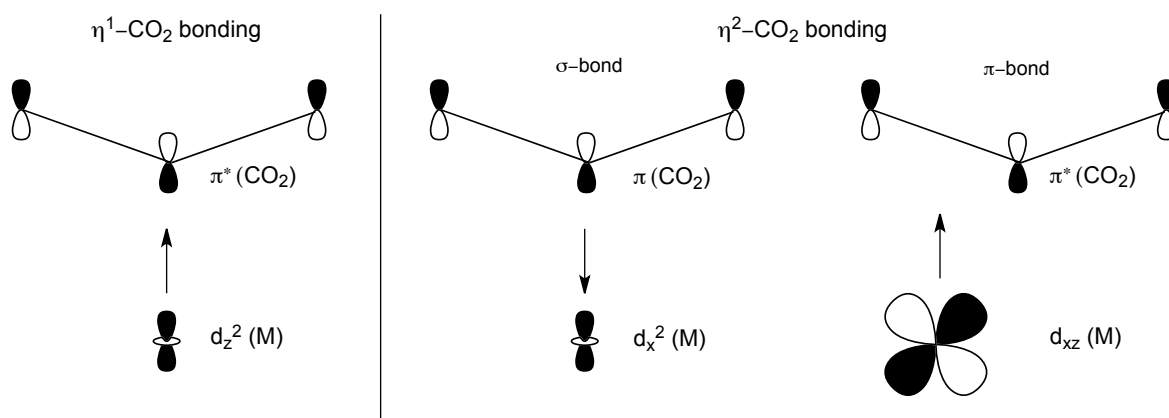

FIGURE 1.2: η^1 (left) and η^2 (right) -CO_2 bonding.

On the other hand, the η^2 bond is similar to olefin-metal bonds. Figure 1.2 (right) illustrates σ bonding between the π orbital of CO_2 and a vacant d_{x^2} orbital of the metal and a simultaneous π bonding between a filled d_{xz} metal orbital and a vacant antibonding orbital of CO_2. This

mode is often favoured in high lying d orbitals for π bonding as the interaction with the CO_2 antibonding orbital is stabilized.

1.3.2 Complexes of Carbon Dioxide

Metal-CO_2 complexes are usually formed by reaction of a metal complex with CO_2. These metal-containing precursors usually have an empty coordination site or ligands that readily leave. They are also highly nucleophillic, flanked with electron-donating ligands that directly bind CO_2. The first CO_2-complex ever reported was a η^2-CO_2 complex discovered by Aresta in 1975.[16]
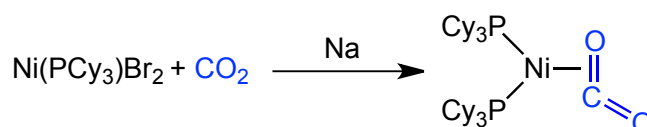
SCHEME 1.2: The synthesis of the first CO_2-metal compound by Aresta.

In this complex, the geometry at the nickel centre is planar. The C=O bonds of the coordinated CO_2 molecule are also non-equivalent, with the one bonded to nickel being slightly longer (1.22 Å and 1.17 Å). The O-C-O bond angle is also wide at 133°. The nickel complex was initially characterised as a toluene-bonded crystal but was later successfully characterised solvent-free by Romao.[18] Another early complex discovered is a niobium centered η^2-CO_2 complex, $Cp_2Nb(CO_2)(CH_2SiMe_3)$ by Lappert.[20] It has properties comparable to that of the nickel complex by Aresta. A similar niobium complex, $Cp_2Nb(CO_2)(CH_2Ph)$ was also reported a few years later by Nicholas *et al.*[21,22]

The side-on η^2 (C, O) coordination mode is the most common based on literature. Following the discovery of Aresta, many other η^2-CO_2 complexes were reported. The complexes were far and varied with different transition metal centres such as palladium[23], molybdenum[24–26], iron[27–29], cobalt[30] and tungsten[31]. A η^2 (C, O) bis(CO_2) compound at a molybdenum centre was also reported by Poveda.[24] The compound *trans*-$[Mo(CO_2)_2(PMe_3)_3(CN-i\text{-}Pr)]$ had equivalently ligated CO_2 molecules with C−O bond lengths of 1.22 Å and 1.26 Å for both CO_2 ligands. Consistent with other η^2 complexes, the O-C-O angles are wide at 133° and 134°. A closely related compound, *trans*-$[Mo(CO_2)_2(PMe_3)_3(CNCH_2Ph)]$ was later reported but it showed greater differences in bond lengths between the two ligated CO_2 molecules.[26] The O-C-O bond angle was also smaller. However, in both compounds, X-Ray structure studies showed that both the metalalactone rings were orthogonal.

η^1-CO_2 complexes, on the other hand are usually unstable and require manipulation in inert conditions[32]. In the late 1970s, Herskovitz was the first to report η^1 (C) rhodium and iridium CO_2 complexes, $Rh(diars)_2(Cl)(CO_2)$ and $Ir(dmpe)_2(Cl)(CO_2)$.[33,34] Cobalt complexes were also reported by Zanazzi.[35,36] Following their discovery, ruthenium complexes were also later reported.[37,38] It was mentioned in Section 1.3.1 that η^1 (O) complexes are lesser known.

The only reported compound to date is that of Meyer in 2004. As expected, the CO_2 molecule was reported to be almost linear with a O-C-O bond angle of 178°.[39]

Other modes of coordination include a bridging mode, where CO_2 inserts between 2 metal complexes. The simplest type involves the coordination of the carbon to one metal centre and the oxygen to another metal centre. Many variations of this coordination mode exist, depending on whether the metal centres are bound to each other, or bridged by other groups.[32] Some types of bridging modes are shown in Figure 1.3.
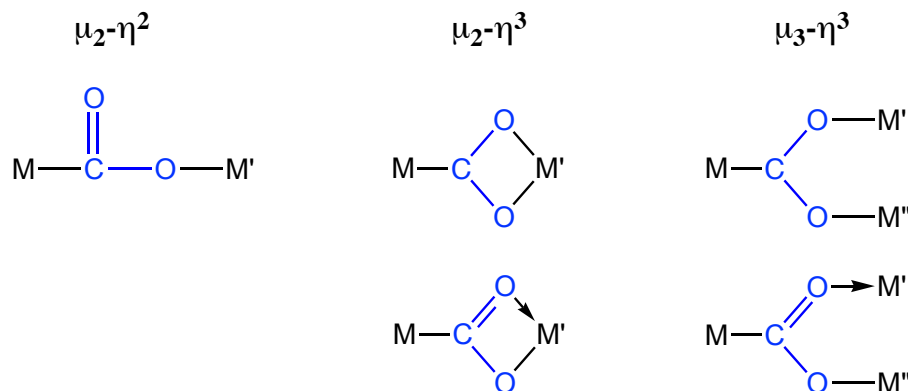

FIGURE 1.3: General binding modes in CO_2-bridged polynuclear complexes, where μ_n denotes the number of metal centres, n, involved in the coordination.

The coordinated oxygen atoms in these structures can still be involved in further interactions with other metal centres in the solid state.[35,40] For a $\mu_2 - \eta^2$ type compound, additional M-M' interactions have been observed.[41,42]

Carbon Dioxide Complexes of Palladium

One of the focuses in this thesis is the use of palladium for CO_2 activation. Palladium is one of the most frequently used metals in catalysis due to its excellent ability of coupling electrophiles and nucleophiles.[43,44] This was also recently highlighted and celebrated in 2010 as Professors Negishi, Suzuki and Heck won the Nobel Prize for their contribution to palladium catalysed cross coupling reactions. A general catalytic cycle depicting cross coupling reactions is shown in Scheme 1.3

The ability of palladium to shift between oxidation states Pd(II) and Pd(0) with ease is precisely why its complexes are being studied for many other catalytic applications. Phosphine ligands, both mono- and bidentate are usually used as ancillary ligands with bulky phosphines being most effective as it results in an electronically dense metal centre.[45]

Palladium complexes with carbon dioxide are also rare despite their usefulness in organic synthesis and their potential use for CO_2 fixation. To date, there is only one known palladium-CO_2 complex that was discovered by the group of Yamamoto.[23]
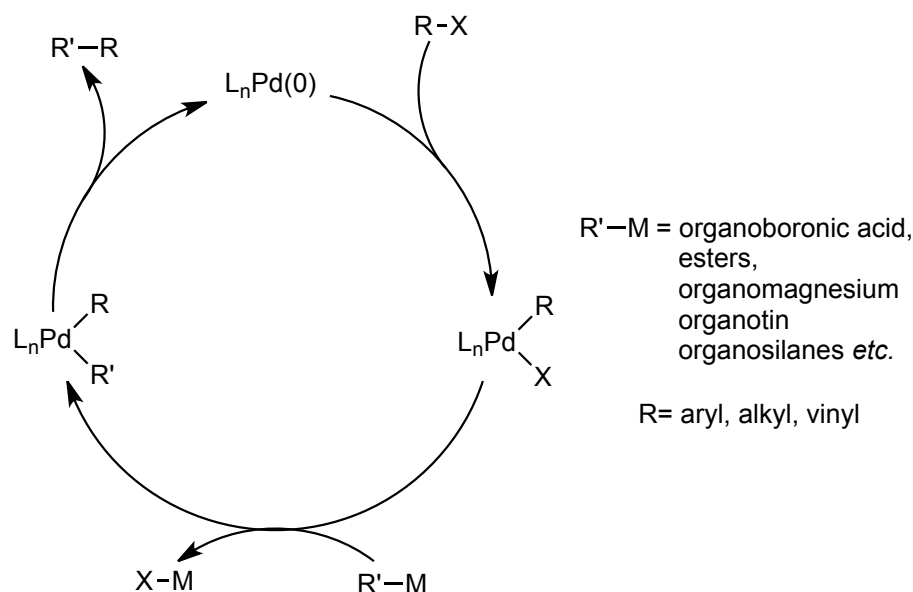
SCHEME 1.3: General catalytic cycle for cross coupling reactions.
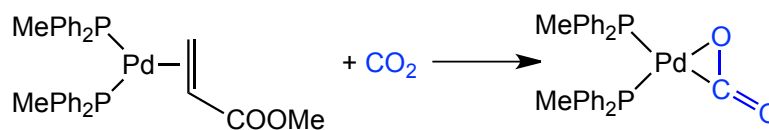
SCHEME 1.4: The first Pd-CO_2 complex isolated by Yamamoto.

It was isolated by reacting a palladium-methyl acrylate complex with 20 bar of CO_2 for 12 hours at room temperature. This complex however, is only stable under an atmosphere of CO_2, which indicates the volatile instability of the complex.

1.3.3   Characterization Techniques of Carbon Dioxide Complexes

Nuclear magnetic resonance (NMR) and infrared (IR) spectroscopy are common techniques used in quantitative measurements or to determine the state of the CO_2 molecule. The chemical shift of CO_2 in ^{13}C NMR spectroscopy varies from 124-126 ppm depending on the solvent[46] and shifts when CO_2 is bonded to a metal centre. Metallocarboxylates (anions, acids, esters, CO_2 complexes usually show a low field resonance in ^{13}C NMR due to their similarities to organic analogues.

Previously discussed in Section 1.1, CO_2 contributes to the greenhouse effect by trapping heat within the boundaries of the atmosphere. This is because CO_2 absorbs energy in the IR wavelengths, allowing IR spectroscopy to be a suitable diagnostic tool for CO_2 chemistry. The vibrational modes of CO_2 are shown in Figure 1.4.

There are three general vibrations for a CO_2 molecule: an asymmetric stretch, a symmetric stretch and a bending mode. The asymmetric stretch is most distinct as it gives a strong band in IR spectroscopy at 2350 cm^{-1}. The two scissoring modes are equivalent and therefore have
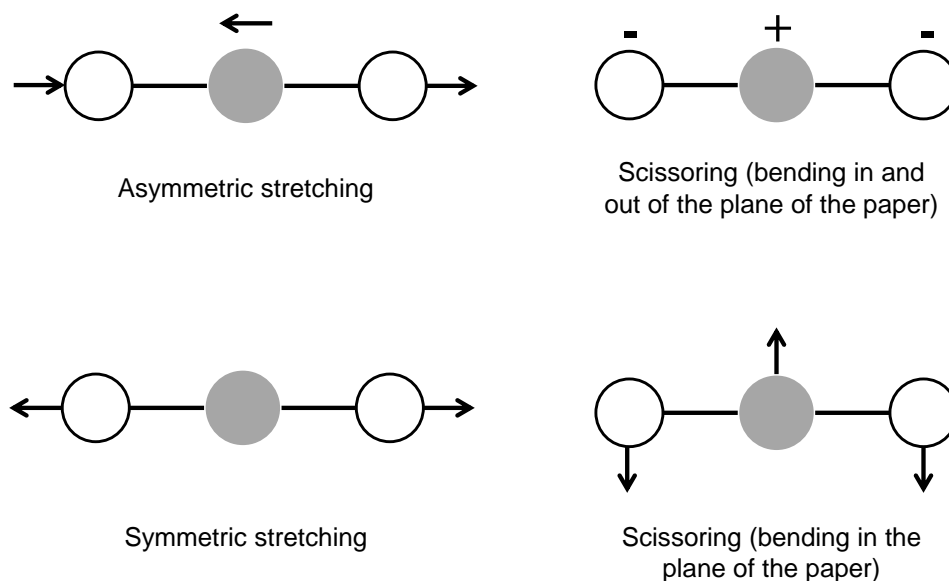
FIGURE 1.4: Vibrational modes of CO_2.

the same absorption frequency (degenerate) at 667 cm $^{-1}$. The symmetric stretch, however, is inactive in IR spectroscopy as it does not produce a net change in dipole moment of the molecule.

However, it is expected for the coordinated CO_2 molecule to have IR bands slightly shifted from that of the free molecule. Coordinated CO_2 bands have been theoretically predicted to appear at 1677, 1405 and 607 cm^{-1}.[47]

Another useful technique is X-Ray diffraction (XRD) studies. It has allowed the determination of how CO_2 is anchored to a metal center and has ascertained the various bonding modes shown in Figure 1.1 and Figure 1.3. While this method gives the highest certainty on the structure of the compound, complexes of CO_2 are usually unstable in solution and crystal growing is challenging. In addition, a solid state structure would not give information on its properties in solution like catalytic activity or reactivity.[48] It would also be questionable if the metal-CO_2 molecule maintains the same configuration in solution.

### 1.3.4 Catalytic Conversion of Carbon Dioxide by its Complexes

Having discussed the different coordination modes of CO_2 in Section 1.3.1, it is understood that CO_2 is in an activated state when the central carbon atom is involved in bonding. The activation is apparent from structural data like the bent geometry and increased C−O bond lengths and also from spectroscopic evidence like low field shifts observed in ^{13}C NMR and low absorption

bands in IR spectroscopy observed when CO_2 is coordinated to a metal centre. This activation is also evident in the reactivity of coordinated CO_2.

The reaction between CO_2 and organometallic complexes is of interest as it provides a one-carbon homologization of the substrate. The most interesting and beneficial reactions of CO_2 are those that form new bonds between the carbon atom and another group. These reaction types are known to proceed with stoichiometric or catalytic amounts of metal complexes.

Formation of New C-C Bonds

Carbon nucleophiles have garnered much attention in recent years due to their diversity, versatility and potential of forming a C-C bond when it attacks the weak electrophillic carbon centre of the CO_2 molecule.
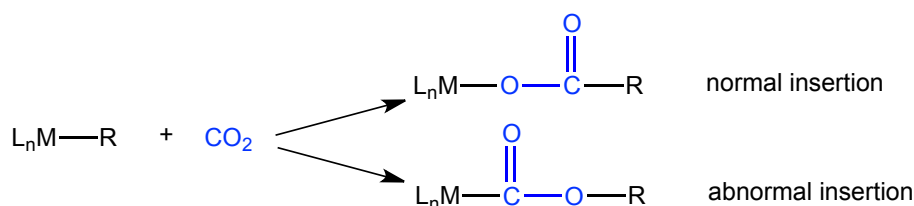

SCHEME 1.5: Insertion of CO_2 into a M-C bond.

There are two ways that CO_2 can insert into a metal-carbon bond of a complex as shown in Scheme 1.5. The normal mode of insertion leads to a carboxylate complex and the abnormal insertion would lead to an alkoxycarbonyl complex. Reactions of this type are the most interesting and valuable from a synthetic point of view as CO_2 acts as a carbon source.

Following the first η^2 CO_2 nickel complex discovered by Aresta, many others began studying the interactions and capabilities of the activated, metal-bound CO_2 molecule. Early studies by the groups of Hoberg, Walther and Inoue showed that the nickel-CO_2 complex was active towards unsaturated compounds.[14] Hoberg and co-workers coupled a variety of alkenes such as ethylene,[49] allenes,[50] 1-3 butadiene[51] and styrene[52] with CO_2 at a nickel centre, forming stable cyclic nickelalactone systems.

The nickel (0) starting complex, for instance $Ni(COD)_2$[53] or $Ni(cdt)$[54] reacts with bulky σ-donor ligands like phosphines or bidentate ligands like bipy, dcpe or dbu, forming a highly nucleophillic 14 electron Ni (0) species, NiL_2. This nucleophile then binds with unsaturated compounds, before the insertion of CO_2 to form the metallacycle. This step is reversible and introduction of a new olefin at this point would result in olefin substitution and a new nickelalactone (see Scheme 1.6). The lactone could be hydrolysed by an acid like HCl to form a carboxylic acid product, with the simultaneous decomposition of the nickel complex. Bernskoetter and Tyler have also recently suggested that not only can the oxidative coupling occur step-wise as

previously discussed, but it can also be a concerted reaction, where both CO_2 and ethylene are bound to the metal centre before forming the acrylates.[55]
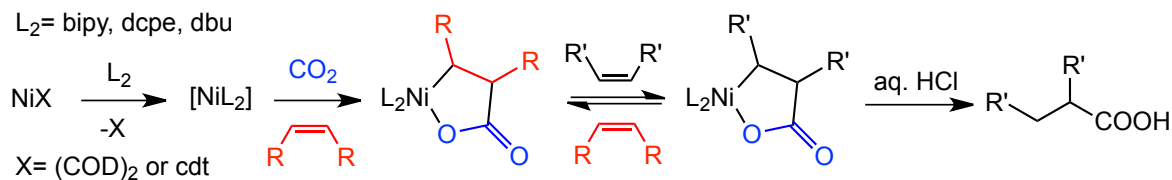

SCHEME 1.6: Synthesis of nickelalactones leading to the formation of a carboxylic acid by acid hydrolysis.

On the basis of this cyclic intermediate, studies have been extended to enynes and diynes at other metal centres like palladium, copper, titanium, zirconium and vanadium.[56,57]

One of the focuses of this thesis involves the coupling of CO_2 with ethylene at palladium centres (see chapter 3).

Formation of New C-O Bonds

$C-O$ bonds are formed by the insertion of CO_2 into $M-OH$ or $M-OR$ bonds.
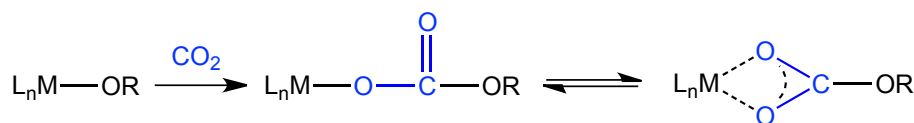
SCHEME 1.7: Insertion of CO_2 into M-OR groups.

When R is an organic moiety, the insertion would result in alkyl or aryl carbonate species. When R is hydrogen, the insertion would give hydrogen carbonate species.[57] This has been demonstrated by the work of Reibenspies, Orchin and Bergman (to name a few) that involve various transition metals.[58–60] Some of these insertions have also been shown to be reversible when CO_2 is removed *in vacuo*.[60,61]

Peroxocarbonates have also been observed to form for Aresta's first η^2 nickel complex with molecular oxygen.[16,62] It was later discovered that the reaction of dioxygen complexes with CO_2 at platinum and rhodium centres could also give peroxocarbonates.[63,64]

A large application that capitalises on the formation of $C-O$ bonds on an industrial scale is the synthesis of cyclic carbonates which will be further discussed in Section 1.4.2.

Formation of New C-N Bonds

The formation of a new C-N bond by the insertion of CO_2 in the M-N bond forms a carbaminato complex. A recent comprehensive review by He and co-workers showed the plethora of
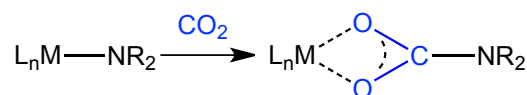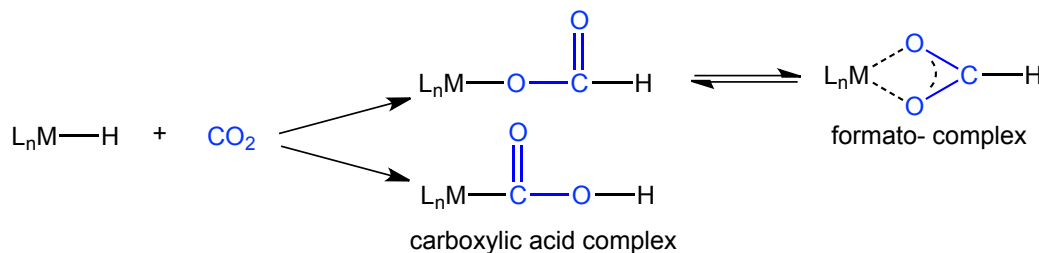
SCHEME 1.8: Insertion of CO_2 into a M-N bond.

products that could be formed through CO_2 capture by nitrogen-containing substrates.[65] The nucleophillic attack of nitrogen is a key step in this insertion reaction.[66,67] Roundhill and co-workers have shown that it is the metal bound nitrogen which attacks carbon dioxide. This pathway was proven by the formation of a carbamic acid intermediate bound to the metal centre (Scheme 1.9).[68]
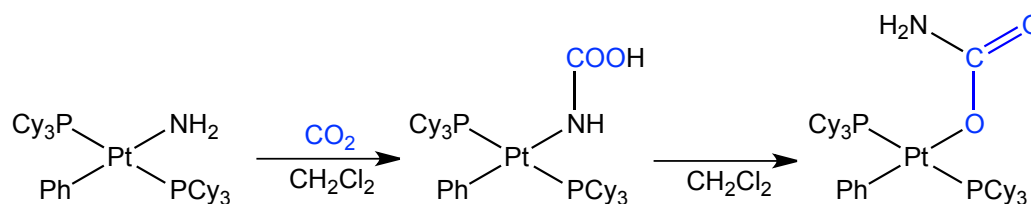
SCHEME 1.9: Nucleophillic attack of the metal-bound nitrogen at CO_2 resulting in a new C-N bond.

Mechanistic studies have also shown that small amounts of free amine may significantly accelerate the reaction by forming carbamic acid with CO_2, which then reacts with the metal-amine complex.[66] This was also supported by a study by Chisholm and Extine, where a rapid exchange of $^{13}CO_2$ with unlabelled CO_2 at a titanium centre was observed, suggesting that CO_2 is only loosely bound, acting as carriers.[69,70]

Formation of New C-H Bond

The insertion of CO_2 into a M-H bond would result in a formato complex or a metallocarboxylic acid complex as shown in Scheme 1.10.

SCHEME 1.10: Insertion of CO_2 into a M-H bond.

The predominant reaction pathway is the formation of a monodentate formato-metal complex which is in equilibrium with a bidentate formato-metal complex. The other pathway forms a metallocarboxylic acid complex which is uncommon primarily due to its instability.

The first step of this reaction involves the nucleophillic attack of the metal hydride on the electrophillic carbon of CO_2, forming the polar transition states shown in Figure 1.5. Subsequent rearrangement of the transition states would afford the formato complex.

FIGURE 1.5: Polar transition states formed between a metal hydride and CO_2.

1.4 Transformation of Carbon Dioxide to Value Added Products

Some typical CO_2 transformations are shown in Figure 1.6. Some of these routes are heavily used in industry, for instance the production of urea, salicylic acid and cyclic carbonates. For releva: s and the sy
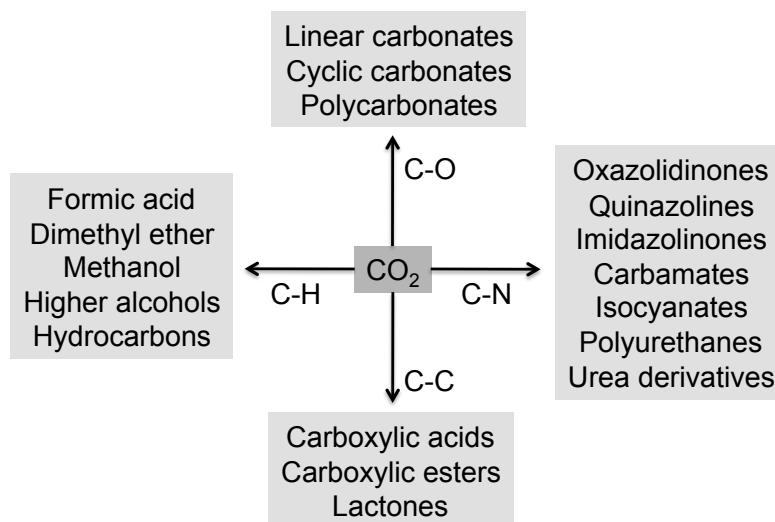
FIGURE 1.6: Transformation of CO_2 into value-added products.

1.4.1 Synthesis of Acrylic Acid and its Derivatives

Acrylic acid is an unsaturated carboxylic acid that is consumed on a large industrial scale as a raw material for water absorbent polymers. Currently, acrylic acid is synthesized in industry by the SOHIO process, which involves the oxidation of acrolein at 300-360°C over a bismuth/vanadium oxide catalyst.[71] Due to the high temperatures needed, there is a motivation to develop a milder, cost efficient route. The oxidative coupling of ethylene and CO_2 to form this bulk

chemical is therefore an attractive route as both ethylene and CO_2 are cheap and abundant starting materials.
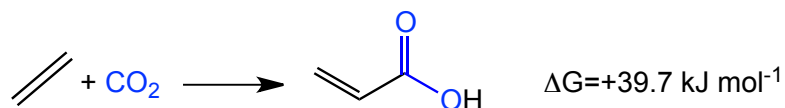
SCHEME 1.11: The "dream reaction": forming acrylic acid from ethylene and CO_2.

However, this reaction is thermodynamically unfavoured (endergonic) and would therefore require a suitable catalyst to lower the barrier of the more energetically demanding step. Scheme 1.12 shows a theoretical catalytic cycle proposed by Hoberg and co-workers. It was postulated that ethylene could oxidatively couple with CO_2 at a nickel (0) centre to form nickelalactones. The lactone would then undergo β-H elimination, forming an acrylic acid-nickel complex which then regenerates the nickel (0) complex after releasing acrylic acid.
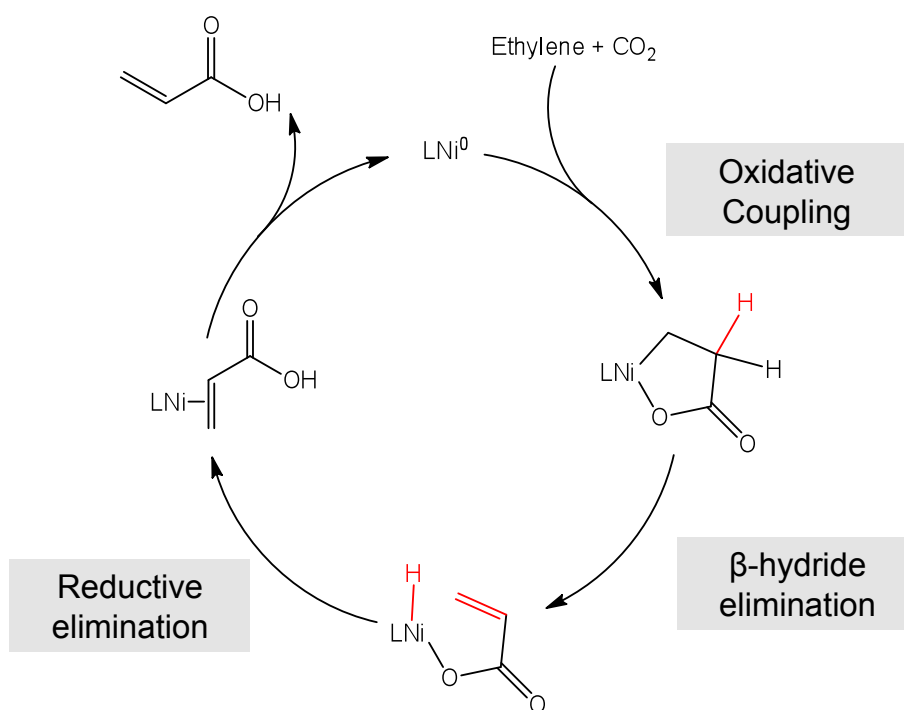
SCHEME 1.12: Theoretical catalytic cycle for the synthesis of acrylic acid from ethylene and CO_2 proposed by Hoberg.

While the catalytic cycle appears feasible on paper, in reality the cycle is thermodynamically impeded. Ethylene and CO_2 couples rapidly at nickel (0) but the β-hydride elimination step is thermodynamically unfavoured so much so that the nickelalactone is a dead end. In addition, the coordination of acrylic acid to the nickel center would hinder a new coordination of ethylene and CO_2. The stability of the lactone can be attributed to steric factors as it is rigid and flat, disallowing the β-hydride to approach the nickel for elimination.

Evident from Scheme 1.6 and the high stability of the lactone, studies of the oxidative coupling between CO_2 and ethylene are still largely non-catalytic. The products, carboxylic acid or

methyl carboxylate ester stem from acid hydrolysis (aq. HCl) or methanolysis (MeOH/aq. HCl) respectively, and result in the subsequent decomposition of the metal catalyst.
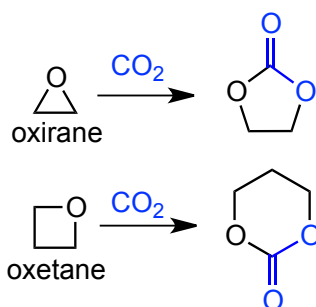
1.4.2 Synthesis of Cyclic Carbonates

The incorporation of CO_2 into carbonates is a potentially significant transformation to reduce the net amount of CO_2 released especially if conducted under ambient conditions. These carbonates are classified into inorganic (metal) and organic carbonates.[72] The latter can be further divided into cyclic, acylic and polycarbonates.

There are many applications for organic carbonates as they are impact resistant and optically transparent.[56,72,73] They are currently used in the manufacture of a plethora of products including DVDs, optical lenses and aircraft windows. Organic carbonates are also key raw materials for the synthesis of polyurethane, urea derivatives and are suitable alternatives for the insidiously poisonous phosgene gas or carcinogenic and poisonous dimethyl sulfate in methylation reactions.[74]

Carbonates could be synthesized by reacting alcohol with the aforementioned phosgene, with pyridine as solvent and base. While this process gives high yields and is flexible as it allows functionalization of the carbonates, it makes use of toxic starting materials (phosgene, pyridine) and produces copious amounts of corrosive hydrogen chloride. The large excess of basic pyridine has to be neutralised and by products have to be removed.[72] An alternate route, commercialised in 2002, is the Asahi-Kasei process, where carbonates were afforded through a phosgene-free route.[75]

Cyclic carbonates can also be obtained by the coupling of CO_2 and strained heterocycles like oxiranes and oxetanes, forming five and six membered rings respectively as shown in Scheme 1.13.[76–78] This method does not use phosgene as a reagent and is 100% atom economical, making it a very desirable transformation. Cyclic carbonates have been commercialised since the 1950s and are used as polar aprotic solvents, electrolytes for lithium ion batteries and as intermediates for fine chemicals.[1,56,72,73,79–82]


SCHEME 1.13: Synthesis of cyclic carbonates from oxirane and oxetane.

The cycloaddition of CO_2 with oxiranes typically proceeds in the presence of an onium salt like TEAB[76] and TBAB[83] or metal halides[84] as catalyst. Other homogenous catalysts include salen complexes of aluminum[85–88], chromium[89,90] and zinc.[91] It has been reported that metal complexes, combined with organic compounds like crown ethers, onium salts or phosphines significantly improved the catalytic activity of the metal.[92–96] Some studies also report the synthesis of cyclic carbonates in the presence of ionic liquids.[97–100] Ionic liquids proved to be advantageous due to the ease of catalyst recovery and product purification[101,102] as a requirement for industrial homogenous catalysis is not to produce solids during the catalyst separation when the product is evaporated.

Mechanism

The reaction of CO_2 and epoxides can generate two types of products: cyclic carbonates and polycarbonates (**a** and **b** in Scheme 1.14). It has also been reported that consecutive insertions of two molecules of epoxides may occur, leading to polycarbonate **c** (Scheme 1.14).[103,104] As discussed in Section 1.2, the carbon atom in CO_2 acts as an electrophile and the oxygen atoms as nucleophiles. The activation of CO_2 can then occur by both an electrophillic or nucleophillic attack. This is also reflected in most catalytic systems for this reaction: they contain Lewis acid sites for the electrophillic activation of epoxide and/or CO_2 and contain Lewis basic nucleophiles. These two sites may belong to two different components - the metal as Lewis acid and the co-catalyst as Lewis base. Alternatively the sites may be present in one compound where the complex contains a cationic metal centre and a labile anionic ligand.[105]
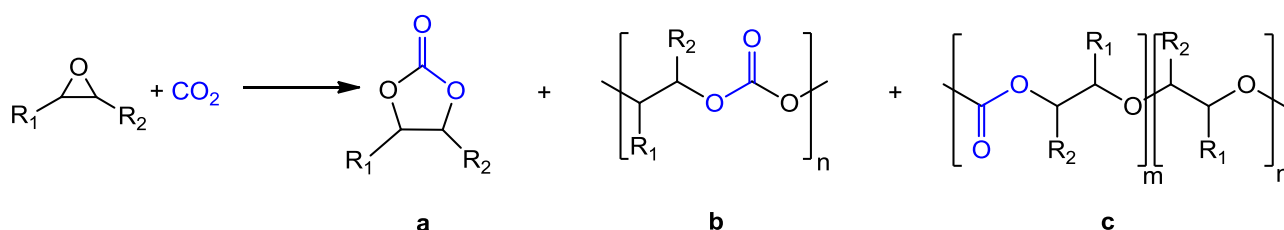

SCHEME 1.14: Possible products from the reaction of CO_2 and epoxides: cyclic carbonates (**a**), polycarbonates (**b**) and polycarbonate containing ether linkages (**c**).

The most widely studied type of catalysts for the reaction of CO_2 and epoxides are homogeneous metal complexes, which can be used alone if they have ligands that can act as a nucleophile or in combination with a co-catalyst to provide the nucleophillic species. Many metal centres acting as Lewis acid sites have been studied, most commonly Al, Cr, Mn, Co, Mg and Fe.[103,104] The ligands on the metal centres are usually salen-type ligands, phenolates and porphyrins.[106] Non metallic homogenous catalysts have been reported as well.

A typical mechanism involving a metal centre and a nucleophile is shown in Scheme 1.15. The epoxide coordinates to the Lewis acidic metal centre and is activated for nucleophillic attack.

This causes the epoxide ring to open, forming a metal bound alkoxide which is now a nucleophile and is able to activate CO_2. The CO_2 molecule inserts into the M−O bond, forming a metal carbonate intermediate. The carbonate species then rearranges to form the cyclic carbonate or further propagates by subsequent addition of epoxide and CO_2, forming a polycarbonate. This mechanism has also been supported by a labelling experiment performed by Shi *et al.* in 2003.[107]
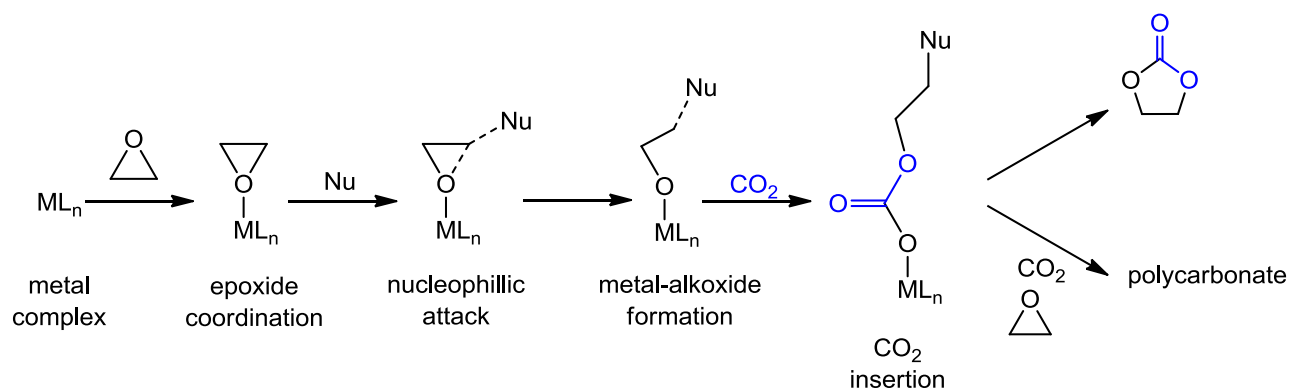
SCHEME 1.15: Mechanism of the formation of carbonates from propylene oxide and CO_2 involving a metal complex and a nucleophile. The nucleophile may originate from the metal complex or from a co-catalyst.

Other pathways involving bimetallic complexes, two nucleophiles or even non-metallic catalysts exist. Salts of organic cations have also been used as catalysts, in particular, ionic liquids. They have been studied as both homogeneous and heterogeneous[108] catalysts. CO_2 also dissolves relatively well in ionic liquids, implying that these ionic liquids could act as both solvent and catalyst. However, reactions involving ionic liquids alone without the complement of a metal centre usually require high temperatures ($\geqslant 80°C$) to give good product yields and selectively forming the more thermodynamically stable cyclic carbonate.

Metal Containing Catalysts

The nature of the metal centre in metal complexes plays an important role in their catalytic performance. As shown in Scheme 1.15, the mechanism involves an alkoxide species containing a metal-oxygen bond. The strength of the bond greatly influences the selectivity and activity of the catalyst. A metal-oxygen bond that is too strong would render the intermediate inactive towards multiple insertions which leads to propagation and copolymer production. It would also result in an intermediate that is resistant towards ring closure, resulting in a linear carbonate. On the other hand, if the metal-oxygen bond is weak, it can then be displaced by a nucleophile or solvent molecule, which would result in lower activity but favour the back biting reaction, increasing selectivity towards the cyclic carbonate. Therefore an intermediately strong bond would be needed for optimal catalytic performance. The bond strength can be adjusted by choosing an appropriate metal centre.

The choice of ligand is also instrumental in this reaction as the type of ligand dictates if the complex has a rigid or flexible structure. Two of the most widely studied ligands used in the metal complexes for this reaction are the porphyrin and salen ligands. Both ligands result in a planar complex with tetradentate coordination to the metal centre. Depending on the metal centre, the complex can accomodate additional ligands in the axial positions. These axial ligands are generally labile and are good leaving groups as they are readily displaced during the reaction.

Co-Catalysts

It has been reported that the catalytic performance of a catalyst can be further enhanced by a Lewis base as co-catalyst.[104,109] The co-catalyst either attacks and opens the epoxide ring that is coordinated to the metal centre or it behaves as a nucleophile that coordinates to the metal centre, increasing its electron density and weakening the bond with other nucleophillic species (if more than one nucleophile is present, usually in a polymeric chain). For good activity, the co-catalyst should not be bound too strongly to the metal centre so that it can easily leave, while still being a good nucleophile to open the ring of the epoxide. Being a good leaving group would also promote back biting reactions for the metal-bound carbonate intermediates, favouring the formation of cyclic carbonates. A co-catalyst with poor leaving abilities would supress the formation of cyclic carbonates and be more selective towards polycarbonates.

Co-catalysts can be neutral, like an organic base, or ionic, like an ammonium salt. Common co-catalysts are shown in Figure 1.7. For ionic catalysts, the anion has a greater nucleophillicity towards the epoxide if the corresponding cation is bulky as it would exert lower ion-pair electrostatic attraction towards the anion.[108]
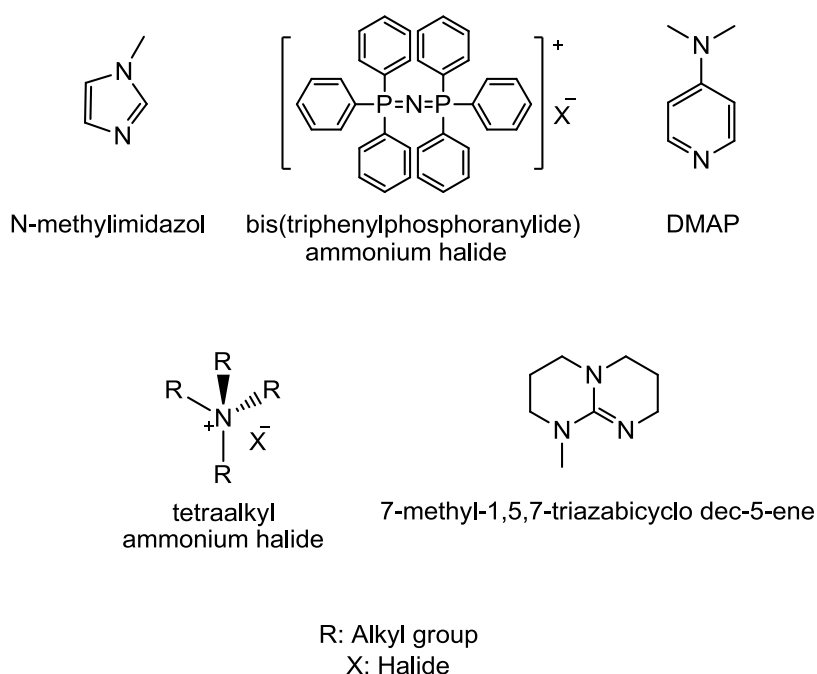

FIGURE 1.7: Common co-catalysts used in the reaction of carbon dioxide and epoxides.

The ratio between catalyst and co-catalyst also affects the selectivity of carbonate formation. A higher co-catalyst to catalyst ratio has been reported to favour the formation of cyclic carbonate over polycarbonates. The excess co-catalyst would displace the metal-carbonate intermediate, favouring the back biting reaction for cyclization.[104,110,111]

The importance of a co-catalyst can be observed in aluminum tetraphenylporphyrin complexes. Without a co-catalyst, CO_2 is minimally incorporated in the polymer chain of propylene oxide. However, when DMAP was added as co-catalyst, co-polymerization of propylene oxide and CO_2 was prevalent.[112]

Ionic liquids can also be used as co-catalysts for carbonate formation. These non-metallic compounds can be used as both homogeneous and heterogeneous catalysts (immobilised on a support).

Substrates

The rate and selectivity of the formation of carbonates does not only depend on the features of the catalytic system but also on the epoxide substrate due to steric and electronic effects.

Steric bulk around the epoxide ring would cause a lower conversion rate as it would hinder nucleophillic attack by the co-catalyst. This is usually observed for internal epoxides like cyclohexene oxide or α-disubstituted epoxides like 1,1-dimethyloxirane when compared to epoxides with a linear alkyl chain like propylene oxide.

The nature of the substituents on the epoxide ring also affects selectivity for cyclic or polycarbonates. Terminal epoxides like propylene oxide would have nucleophillic attack primarily occuring at the less hindered carbon site i.e. the β-carbon due to the higher accessibility and the electron-donating effect of the alkyl group. On the other hand, epoxides like styrene oxide that have an electron-withdrawing group on the α-carbon would promote nucleophillic attack on the electron deficient α-carbon instead of the β-carbon. Upon CO_2 insertion, this would form cyclic styrene carbonate as back biting reaction would be favoured by the electron withdrawing phenyl group (Figure 1.8).
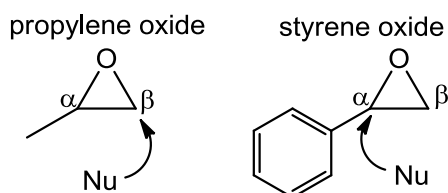

FIGURE 1.8: Most probable sites of nucleophillic attack for different epoxides.

It is crucial to have a fine balance of the components discussed above (metal centre, substrate, co-catalyst) to obtain the desired selectivity of this reaction. This will be further discussed in Chapter 5.

Chapter 2

Objectives and Outline

CO_2 has been shown to be ubiquitous and inexpensive and its utilization could contribute to alleviate the current climate situation. It is also an ideal C-1 building block. Due to its inherent stability, the development of suitable organometallic catalysts is crucial for its activation.

The formation of new C-C and C-O bonds have been discussed in Section 1.3.4. It was later shown that the oxidative coupling of CO_2 and ethylene at a nickel centre results in a very stable nickelalactone (Section 1.4.1). One of the objectives of this work is to extend this study to other group 10 metals like palladium. Since the atomic radius of palladium is about 20 pm larger than nickel[113], it would follow that palladium would form less stable metalalactones that would then be able to undergo β-hydride elimination with greater ease. The direct synthesis of palladalactones from ethylene and CO_2 has also not been reported.

The work with palladium is split into 2 parts:

1. The synthesis of palladalactones from ethylene and CO_2

2. Inducing β-hydride elimination in palladalactones by electrophiles to form acrylates

The formation of cyclic carbonates from epoxides and CO_2 have also been discussed in Section 1.4.2 and many different types of catalysts have been used in this reaction. However, simple catalytic systems in mild conditions are not widely reported and few mechanistic studies have been done. After a preliminary screening of different catalyst and co-catalyst systems, it is found that a $NbCl_5$/DMAP or a $NbCl_5$/TBAB system shows high activity for the synthesis of cyclic carbonates under ambient conditions.[114] The synergistic catalyst/co-catalyst relationship was intricately studied under varying catalyst/co-catalyst ratios and CO_2 pressure. Reaction rates were also studied with ionic liquids as co-catalyst.

Chapter 3

# Synthesis of Palladalactones from Pd Complexes, Ethylene and Carbon Dioxide

3.1   Introduction

The formation of metallactones from ethylene and CO_2 have been reported for several other metals (Zr[115], Ti[116], Rh[117], Fe[118]) after Hoberg's discovery of the nickelalactone in 1982.[49] While the nickel lactone has been studied by many, the formation of a palladalactone (and subsequently acrylic acid/acrylates) by ethylene and CO_2 has not been reported to date. Aresta was the closest to realizing this as he successfully obtained methyl acrylate, ethyl acrylate and methyl methacrylate from ethylene and CO_2 by way of palladium centred salts though not catalytically.[119] In the same study, DFT calculations were performed in an attempt to isolate the intermediates which were hypothesized to be complex, unusual and non-trivial. Although they were unsuccessful, a mechanism for methyl acrylate formation was proposed (see Scheme 3.1).

One of the challenges in this work was the synthesis of zerovalent palladium-alkene complexes. They are usually used as starting materials for the synthesis of other zerovalent complexes with phosphine or nitrogen-based ligands. The stability of these complexes is determined by a fine balance of electron-donating and withdrawing capabilities of the ligand and the palladium centre respectively.

The bonding of an alkene to palladium consists of two parts:

- A forward donation from the π orbital of the alkene into the empty d orbital of palladium, forming a σ bond (Figure 3.1, left)
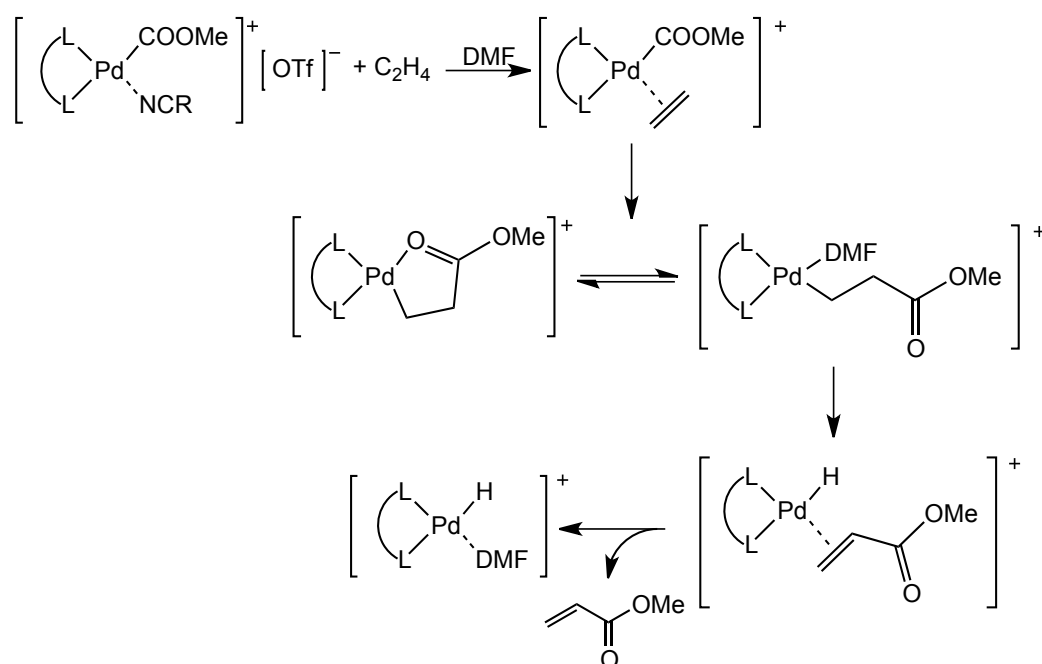
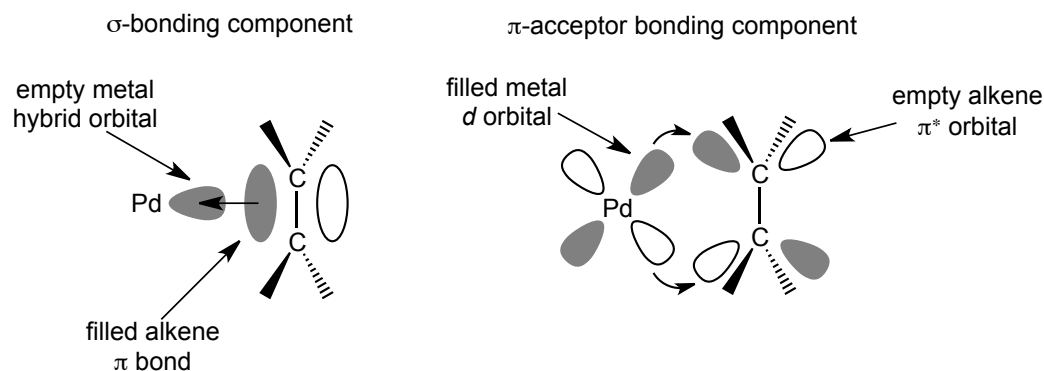SCHEME 3.1: Aresta's proposed mechanism for methyl acrylate formation.

FIGURE 3.1: The bonding of an alkene to a palladium centre.

- A back donation from a filled d orbital of palladium into the empty π orbitals of the alkene, forming a π bond (Figure 3.1, right)

To form stable olefin complexes, the orbitals must have the right symmetries and the metal must possess a high electron affinity to be a good σ acceptor and a low promotional energy (the "cost" of bonding to a low lying excited state of the metal ion (d^n or $d^{n-1}s^1$) instead of the ground state) to improve the π backbonding.[120]

Many palladium(II)-olefin complexes of the type [PdCl$_2$(olefin)] have been prepared and their catalytic reactions with nucleophiles have been studied at length.[121,122] However, palladium(0)-olefin complexes are relatively limited unlike its nickel(0) and platinum(0) analogs. The scarcity of palladium(0)-olefin complexes could be attributed to their instability as shown in Table 3.1. Pd(0) has a low electron affinity (compared to Pd(II)) and high promotional energy compared to the other metals in its group. Ionization potential also increases from Ni < Pt < Pd, resulting

TABLE 3.1: Electronic properties of Group 10 metals to form stable olefin complexes.

Atom	Ground State	Promotional Energy $d^{10} \to d^9 s^1$ or $d^8 \to d^7 s^1$	Promotional Energy $d^{10} \to d^9 p^1$ or $d^8 \to d^7 p^1$	Electron Affinity $d^{10} \to d^{10} s^1$ or $d^8 \to d^7 s^1$	π Donor Character	σ Acceptor Character
Ni (0)	$d^8 s^2$	-1.80	1.72	1.20	very good	poor
Pd(0)	d^{10}	0.81	4.23	1.30	good	poor
Pd(II)	d^8		3.05	18.56	good	very good
Pt(0)	$d^9 s^1$	-0.76	3.28	2.40	good	poor
Pt(II)	d^8		3.39	19.42	good	very good

in an unfavourable back donation, rendering the Pd(0) olefin complex the least stable among the three.[123]

Another reason accounting for the lack of Pd(0)-olefin complexes in literature is that there is no suitable route to form these complexes. For stability, electron rich phosphines or nitrogen based ligands are usually used. However, in the case of Pd(0), these ligands would compete with the olefin for coordination to the metal centre, hindering the approach of the olefin. Regardless, several known Pd(0) alkene complexes were synthesized to attempt to couple them with CO_2.

3.2   Results and Discussion

Several palladium (0) and palladium (II) complexes were synthesized and they were first reacted with ethylene for a period of time before CO_2 was introduced into the reaction vessel in an attempt to recreate the early nickel experiments by Hoberg (Section 1.4.1).[49] The experiments were performed in both a steel autoclave and an *in situ* IR setup.

3.2.1   Reaction of Palladium Complexes with Carbon Dioxide

The palladium complexes used in this study are shown in Figure 3.2 and were synthesized according to published procedures.

The diethyl palladium complex, **1** was chosen as it was reported to be a convenient precursor for Pd(0)-alkene complexes.[123] The ethyl groups easily leave in solution in the presence of an olefin, leaving a coordinatively unsaturated Pd(0) complex that is capable of coordinating to alkenes. Unfortunately the addition of ethylene and CO_2 led to the decomposition of **1**.
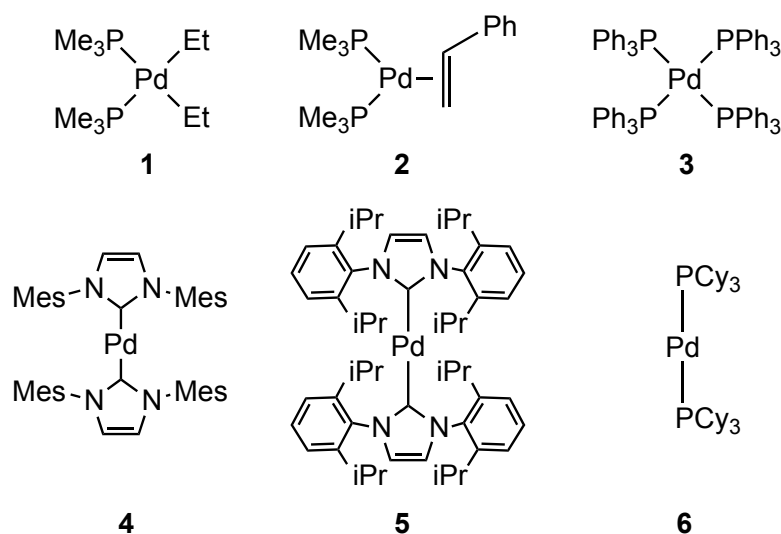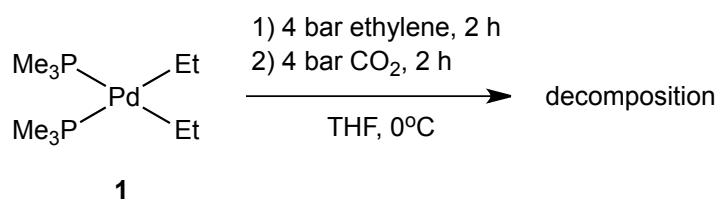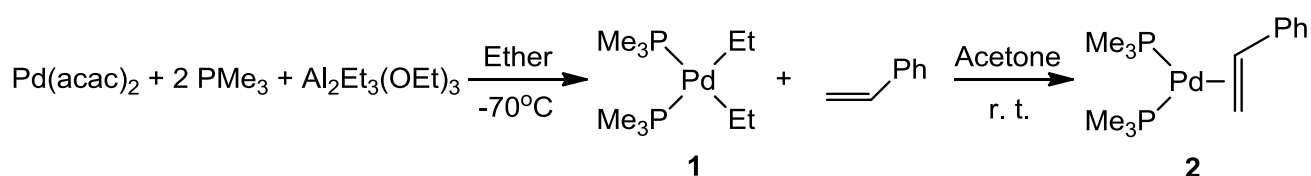
FIGURE 3.2: Pd-alkene complexes synthesized.

SCHEME 3.2: Reaction of **1** with ethylene and CO_2.

SCHEME 3.3: Synthesis of **1** and **2**.

Scheme 3.3 shows the synthetic route towards **1** and **2**. The alkylation of Pd(acac)$_2$ by an alkylaluminum compound is advantageous over conventional alkylation methods that use palladium halides, alkyllithium or Grignard reagents because the final product can be isolated by filtration and washing with organic solvents like hexane.[124] This is especially useful since the dialkylpalladium (II) complex is susceptible to water and more importantly, is only stable at low temperatures. **1** is diamagnetic, air sensitive, thermally unstable and decomposes at room temperature even under an inert atmosphere. The products of thermal decomposition have been reported to be a mixture of ethylene, ethane and butane.[125]
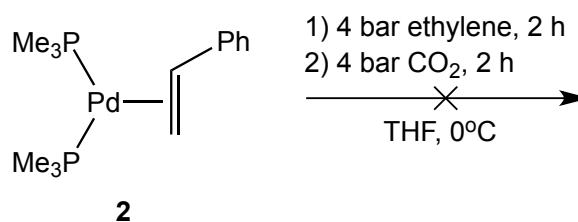
SCHEME 3.4: Reaction of **2** with ethylene and CO_2.

The styrene complex **2** was synthesized from **1**, by stirring with styrene for 6 hours and isolated by recrystallization. CO_2 was introduced to the styrene complex directly however, no reaction was observed by comparing their NMR spectra. Also when **2** was first reacted with ethylene, no exchange of styrene with ethylene was observed. Ethylene was unable to displace styrene as it was more electron rich and therefore has a poorer coordinating ability. Styrene, however has an electron withdrawing phenyl group, which decreases electron density on the double bond and preferentially coordinates to the palladium centre.
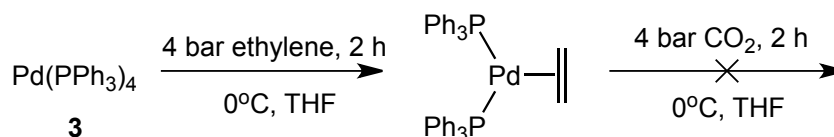
SCHEME 3.5: Reaction of **3** with ethylene and CO_2.

For the tetrakis palladium complex **3**, reaction with ethylene gave the ethylene coordinated complex, as seen in NMR. The coordinated ethylene molecule has a slightly down field chemical shift (5.50 ppm) as compared to the free molecule (5.25 ppm) due to the added deshielding of the C=C. The ethylene coordinated compound was subsequently found to be inactive towards CO_2. Using 10 bar of ethylene and 20 bar of CO_2 in a steel autoclave for 6 hours also did not show any reaction towards CO_2.

Carbene complexes **4** and **5** were fluorescent in solution and inactive towards ethylene. However, when CO_2 was added, the fluorescence had noticeably faded. A white solid was observed to have precipitated over a few days and NMR studies, in comparison with literature,[126] showed that the solid was a carboxylate adduct of the imidazolium salt and no insertion of CO_2 had occurred. (Scheme 3.6) In this case, the carbene ligands were cleaved from the palladium centre and then bonded to CO_2, independent of the palladium centre.

Complex **6** showed some degree of activation towards ethylene and CO_2 as NMR-scale studies showed the coordination of ethylene to the palladium complex. The ethylene coordinated complex was also successfully crystallized and analysed by X-Ray studies which confirmed its identity (see Figure 3.3). Upon introducing CO_2, there was a visible shift in the NMR spectrum but the identity of the resulting product could not be ascertained. IR studies performed on the reaction mixture showed a new peak at 1666 cm^{-1}.

R = mesityl (**4**), diisopropylphenyl (**5**)
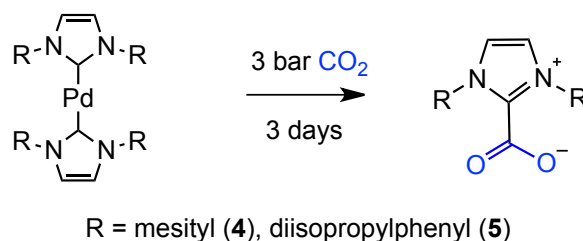
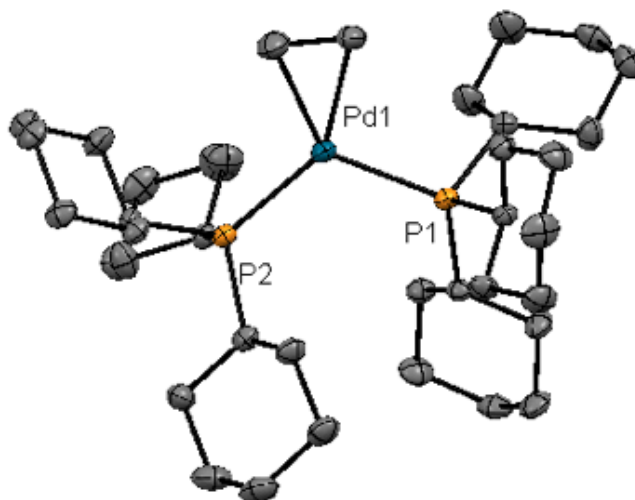SCHEME 3.6: Formation of a carboxylate upon reacting bis(carbene) palladium compounds with CO$_2$.

FIGURE 3.3: ORTEP drawing of the palladium-ethylene complex, where ethylene is η^2-coordinated to palladium.

The reaction was scaled up and performed in an in situ IR setup in an attempt to identify the product. Subsequent removal of the solvent in a schlenk afforded a yellow solid. IR studies on the solid also confirm the presence of the peak at 1666 cm^{-1}. However, this reaction was not reproducible. It was also found that the same solid rapidly forms when the reaction mixture was exposed to air. This suggested that the solid might be formed due to oxidative addition of CO$_2$ rather than the desired reaction between ethylene and CO$_2$. A series of experiments were then performed to determine the exact combination of gases between C$_2$H$_4$, CO$_2$ and O$_2$ that were responsible for the formation of the precipitate.

When Pd(PCy$_3$)$_2$ was reacted with O$_2$, a slight colour change was noted and there was a shift of about 3 ppm in the ^{31}P NMR spectrum. Shifts were also observed in both the proton and carbon NMR spectra. Further IR and NMR studies with different gas pair combinations established that the solid with absorption peak at 1666 cm^{-1} was formed by the oxidative coupling of CO$_2$ and O$_2$ on Pd(PCy$_3$)$_2$. A comparison of the IR spectra is shown in Figure 3.5. Minor differences could be due to varying humidity levels. The ^{13}C NMR spectrum of this compound showed a peak in the carbonyl region at 167 ppm.
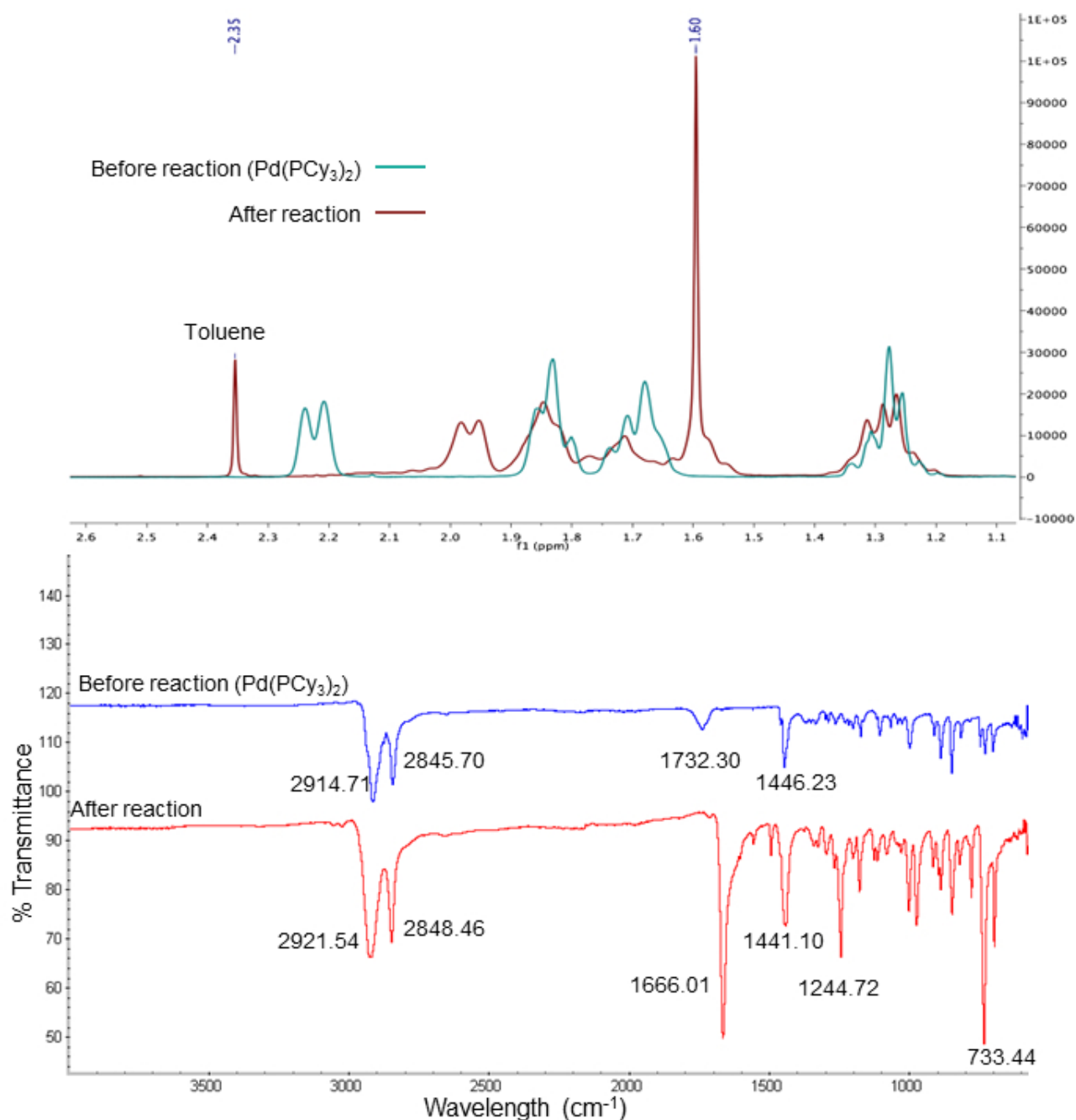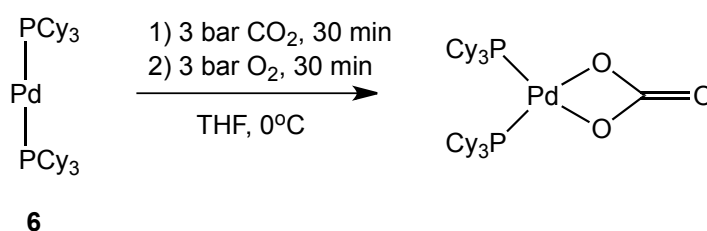
FIGURE 3.4: Proton NMR spectrum (top) and IR spectrum (bottom) of $Pd(PCy_3)_2$ before and after reaction with CO_2.

SCHEME 3.7: Reaction of **6** with CO_2 and O_2.

To fully elucidate the structure of this compound, single crystals suitable for X-Ray analysis were grown over several weeks. It was found that a palladium peroxocarbonate[127] complex was
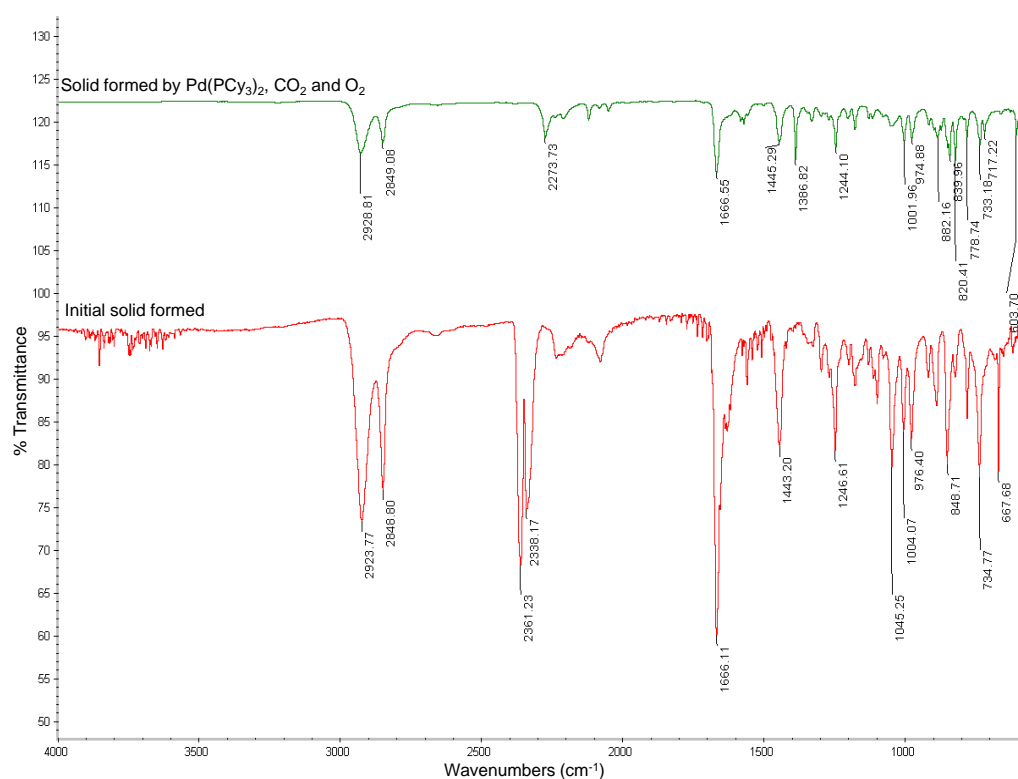
FIGURE 3.5: Comparison of IR spectra of the solid formed with oxygen and the initial solid formed.

formed as a product of this reaction instead of the peroxo complex. An ORTEP drawing of the compound is shown in Figure 3.6. Interestingly, similar palladium peroxocarbonates were also reported as rearranged products of CO_2 addition and hydrolysis of dimethyl palladium complexes.[128]
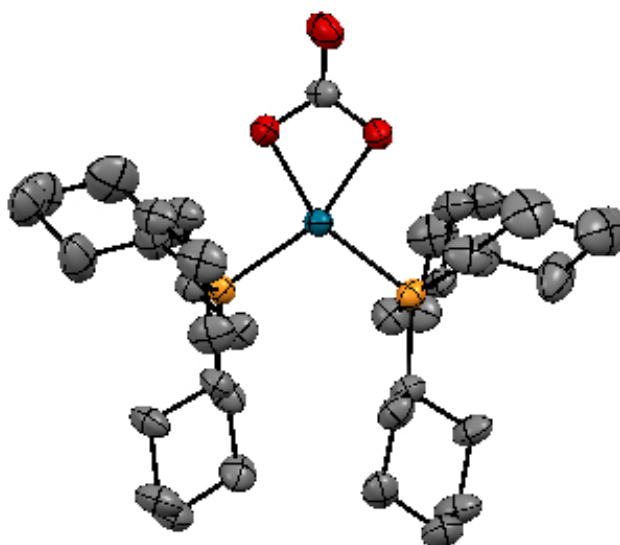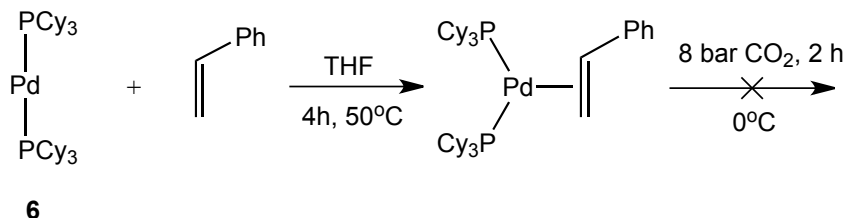

FIGURE 3.6: ORTEP drawing of the Pd-peroxocarbonate complex.

3.2.2 Reaction of bis(tricyclohexyl)phosphine palladium (0) with Styrene and Carbon Dioxide

SCHEME 3.8: Reaction of **6** with styrene and CO_2.

$Pd(PCy_3)_2$ was also reacted with styrene in an attempt to diversify the alkene substrates. Similar to the results with ethylene, styrene was observed to have coordinated to the palladium centre. The NMR spectrum showed a upfield shift in the ^{31}P NMR spectrum and diminished and broadened peaks belonging to the alkenyl moiety in styrene, which was consistent with coordination. Unfortunately, attempts to grow single crystals were unsuccessful and the identity of the complex could not be confirmed. Reacting the styrene coordinated complex with 8-20 bar of CO_2 for 2-8 hours did not show any activity.

3.3 Experimental

3.3.1 General Information and Materials

All air sensitive manipulations were performed in an inert argon atmosphere using Schlenk techniques or a glovebox. Glassware was washed in an isopropanol/KOH base bath followed by a dilute hydrochloric acid bath and then deionised water. All glassware were dried overnight in a 120°C oven and flame dried *in vacuo* at 350°C before using for air sensitive reactions. Steel autoclaves were washed with detergent and deionised water and dried in a 120°C oven before use.

Chemicals

Palladium (II) chloride (99%), triethylaluminum solution (1.3 M in hexanes), 1,5-cyclooctadiene (99%), palladium (0) tetrakistriphenylphosphine (99%), styrene (99%), tricyclohexylphosphine, trimethylphosphine solution (1 M in THF) and tri(o-tolyl)phosphine (97%) were purchased from Sigma Aldrich and used without further purification. Palladium (II) acetylacetonate (99%) was purchased from Acros Organics and also used as received. The pyrophoric triethylaluminum and all phosphines were stored in the glove box.

Solvents

Hexane, pentane, dichloromethane, diethylether and toluene were purified over activated alumina. THF was dried with sodium wires, methanol and ethanol with CaH_2 and acetone over $CaSO_4$, refluxed and distilled. The solvents were also degassed by the freeze-pump-thaw method and stored over 3 Å or 4 Å molecular sieves. The water content of the solvents (except acetone) were regularly analysed by a Karl-Fischer titrator. All deuterated solvents were also dried in the usual way, distilled under reduced pressure, degassed and stored over 3 Å or 4 Å molecular sieves in the glovebox.

3.3.2 Instruments

In situ IR spectroscopy was carried out on a Mettler Toledo ReactIR 45/Multimax RB 04-50 station with 50 mL stainless steel autoclaves. The autoclaves are equipped with diamond probes at the base which act as the multiple reflection ATR element. The autoclaves were connected to a CO_2 cylinder by a Mettler Toledo LMPress60 pressure regulator which provided and maintained con   ted ever
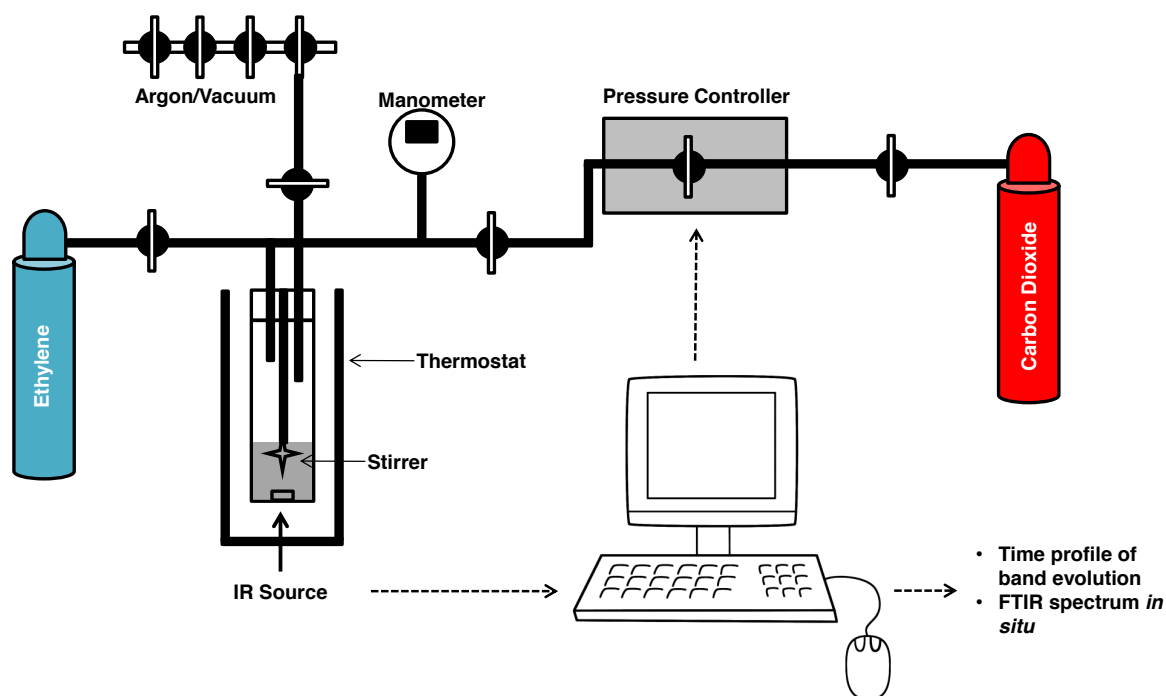

FIGURE 3.7: *In situ* IR experiment setup

NMR scale reactions were performed in a high pressure J Young NMR tube that was connected to a gas manifold which was connected to an ethylene cylinder followed by a CO_2 or O_2 cylinder. Other experiments involving gaseous substrates were performed in a regular autoclave with a pressure gauge and was connected to the same gas manifold as the NMR experiments.

FTIR measurements were performed on a Thermo Scientific Nicolet 6700 FT-IR spectrometer with a diamond probe. The transmittance spectra were processed with the accompanied OMNIC software.

NMR measurements were performed on 400, 500, 600 or 700 MHz Bruker AVANCE spectrometers. Chemical shifts are reported in ppm (δ values relative to TMS) with the solvent residual peak as an internal standard.

X-Ray experiments were performed on a single crystal coated with paratone oil and mounted on a Kaptan loop. The crystal was kept on a stream of nitrogen during data collection by an X-Ray diffractometer equipped with an APEX II κ-charge-coupled device detector and a rotating anode (Bruker AXS FR591). ORTEP structures were visualised by the Mercury software.

3.3.3 Synthesis of Palladium Precursors

Synthesis of Pd(COD)Cl$_2$: $PdCl_2$ (3.24 g, 18.2 mmol) was dissolved in conc. HCl (37%) warmed to 50°C. After all solids had dissolved, the solution was left to cool and was diluted with ethanol (150 mL). The solution was filtered to remove any remaining undissolved matter and washed with excess ethanol. COD (4.40 mL, 36.4 mmol) was then added, immediately precipitating the product as a yellow solid. The suspension was stirred for 20 minutes to allow for complete precipitation. The product was then filtered and washed with diethyl ether. Yield=90%

Synthesis of Pd[P(o−tolyl)$_3$]$_2$ (modified from literature)[129]: NaOH (1.48 g, 37 mmol) was first dissolved in methanol (8 mL) and added to a solution of Pd(COD)Cl$_2$ (5.23 g, 18 mmol) in toluene (30 mL). The mixture was left to stir for 30 minutes and subsequently removing the precipitated NaCl by filtration. P(o−tolyl)$_3$ (11.15 g, 37 mmol) was then dissolved in toluene (50 mL) and added to the resulting filtrate at -20°C in an ice/NaCl cooling bath and stirred for 1 hour. The reaction was warmed to 0°C and stirred for another hour. The reaction was then brought to room temperature and stirred overnight where a yellow solid was formed. The solid was filtered, washed with methanol and dried *in vacuo*. Yield=63%

^{1}H NMR (C$_6$D$_6$, 10°C, 400MHz): δ (ppm) 7.28 (s, 18 H), 6.95 (m, 6 H), 3.09 (s, 18 H)
^{31}P NMR (C$_6$D$_6$, 10°C, 100MHz): δ (ppm) 7.40

Synthesis of PdEt$_2$(PMe$_3$)$_2$, (modified from literature)**1**[124]: A solution of Al$_2$Et$_3$(OEt)$_3$ was first prepared by adding ethanol (0.97 g, 0.021 mol) dropwise and cautiously to triethylaluminum (10.76 ml, 0.014 mol) at -20°C in an ice/NaCl cooling bath. The solution was stirred for an hour. Pd(acac)$_2$ (1.0 g, 3.28 mmol) was dissolved in diethyl ether (10 mL) and cooled to -78°C in an isopropanol/dry ice cooling bath. PMe$_3$ (6.89 mL, 6.89 mmol) was added dropwise, followed by the prepared Al$_2$Et$_3$(OEt)$_3$ solution in excess. The reagents were left to stir for 15 minutes, before transferring to an ice bath at 0°C and left to stir further for 1 hour at 0°C. The solution

was then concentrated and placed into a freezer at -20°C for crystallization. Colourless crystals precipitated overnight and were filtered and stored in the freezer in the glovebox. Yield=70%

^{1}H NMR (C$_6$D$_6$, 10°C, 400MHz): δ (ppm) 1.53 (t, 6 H) 1.07 (s, 18 H), 0.82 (q, 4 H)
^{13}C NMR (C$_6$D$_6$, 10°C, 100MHz): δ (ppm) 17.59, 13.76, 4.79

Synthesis of Pd(IMes)$_2$, 4 [130]: A solution of 1,3-bis-(2,4,6-trimethylphenyl) imidazol-2-ylidene (2.68 g, 8.80 mmol) was dissolved in toluene (30 mL) and added to a separately dissolved Pd[P(o−tolyl)$_3$]$_2$ (2.47 g, 3.45 mmol) in toluene (30 mL). An orange solution formed instantaneously and was left to stir for 1 hour. The solvent was removed *in vacuo* and the orange residue was washed with cold hexane (0°C) to remove all traces of phosphine. Yield=67%

^{1}H NMR (C$_6$D$_6$, 10°C, 400MHz): δ (ppm) 6.82 (s, 8H), 6.14 (s, 4H), 2.34 (s, 12 H), 2.04 (s, 24 H)
^{13}C NMR (C$_6$D$_6$, 10°C, 100MHz): δ (ppm) 198.9, 139.2, 136.5, 136.1, 129.0, 119.1, 21.7, 19.1

Synthesis of Pd(IPr)$_2$, 5 [130]: Procedures were the same as **4** with Pd[P(o−tolyl)$_3$]$_2$ (541 mg, 0.76 mmol) and 1,3-bis-(2,6-diisopropylphenyl)imidazol-2-ylidene (2.68 g, 8.80 mmol). Yield=58%

^{1}H NMR (C$_6$D$_6$, 10°C, 400MHz): δ (ppm) 7.29 (t, 4 H), 7.09 (d, 8 H), 6.27 (S, 4 H), 2.89 (m, 8 H), 1.20 (d, 24 H), 1.11 (d, 24 H)
^{13}C NMR (C$_6$D$_6$, 10°C, 100MHz): δ (ppm) 198.6, 144.2, 139.5, 128.5, 126.2, 121.1, 28.7, 24.8, 23.8

Synthesis of Pd(PCy$_3$)$_2$, 6: NaOH (0.94 g, 23.5 mmol) was dissolved in MeOH (5 mL), added to a solution of Pd(COD)Cl$_2$ (1.67 g, 5.9 mmol) in toluene (10 mL) at -20°C and left to stir for 20 minutes. The precipitated NaCl was filtered and PCy$_3$ (3.29 g, 11.7 mmol) was added. The reaction was stirred for 1 hour at -20°C and 1 hour at 0°C. Methanol (50 mL) was added and left to stir for 10 minutes to precipitate the desired product. The suspension was filtered, washed with copious amounts of methanol and dried *in vacuo*, giving the final product as a yellow solid. Yield=68%

^{1}H NMR (C$_6$D$_6$, 10°C, 400MHz): δ (ppm) 2.34 (d, 12 H), 1.94 (m, 18 H), 1.39 (m, 18 H)
^{31}P NMR (C$_6$D$_6$, 10°C, 100MHz): δ (ppm) 39.0

3.3.4 Reaction of Palladium (0) and (II) Complexes with Alkenes and Carbon Dioxide

General Procedures for NMR Scale Reactions

The palladium complex (20-30 mg) was weighed into a high pressure J. Young NMR tube and dissolved in thf-d8 (0.4 mL). The tube was then cooled in an ice bath to 0°C before introducing

4 bar of ethylene. The low temperature would allow for better gas solubility. Ethylene pressure was kept for 2 hours before introducing an additional 4 bar of CO_2. The maximum pressure capacity of the tube was 8 bar. CO_2 pressure was kept for 2 hour. NMR was measured with the tube under gaseous pressure.

Reaction with Styrene and CO₂

Complex **2** was generated *in situ*. Complex **1** (26 mg, 0.08 mmol) was dissolved in acetone-*d6* (0.4 mL) in a pressure resistant J. Young NMR tube. Styrene (37.6 μL, 0.328 mmol) was then added via a micro syringe. The tube was heated to 40°C and left for 3 hours to allow for the coordination of styrene. 8 bar CO_2 was then introduced via the gas manifold.

In the case of complex **6**, 30 mg (0.05 mmol) was dissolved in thf-d8 (0.4 mL) and reacted with styrene (5.175 μL, 0.05 mmol) at 50°C for 4 hours. The high pressure J Young tube was then cooled to 0°C and 8 bar CO_2 was introduced and left to stand for 2 hours.

Reaction with O₂

Complex **6** (30 mg, 0.05 mmol) was dissolved in THF-*d8* (0.4 mL) in a pressure resistant J. Young NMR tube. The tube was immersed in an ice bath at 0°C and 4 bar CO_2 was introduced via the gas manifold and left under pressure for 1 hour. The O_2 cylinder was then connected and 4 bar of O_2 was introduced. The formation of the yellow palladium peroxocarbonato complex was immediate. The tube was brought into the glove box and its contents transferred into a schlenk for work up and subsequent NMR analysis.

General Procedures for *in situ* IR Reactions

The autoclave was first cooled to 0°C. The appropriate palladium complex (e.g 0.10 g, 0.150 mmol of **6**) was dissolved in 8 mL of toluene and injected into the autoclave under a stream of argon. IR data collection was started. The solution was mechanically stirred at 500 r.p.m and left to equilibriate for 5 minutes before introducing 4 bar of ethylene by adjusting the regulator attached to the cylinder. The reaction was left to stir under ethylene for 1 hour before 4 bar CO_2 was added. In subsequent reactions, the ethylene and CO_2 pressure were increased to a maximum of 10 and 20 bar respectively. Unfortunately as discussed, higher pressures did not bring the activation to fruition. Upon completion of reaction, the contents of the autoclave was transferred into a schlenk flask by syringe and evacuated *in vacuo*.

General Procedures for Reactions in an Autoclave

The palladium complex (e.g. 0.125 g, 0.108 mmol for complex **3**) was first dissolved in toluene (5 mL) and injected into the autoclave in a glove box. A magnetic stirrer was also added to the

autoclave. The autoclave was cooled to 0°C by placement into an ice bath before introducing 10 bar ethylene for 30 minutes. The ethylene cylinder was then replaced with a CO_2 cylinder and 20 bar CO_2 was introduced and left to stir overnight. The cylinder was depressurized, opened in the glove box, its contents emptied into a schlenk and volatiles were removed *in vacuo*.

Reactions with Styrene

For palladium-styrene complex **2**, complex **1** (0.20 g, 0.632 mmol) was first dissolved in dry acetone (8 mL). Styrene (0.289 mL, 2.53 mmol) was added and the reaction was left stirred at 30°C for 6 hours to form the styrene coordinated complex **2**. The reaction mixture was then transferred into an autoclave in a glove box. The autoclave was then brought out of the glove box and connected to a CO_2 cylinder via a gas manifold. 10 bar of CO_2 was then introduced. The cylinder was depressurized, opened in the glove box, its contents emptied into a schlenk and volatiles were removed *in vacuo*.

Reactions with O₂

Complex **6** (0.20 g, 0.300 mmol) was weighed into the autoclave and a magnetic stirrer was added. The complex was dissolved in toluene (10 mL), the autoclave was closed, brought out of the glove box, connected to the gas manifold and cooled to 0°C after which 10 bar CO_2 was introduced. The autoclave was left to stir under pressure for 1 hour before adding 20 bar of O_2 and leaving to stir for another hour. The autoclave was brought into the glove box and the contents were decanted into a schlenk where the solid was isolated by cannular filtration. The solid was dissolved in $CDCl_3$ and analysed by NMR. Crystals suitable for X Ray studies were grown by dissolving the solid in chloroform and layering with toluene.

3.4   Conclusion

The formation of palladalactones from palladium complexes have been investigated. The palladium complexes implemented in this study were largely inactive towards the coupling of ethylene or styrene with CO_2 under our experimental conditions (2-8 hours, 4-20 bar, 0 °C). While styrene and ethylene coordinates to the palladium centre, the resulting complex is inactive towards CO_2. The palladium (0) carbene complexes gave instead a carboxylate adduct upon reaction with CO_2. They were, however, inactive towards ethylene.

A palladium peroxocarbonate complex has also been isolated as a result of the reaction between CO_2 and O_2, consistent with the findings of Dibugno *et al*. Although the reaction was not the desired coupling, it allowed for the crystal structure of the peroxocarbonate to be measured.

Chapter 4

Ring-Opening of Palladalactones with Electrophiles

4.1 Introduction

Cyclic nickel carboxylates have been widely discussed over the past two decades with regard to their potential of catalysing the "dream" reaction between ethylene and CO_2, to form acrylic acid.[52,131] The generally accepted catalytic cycle has been discussed in Scheme 1.12, which involves an oxidative coupling, a β-hydride elimination and finally a reductive elimination step. While ethylene and CO_2 couple rapidly at a nickel centre,[49,131,132] the resulting nickelalactone formed is so stable and it does not allow β-hydride elimination to yield acrylic acid (see Scheme 1.12). The β-hydride elimination is strongly endergonic ($\Delta G = +164$ kJ mol^{-1}) and has a high activation barrier. This causes the catalytic cycle to be prematurely halted. To date, the entire catalytic process has never been realised experimentally. However, the catalytic cycle has been taken apart and parts of the cycle have been separately investigated.

DFT calculations from Buntine have shown that ring strain and long bond distance between the nickel centre and the β hydrogen disfavours the transformation of the nickelalactone to an acrylate as the Ni$-$C bond scission of the lactone is not spontaneous (see Scheme 4.1).[133] However, experimental data and theoretical calculations have shown that such a transformation is possible, despite the thermodynamic barrier.

Buntine performed DFT calculations for this coupling reaction at nickel with dbu as ligand. His results show an exothermic and exergonic ($\Delta G = -17.2$ kJ mol^{-1}) formation of the lactone, however, ultimately leading to an overall thermodynamically unfavoured reaction (Scheme 4.1, left). The β hydride elimination goes through a thermodynamically unfavoured transition state of very high energy ($\Delta G = +145.20$ kJ mol^{-1}) due to the ring strain. The reaction from lactone to acrylate also proceeds via a cleavage of the Ni$-$O bond before the β hydrogen can approach
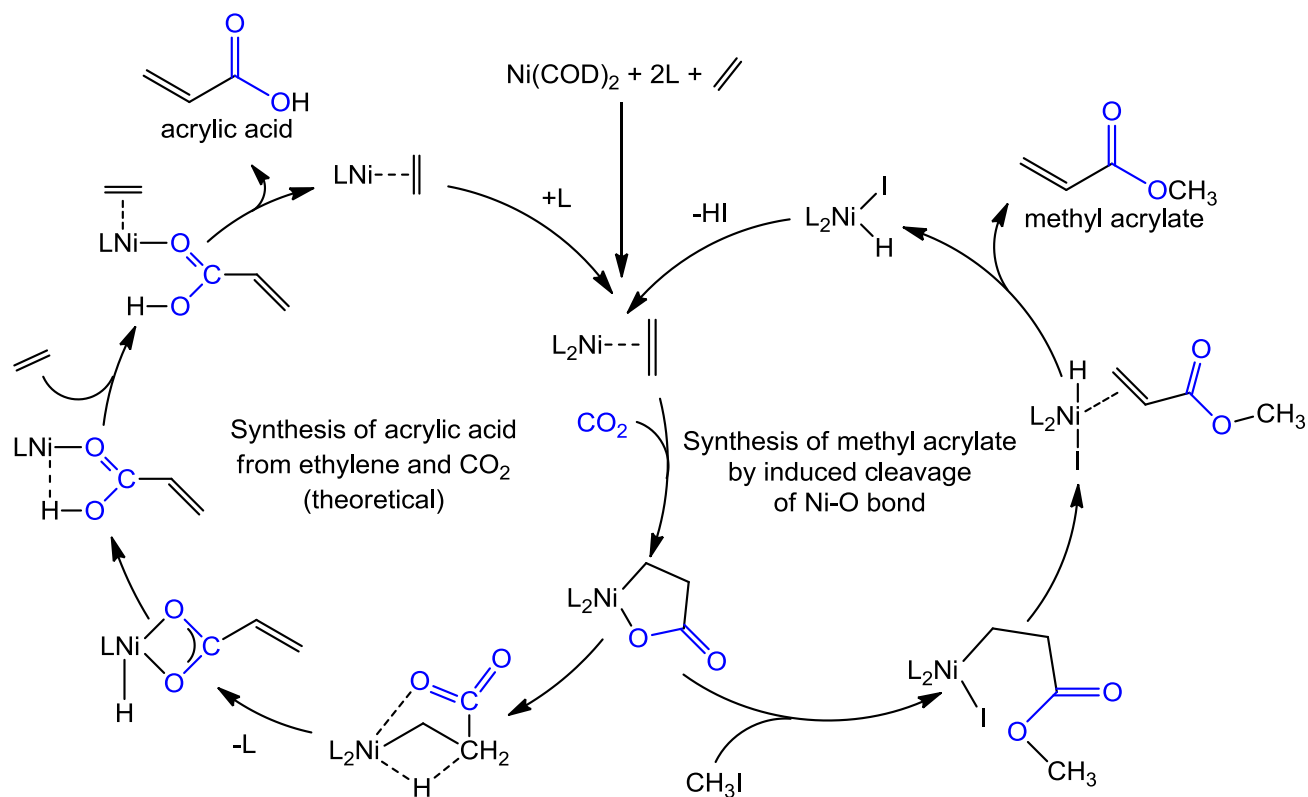
SCHEME 4.1: Left: Hypothetical catalytic cycle for the coupling of CO_2 and ethylene, proposed by Buntine. Right: The synthesis of methyl acrylate by electrophile-induced β-hydride elimination, proposed by Rieger.

the nickel centre to form an intermediate nickel-hydrido-acrylate species before forming acrylic acid. In turn, this nickel-hydrido-acrylate species also needs to reductively eliminate the acrylate and hydride ligands, which is challenging given the high $M-O$ bond dissociation energies of the acrylate intermediates. The DFT studies also suggested that ring opening of the lactone could induce β-hydride elimination. Early experimental studies by Walther[132] and Hoberg[134] have also shown that β-hydride elimination could indeed occur.

With this, the group of Rieger then proposed a methylation step with methyl iodide to induce ring opening of the nickelalactone.[135] While their attempt was valiant, being the first to successfully obtain acrylates from nickelalactones, the reaction remained non-catalytic and the yields are low (maximum 33%).

Quite recently, the group of Limbach reported that Brønsted bases like alcoholates were also capable of releasing acrylates by deprotonating the carbon atom adjacent to the carbonyl group in the lactone.[136] Several catalytic turnovers were obtained but undesired side reactions between the base and CO_2 formed an alcohol byproduct that deactivated the metal species after a few cycles. They also found through computational calculations[137] that the methylation is more likely to occur through an S_N2 mechanism instead of the one-step, concerted methylation proposed by Kühn[138] and Rieger (Scheme 4.2) as the transition state in the latter has a higher Gibbs free energy.
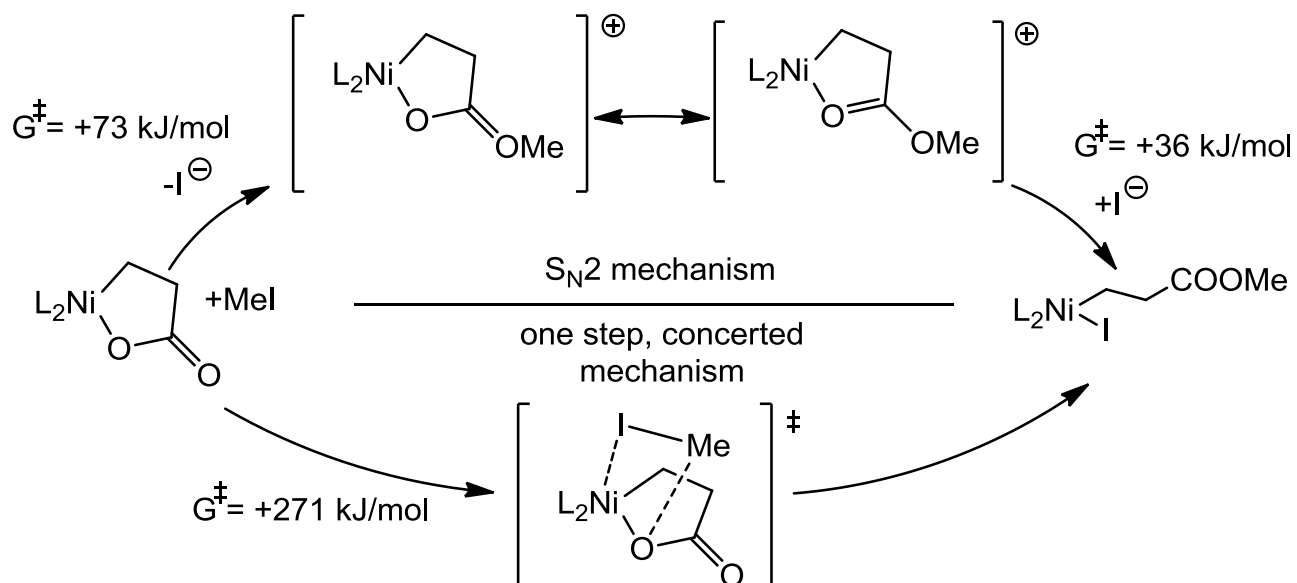
SCHEME 4.2: S_N2 mechanism proposed by Limbach where transition states have lower energies (top). One step, concerted mechanism proposed by Rieger and Kühn (bottom).

As discussed in chapter 3, so far no palladalactones have been synthesized from the coupling of ethylene and CO_2. Therefore, to extend the scope of this study, several palladalactones have been synthesized by "bench" methods. As mentioned in Chapter 2, the study was extended to palladium due to its larger radius, and therefore longer bonds which would ultimately result in a less stable lactone that would be more susceptible towards β-hydride elimination. The reported methylations with methyl iodide have also been shown to have a high thermodynamic barrier as the reactions require large amounts of electrophile (10-100 equiv) and is limited to a small set of ligands. Therefore, other methylation agents were used in this study as well.

4.2 Results and Discussion

A few palladalactones have been reported in literature and shown in Figure 4.1.
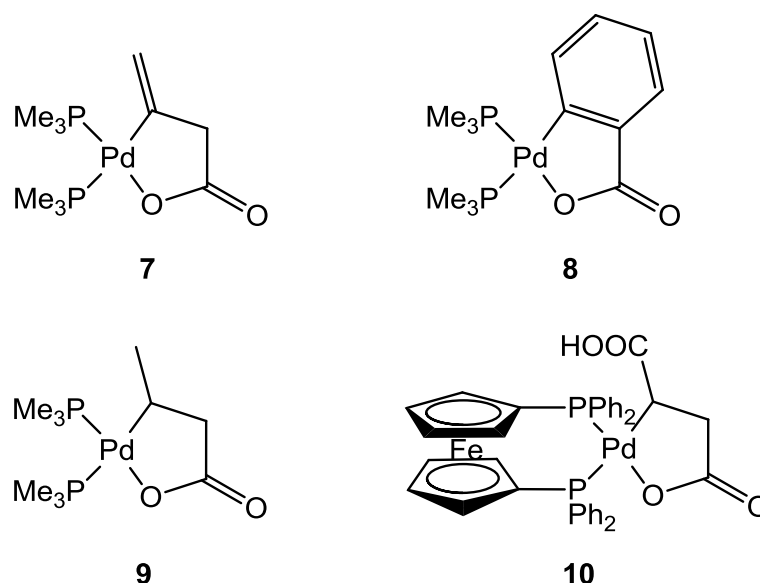
FIGURE 4.1: Palladalactones in literature.

$7^{[139]}$ and $8^{[140]}$ were not suitable for this study due to their inability to undergo β-hydride elimination. Therefore, **9** and **10** were selected as model palladalactones for this study.

The lactones have comparable Pd$-$O bond lengths (**9**: 2.06 Å, **10**: 2.05 Å) and they are longer than typical Ni$-$O bond lengths in the nickelalactones used in this study (1.85-1.89 Å).$^{[138]}$ **9** and **10** differ in the denticity of the phosphine ligands - monodentate PMe$_3$ on **9** and bidentate dppf on **10**. They also both bear substituents on the α-carbon: A methyl group on **9** and a carboxylic acid group on **10**.

4.2.1 Synthesis of Palladalactones
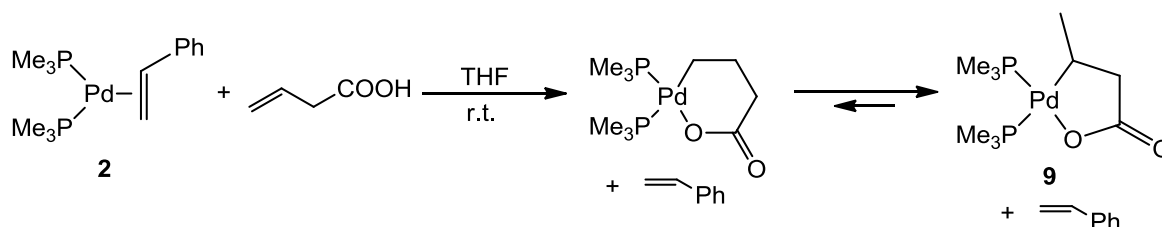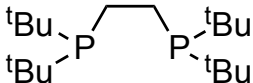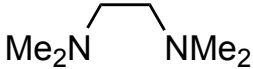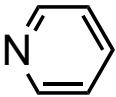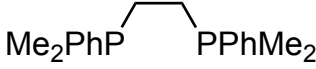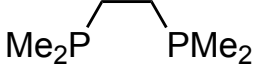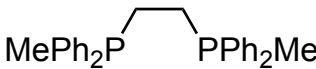
SCHEME 4.3: Synthesis of **9**

9 was synthesized based on modified procedures by Yamamoto.$^{[141,142]}$ Different phosphines were used to synthesize different lactones by the analogous method but were unsuccessful. Lactone **9**, like its precursor, is air and moisture sensitive, but is stable at room temperature.

The reaction of PdEt$_2$(PMe$_3$)$_2$ with styrene gives a coordinatively unsaturated styrene complex which is a suitable precursor for the cyclization with 3-butenoic acid. A six-membered lactone

is initially formed predominantly but it soon undergoes skeletal isomerization to give an equilibrium between the six-membered lactone and the five-membered lactone in a ratio of 5 : 95. Recrystallization affords a pure sample of the desired five-membered lactone.

TABLE 4.1: Different phosphines that were used to diversify complex **2** and lactone **9**.

Phosphines	Dialkylpalladium Complex	Palladalactone
${}^{t}Bu\,{}_{}P\,{}^{t}Bu$ / ${}^{t}Bu\,P\,{}^{t}Bu$ (bridged)	✓	✗
Me_2N ‒ NMe_2	✗	✗
Ph_2P ‒ PPh_2	✗	✗
pyridine (N-ring)	✗	✗
Me_2PhP ‒ $PPhMe_2$	✗	✗
Me_2P ‒ PMe_2	✓	✗
$P{}^{t}Bu_3$	✓	✗
PEt_3	✓	✗
$MePh_2P$ ‒ PPh_2Me	✓	✗

As shown in Table 4.1, the dialkyl palladium complex was obtained for some phosphines but cyclization with 3-butenoic acid to give the lactone did not work for any phosphines other than PMe$_3$.

10 was synthesized according to published procedures by Mukherjee *et al.*[143] In contrast with **9**, lactone **10** is air-stable. The postulated mechanism of formation of **10** is shown in Scheme 4.4. The first step of the mechanism is the coordination of the fumarate to the triflate complex, **A**, which leads to the intermediate **B**, where the double bond is η^2-coordinated to palladium. A hydride from the solvent (methanol) then shifts to the β-carbon and forms an aldehyde *in situ*, **C**. This was qualitatively observed as an orange-yellow precipitate was formed when a solution of 2,4-dinitrophenylhydrazine (standard test for aldehydes) was added drop wise into the reaction mixture. This also suggests that methanol is most likely the hydride source.
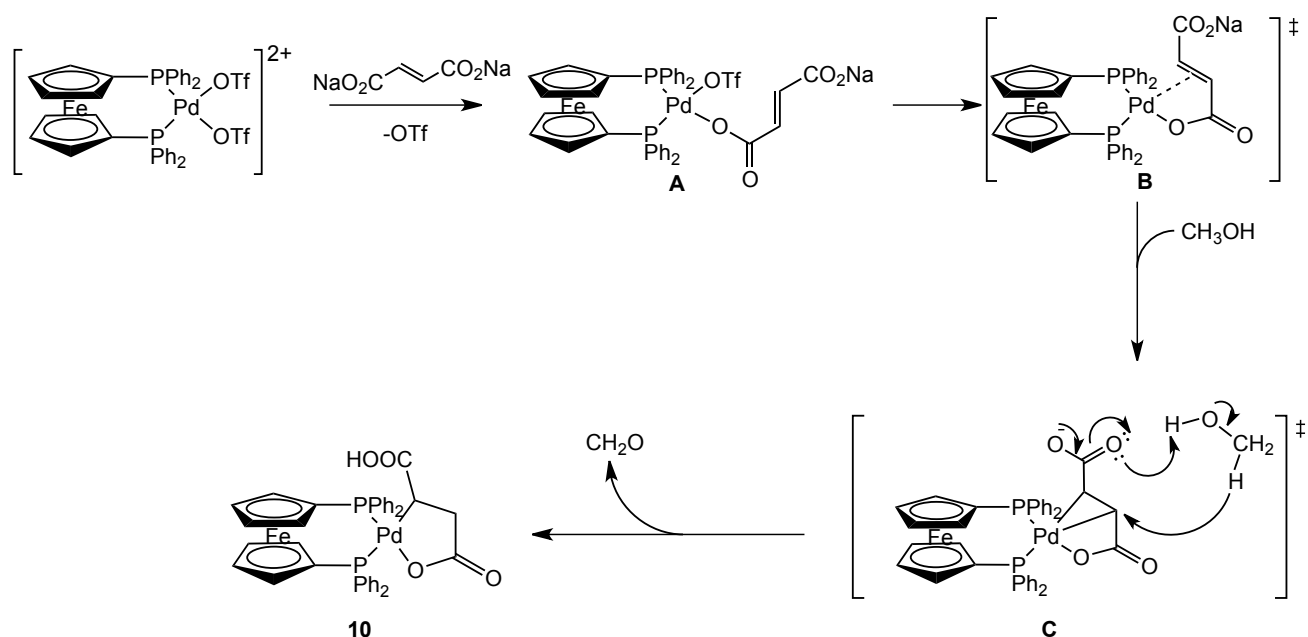
SCHEME 4.4: Proposed mechanism of **10**.

4.2.2 Ring-Opening Reactions with Electrophiles

Prior to this study, an electrophile screening as alternatives to methyl iodide was conducted using the electrophiles shown in Figure 4.2.[144]

The electrophiles ranged from mild and "greener" reactants like dimethyl carbonate , trimethyl phosphate and 2,2-dimethoxypropane to stronger methylating reagents like the Meerwein's reagent analogue - trimethyl oxonium tetrafluoroborate and sulfur containing reagents like methyl triflate and the highly toxic dimethyl sulfate and methyl methanesulfonate. When these electrophiles were used on nickelalactones, the mild reagents and trimethyl oxonium tetrafluoroborate did not show any activity in inducing the cleavage of the Ni-O bond. Methyl triflate showed the most
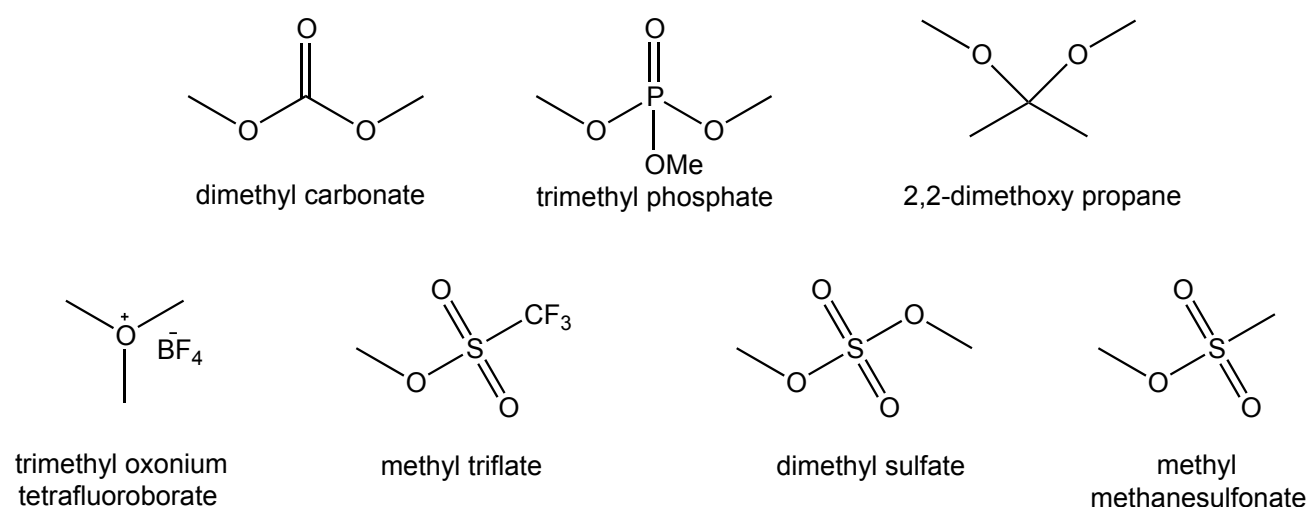
FIGURE 4.2: Electrophiles that were previously screened in an earlier study.

promise while the toxic reagents only showed limited formation of methyl acrylate and were therefore discarded due to their toxicity.

The ring opening of lactone **9** affords either methyl crotonate (**11a**) or 3-butenoic acid methyl ester (**11b**) depending on the initial position of the proton eliminated (**9** has 2 sets of available β-hydrogens that could undergo elimination). This was interestingly observed when MeI was used. However, when MeOTf was used, **11a** was obtained selectively. The ring opening of lactone **10** affords only dimethyl fumarate, **12**.
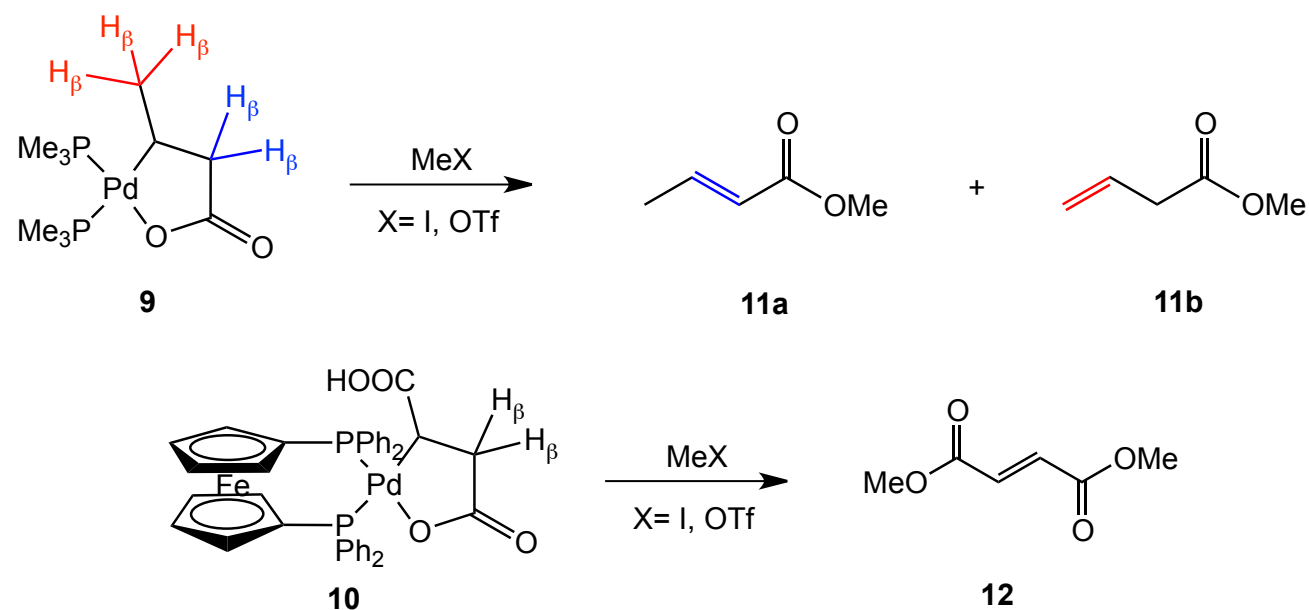
SCHEME 4.5: Products of ring opening by methyl iodide and methyl triflate.

The ring opening reactions were conducted in NMR-scaled experiments. 0.1 mmol of the lactones **9** and **10** were dissolved in 0.5 mL CDCl$_3$ and DMSO-d_6 respectively. CH$_2$Cl$_2$ (for **9**) and CHCl$_3$ (for **10**) were also added as internal standard in addition to the methylating agent. The conversion was then obtained by integrating the peaks found in the NMR spectrum. The results are summarized in Table 4.2.

TABLE 4.2: Yield of **11** and **12** formed by the ring opening of palladalactones **9** and **10** respectively

Entry	Palladalactone	MeX	MeX equiv.	Time (h)	Conv. (**11a, 11b**) (%)
1	**9**	MeI	10	3	22 (14, 8)
2	**9**		100	3	69 (54, 15)
3	**10**		2	24	–
4	**10**		10	24	10
5	**9**	MeOTf	1	0.5	23
6	**9**		1	3	23
7	**9**		1	24	23
8	**9**		10	24	20
9	**10**		2	0.5	39
10	**10**		2	24	45
11	**10**		10	0.5	35
12	**10**		10	24	45

For lactone **9**, the formation of methyl crotonate (**11a**, CAS 623-43-8) in $CDCl_3$ showed the appearance of vinylic protons at 6.96 ppm (m, 1H) and at 5.83 ppm (m, 1H) and methyl ester protons at 3.65 ppm (s, 3H). (Figure 4.3, Figure 4.4) The formation of 3-butenoic acid methyl ester (**11b**, CAS 3724-55-8), showed peaks of vinylic protons at 5.89 ppm (m, 1H) and 5.09 ppm (m, 2H). The methylene protons were observed at 3.05 ppm (d, 2H) (Figure 4.3, Figure 4.4). For lactone **10**, the formation of dimethyl fumarate **12** in DMSO-d_6 (6.67 ppm, s, 2H) was proved by comparison with a pure sample in DMSO-d_6 (Figure 4.5).
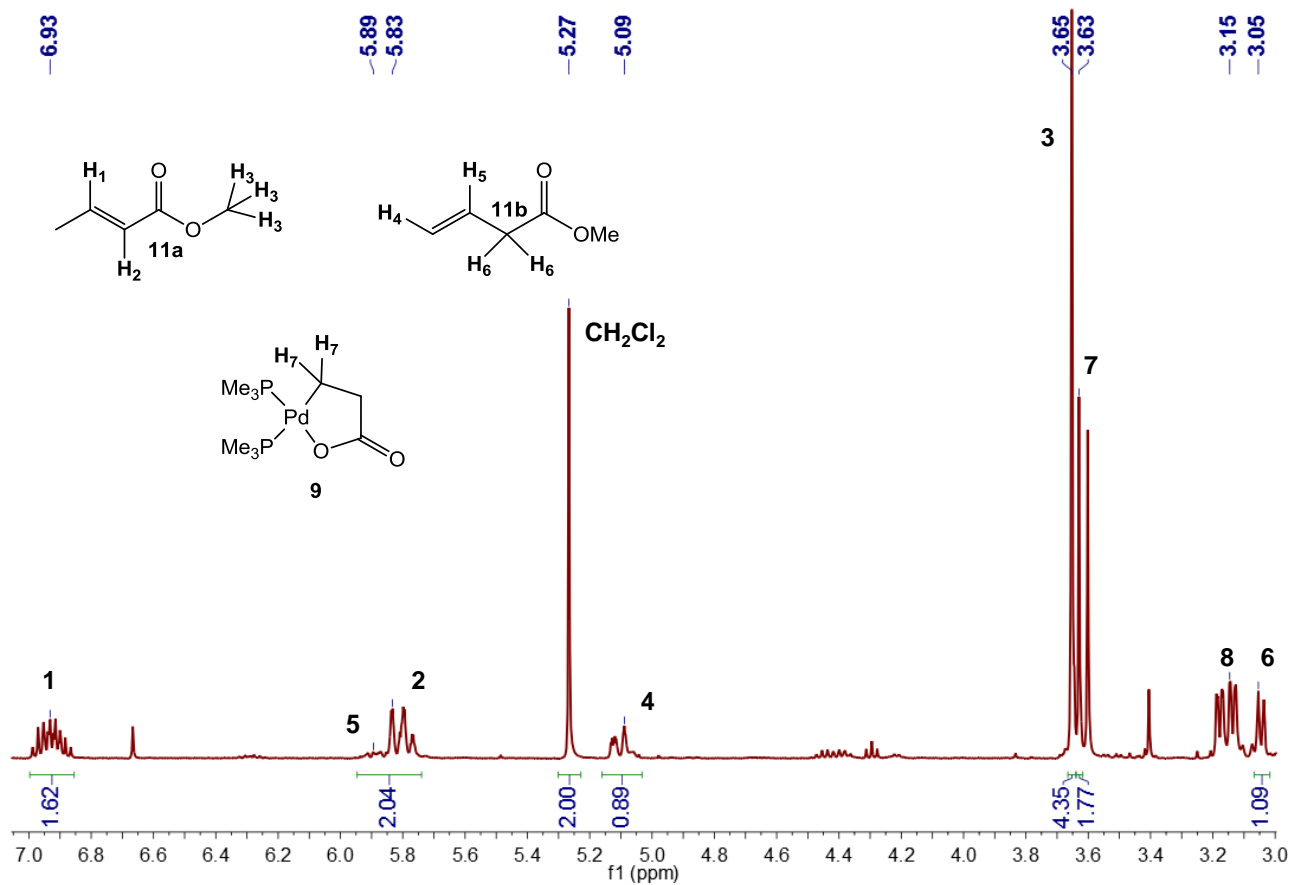
FIGURE 4.3: Proton NMR spectrum of the reaction between **9** and MeI (100 equiv. MeI, 3 h in CDCl$_3$ with CH$_2$Cl$_2$ as internal standard). The concentration of the standard is $\frac{1}{3}$ of the initial concentration of **9** to give **11a** and **11b**. Yield of **11a** $= \frac{1.62}{3} = 54\%$, Yield of **11b** $= \frac{0.89}{3\times 2} = 15\%$
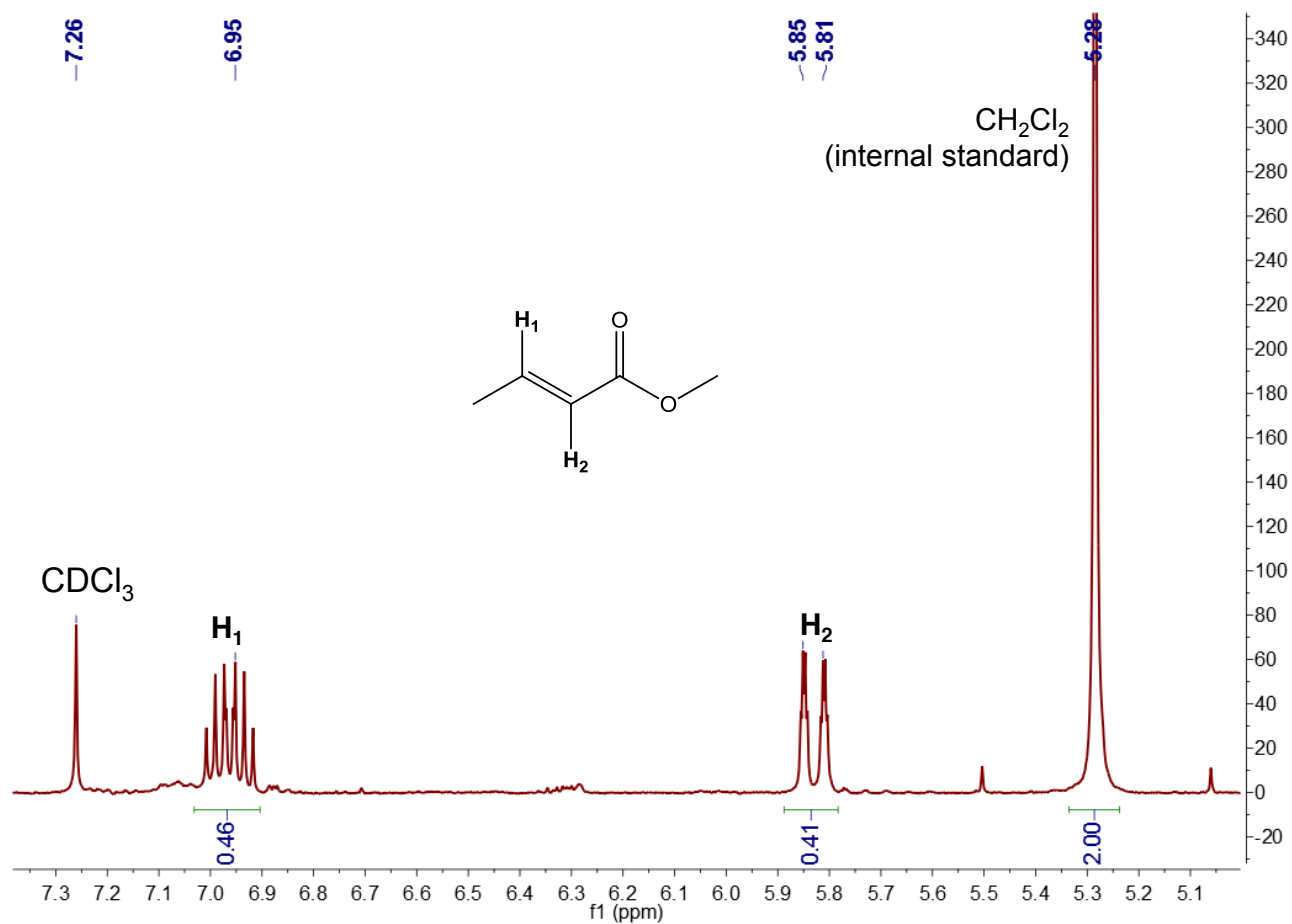
FIGURE 4.4: Proton NMR spectrum of the reaction between **9** and MeOTf (10 equiv. MeOTf, 3 h in $CDCl_3$ with CH_2Cl_2 as internal standard). The concentration of the standard is $\frac{1}{2}$ of the initial concentration of **9** to give **11a** selectively. Yield of $\mathbf{11a} = \frac{0.46}{2} = 23\%$
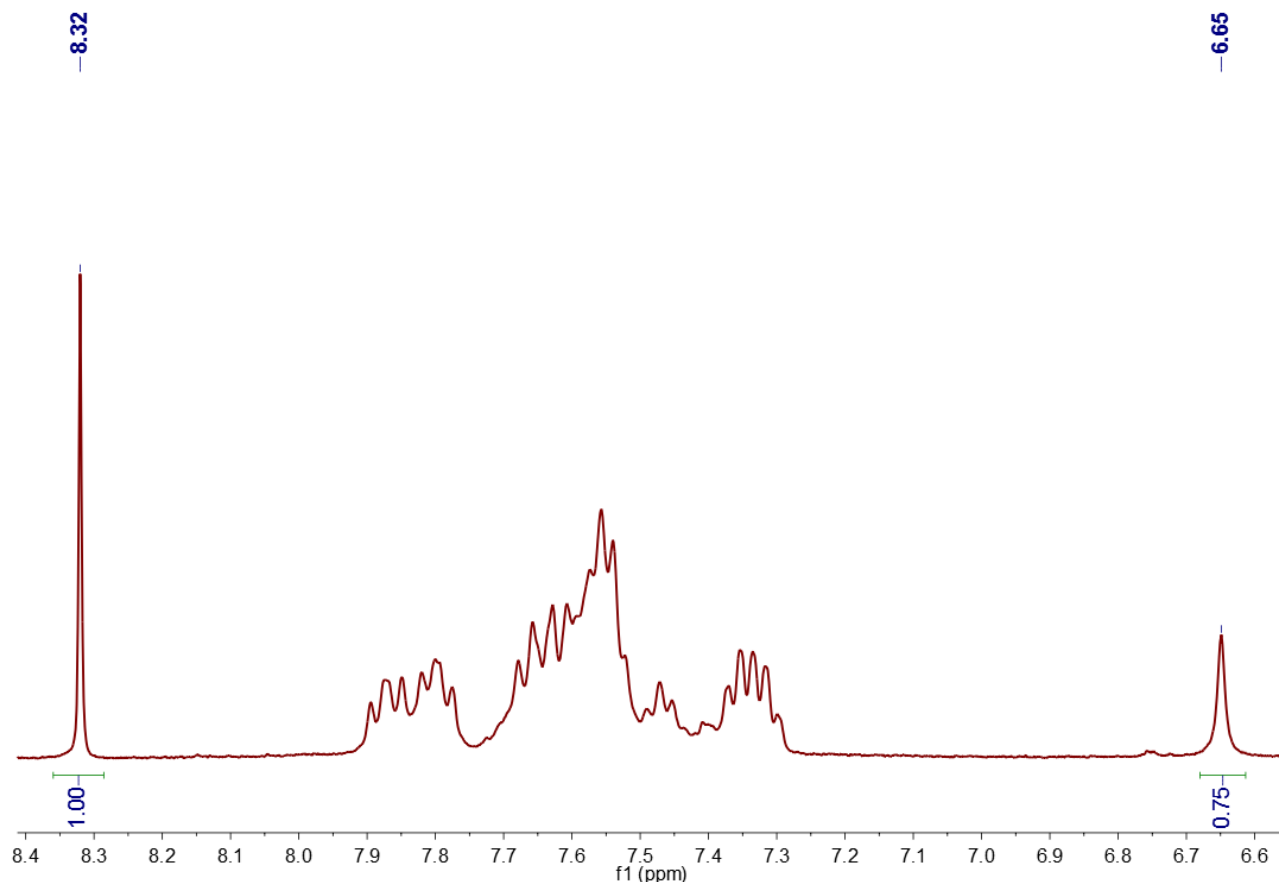
FIGURE 4.5: Proton NMR spectrum of the reaction between **10** and MeOTf (2 equiv. MeOTf, 15 min in DMSO-d_6 with CH_3Cl as internal standard). The concentration of the standard is equimolar to the initial concentration of **10** to give **12**. Yield of **12** $= \frac{0.75}{2} = 37.5\%$

When lactone **9** was reacted with 10-100 equivalents of methyl iodide, the peaks corresponding to **9** were observed to progressively disappear, yielding **11a** and **11b**. A combined conversion of 69% was obtained after 3 hours with 100 equivalents of methyl iodide (Table 4.2, entry 2). The yield of methyl crotonate, however, started to decline after 3 hours as a more complex mixture of organic compounds was formed.

In situ monitoring of the reaction mixture by NMR spectroscopy shows that the palladalactone is almost immediately converted upon addition of methyl triflate and most of the methyl triflate is consumed while new signals appear in the methyl ester region. Figure 4.6 shows an NMR spectrum of a reaction with methyl triflate after only 15 minutes. The peaks corresponding to the starting lactone are already diminished, indicating a rapid reaction. Results also suggest that an equilibrium between the ester product **11a** and the lactone **9** is readily reached (Table 4.2, entries 5-7) when methyl triflate was used as methylating reagent. In addition, product **11a** is selectively formed when methyl triflate was used to open the ring in lactone **9** (Table 4.2, entries 5-7). Increasing the amount of methyl triflate did not affect the yield of the ester (Table 4.2, entry 8).
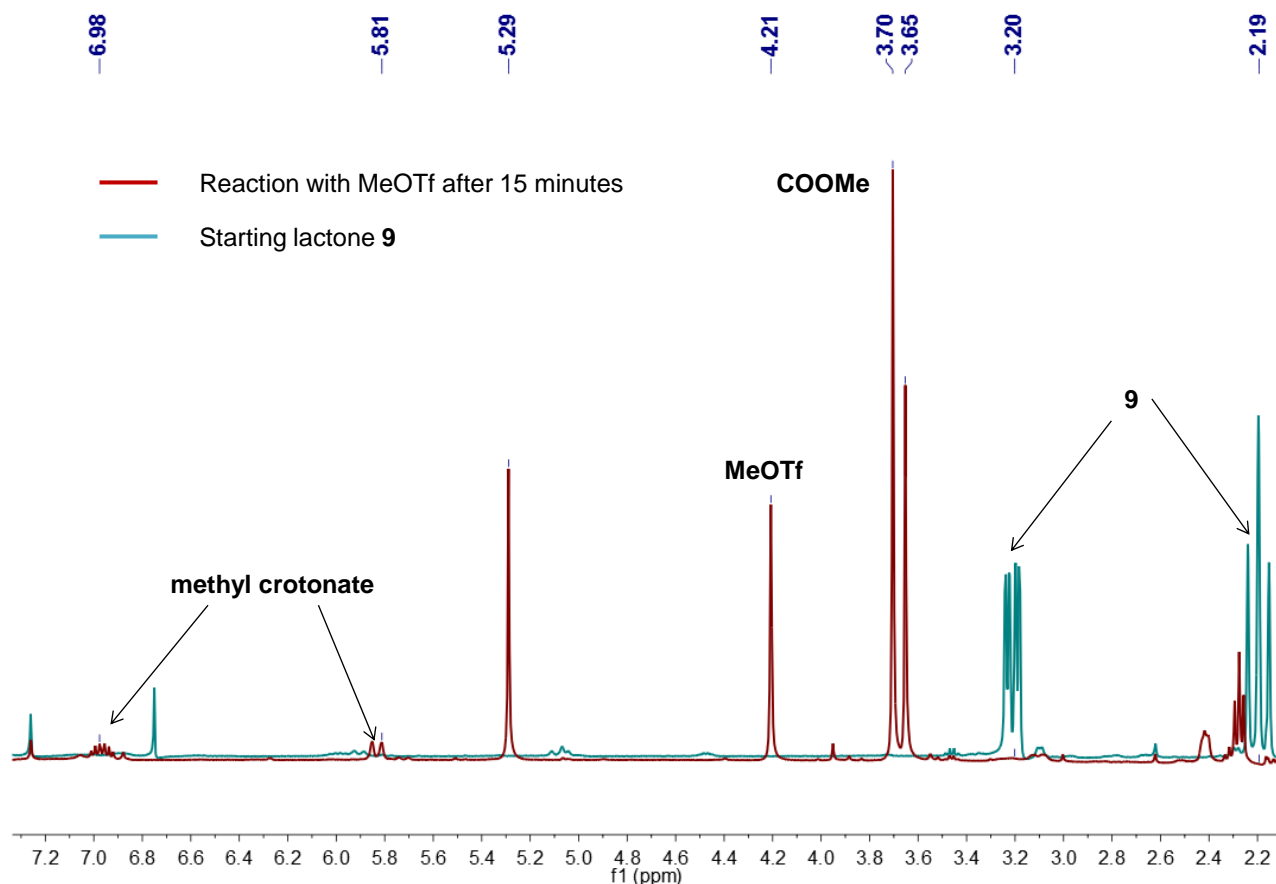
FIGURE 4.6: Proton NMR spectrum of the reaction between MeOTf (1 equiv.) and **9** after 15 min in CDCl$_3$. The signals corresponding to the starting material (blue) disappear to form methyl crotonate and new signals in the methyl ester region as expected upon ring opening of the lactone. The residual peak of the unreacted MeOTf is seen at 4.21 ppm.

For lactone **10**, at least 2 equivalents of electrophile had to be used to account for esterification at the carboxylic acid moiety. 2 and 10 equivalents of electrophile were used but when 100 equivalents of either electrophile were added, the lactone immediately decomposed to palladium black. While methyl iodide proved to be almost ineffective in the ring opening of the lactone (Table 4.2, entries 3 and 4), 2 equivalents of methyl triflate provided moderate yields of **12** within 30 minutes, with the reaction rapidly reaching a plateau (Table 4.2, entries 9 and 10). Similar to the observation for lactone **9**, increasing the amount of electrophile did not lead to an improvement in the conversion values of lactone **10** (Table 4.2, entries 11 and 12).

4.2.3   Comparison with Nickelalactones

A major motivation for this study was to determine if palladalactones were more susceptible to β-hydride elimination as compared to nickelalactones. Ring opening reactions on nickelalactones were carried out in an earlier study.[138,144] The conditions used for the ring opening studies of

nickelalactone are similar to that of those used for palladalactones. The nickelalactones that were investigated are shown in Figure 4.7.
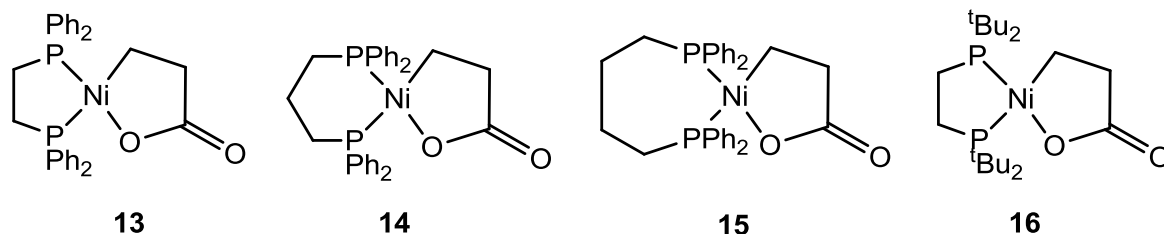
FIGURE 4.7: Nickelalactones flanked with phosphine ligands used in an earlier study.

TABLE 4.3: Comparing conversions obtained with 100 equiv. MeI as methylating agent with pallada- and nickelalactones bearing phosphine ligands.

Entry	Lactone	Temp. (°C)	Time (h)	Conv. (%)
1	**9**	25	3	69
2	**13**	25	24	48
3	**14**	40	48	29
4	**15**	25	24	0
5	**16**	25	24	0

Comparing palladalactone **9** with nickelalactones **13**-**16** that also had phosphine ligands, **9** proved to be more susceptible in undergoing ring opening by methyl iodide and β-hydride elimination as a higher yield of 69% was obtained in a much shorter time of 3 hours (Table 4.3, entry 1). For nickelalactones, they gave lower or no conversions even with a longer reaction period (Table 4.3, entries 2-5).

Both lactones also exhibited similar activities when methyl triflate was used. In both cases, reaction with methyl triflate was quick and almost immediate. A plateau of conversion was also reached. Increasing the loading of methyl triflate did not affect the conversion values for both metallalactones. However, when a large excess of methyl triflate was used, decomposition of the metallalactones to Ni(0) or Pd(0) was observed for both lactones.

4.3 Experimental

4.3.1 General Information and Materials

All air sensitive manipulations were performed in an inert argon atmosphere using Schlenk techniques or a glovebox. Glassware was washed in an isopropanol/KOH base bath followed by

a dilute hydrochloric acid bath and then deionised water. All glassware were dried overnight in a 120°C oven and flame dried *in vacuo* at 350°C before use.

Chemicals

Triethylaluminum solution (1.3 M in hexanes), 1,5-cyclooctadiene (99%), palladium (0) tetrakistriphenylphosphine (99%), styrene (99%), tricyclohexylphosphine, trimethylphosphine solution (1 M in THF), 1,2-bis(diphenylphosphino)ethane (dppe), N,N,N',N'-tetramethane-1,2-diamine (tmeda), triethylphosphine (99%), methyldiphenylphosphine (97%), dimethylphenylphosphine (99%), tri-tert-butylphosphine (99%), 1,2-Bis(dimethyl-phosphino)ethane, pyridine, dppf, and tri(o-tolyl)phosphine (97%) were purchased from Sigma Aldrich and used without further purification. Palladium (II) acetylacetonate (99%) was purchased from Acros Organics and also used as received. 3-butenoic acid was distilled before use to remove the hydroquinone inhibitor. 1, 2-bis (di-tert-butylphosphino) ethane was synthesized according to published procedures. [145]

Solvents

Hexane, pentane, dichloromethane, diethylether and toluene were purified over activated alumina. THF was dried with sodium wires, methanol and ethanol with CaH_2 and acetone over $CaSO_4$, refluxed and distilled. The solvents were also degassed by the freeze-pump-thaw method and stored over 3 Å or 4 Å molecular sieves. The water content of the solvents (except acetone) were regularly analysed by a Karl-Fischer titrator. All deuterated solvents were also dried in the usual manner, distilled under reduced pressure, degassed and stored over 3 Å or 4 Å molecular sieves in the glovebox.

4.3.2 Instruments

NMR measurements were performed on a Bruker AVANCE 400 and 500 MHz spectrometers. ^1H and ^{13}C chemical shifts were referenced to residual solvent resonances ($CDCl_3$: 7.26 ppm, CD_2Cl_2: 5.26 ppm, $(CD_3)_2SO$: 2.50 ppm).

4.3.3 Synthesis of Palladalactones 9 and 10

Synthesis of 9[141]: $PdEt_2(PMe_3)_2$ (1.2 g, 3.78 mmol) was weighed into a Schlenk under an inert atmosphere. It was dissolved in acetone (10 mL) and styrene (1.73 mL, 15.1 mmol) was added. The reaction was left to stir for 6 hours at 35°C and volatiles were removed. The solid was then redissolved in THF (10 mL) at room temperature and 3-butenoic acid (0.353 mL, 4.17

mmol) was added. The reaction was stirred for 24h. Upon completion of reaction, the solution was concentrated and diethyl ether was added to recrystallise the lactone at -20°C. Yield=56%

^{1}H NMR (CDCl$_3$, 25°C, 400MHz): δ (ppm) 3.24 (dd, 1 H), 2.20 (t, 1 H), 1.66 (m, 1 H), 1.45 (dd, 18 H), 1.24 (m, 3 H)
^{31}P NMR (CDCl$_3$, 25°C, 100MHz): δ (ppm) -8.61, -23.24

Synthesis of Pd(dppf)Cl$_2$[146]: Pd(COD)Cl$_2$ (0.5 g, 1.75 mmol) was suspended in benzene (10 mL). Dppf (0.97 g, 17.5 mmol) was stirred in benzene (10 mL) in a separate flask until all solids were dissolved. The solution was then transferred to the flask with Pd(COD)Cl$_2$ by cannular. Reaction was left to stir for 12 hours before filtering by cannular. The solid obtained was dried *in vacuo*. The solid was then dissolved in dichloromethane, toluene and methanol in the ratio of 2:1:1 for recrystallization. The flask was placed in the freezer for 4 days before a dark red crystal was obtained. Yield=68.7%. Anal. Calcd: C= 51.48; H= 3.70. Found: C= 51.48; H= 3.73.

Synthesis of [Pd(dppf)(H$_2$O)$_2$](OTf)$_2$[147]: Pd(dppf)Cl$_2$ (0.3 g, 0.367 mmol) was weighed and stirred in dichloromethane (30 mL) until all solids were dissolved. The solution was then transferred into a schlenk flask with AgOTf (0.283 g, 1.10 mmol) by cannular. The mixture was stirred for 18 hours. The reaction mixture was then filtered to remove the precipitated AgCl. The resulting green solution was stirred in air for 15 minutes and concentrated to about 2 mL. Ether was then added to precipitate the final product. Yield=76.9%. Anal. Calcd: C= 43.46; H= 3.24; S= 6.45. Found: C= 43.20; H= 3.27; S= 6.52.

^{1}H NMR (CD$_2$Cl$_2$, 25°C, 400MHz): δ (ppm) 7.83 (m, 8 H), 7.69 (m, 4 H), 7.53 (m, 8 H), 4.66 (s, 4 H), 4.62 (s, 4 H).
^{13}C NMR (CD$_2$Cl$_2$, 10°C, 100MHz): δ (ppm) 134.7, 133.8, 129.9, 128.4, 127.8, 78.7, 76.5, 69.5, 66.2.
^{31}P NMR (CD$_2$Cl$_2$, 25°C, 100MHz): δ (ppm) 51.1

Synthesis of sodium fumarate: Fumaric acid (1 g, 8.62 mmol) was stirred in a solution of NaOMe (3.2 mL, 30% solution of NaOH in MeOH) for 2 hours. Volatiles were removed to afford pure disodium fumarate as a white solid.

Synthesis of 10[143]: [Pd(dppf)(H$_2$O)$_2$](OTf)$_2$ (0.021 g, 0.0211 mmol) and disodium fumarate (3.376 mg, 0.0211 mmol) were weighed and separately dissolved in MeOH (5 mL). The mixture was stirred at room temperature for 4 hours. Volatiles were then removed *in vacuo*, yielding a yellow solid. Yield=93%. Anal. Calcd: C= 58.75; H= 4.15. Found: C= 58.66, H= 4.22.

^{1}H NMR (CDCl$_3$, 25°C, 400MHz): δ (ppm) 7.80-7.25 (m, 20 H), 4.66-3.31 (m, 10 H), 3.42 (s, 2 H), 3.25 (t, 1 H)
^{31}P NMR (CDCl$_3$, 25°C, 100MHz): δ (ppm) 35.53, 18.19

4.3.4 Ring Opening Reactions with MeX and Palladalactones

9 (34.4 mg, 0.1 mmol) was dissolved in $CDCl_3$. An equimolar amount of CH_2Cl_2 (6.38 μL, 0.1 mmol) was added as internal standard. 1, 10 or 100 equivalents of MeI or MeOTf were then added and the NMR spectrum was measured at 5 minutes, 15 minutes, 30 minutes, 1 hour, 3 hours, 6 hours, 24 hours and 48 hours. The conversion was then obtained by integrating the peaks found in the NMR spectrum.

10 (77.6 mg, 0.1 mmol) was dissolved in DMSO-d_6. An equimolar amount of $CHCl_3$ (8.07 μL, 0.1 mmol) was added as internal standard. 1, 10 or 100 equivalents of MeI or MeOTf were then added and the NMR spectrum was measured at 5 minutes, 15 minutes, 30 minutes, 1 hour, 3 hours, 6 hours, 24 hours and 48 hours. The conversion was then obtained by integrating the peaks found in the NMR spectrum.

4.4 Conclusion

The liberation of esters from palladalactones have been examined. It has been shown that methyl iodide and methyl triflate are able to cleave the Pd-O bond in palladalactones to afford linear esters. Methyl triflate proved to be a better choice, based on atom economy and reaction rates. For lactone **9**, methyl triflate selectively forms methyl crotonate instead of giving a mixture of compounds like methyl iodide.

A similar trend was also observed for both nickela- and palladalactones with methyl triflate as electrophile. The reaction with methyl triflate occurred rapidly, quickly reaching an equilibrium. Increasing the dosage of methyl triflate did not have a positive impact on the final conversion to the ester in both nickela- and palladalactones. A large excess of methyl triflate led to decomposition of the lactone to Ni(0) or Pd(0).

Comparing the results of an analogous study with nickelalactones, it is observed that palladalactones indeed undergo β-hydride elimination more readily than the nickelalactones. This affirmed the initial rationale of extending the study to palladalactones - that they were less stable than their nickel counterparts and would be more susceptible to β-hydride elimination.

A smaller excess of electrophile was also used for the ring opening reaction, which improved the reported ring opening methods of using a large excess of methyl iodide (100 equiv.)[138] or alcoholates (side reactions)[136].

The ability to extend the study to palladium from nickel also shows that this approach is general and can be further extended to other metals. This would be of high interest if the metallacycle could be obtained from the oxidative coupling of ethylene and CO_2 as it could potentially lead to a wide range of possibilities for the study of the catalytic cycle shown in Scheme 4.6.
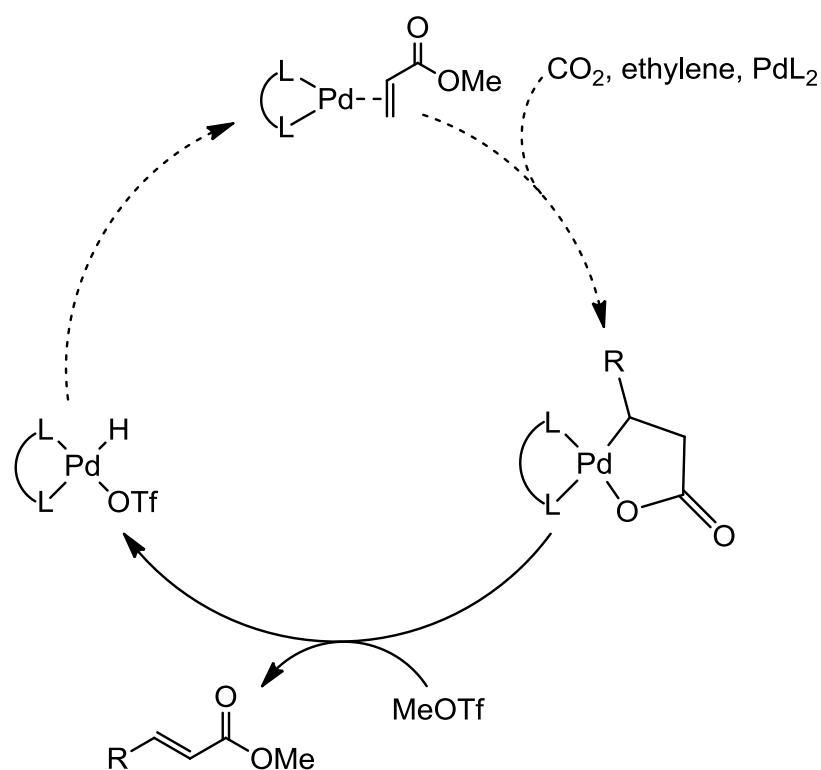
SCHEME 4.6: A potentially viable catalytic cycle for the synthesis of acrylates from carbon dioxide, ethylene and a palladium starting complex. Dashed arrows refer to steps that have not yet been established.

This work was published as part of the article: S. Y. Tina Lee, Amylia Abdul Ghani, Valerio D'Elia, Mirza Cokoja, Wolfgang A. Herrmann, Jean-Marie Basset and Fritz E. Kühn, "Liberation of methyl acrylate from metallalactone complexes via M–O ring opening (M = Ni, Pd) with methylation agents.", *New J. Chem.*, **2013**, *37*, 3512. **DOI**: 10.1039/CNJ00693J

Chapter 5

The Synergy of Catalyst and Co-Catalyst in the Synthesis of Propylene Carbonate from Propylene Oxide and Carbon Dioxide

5.1 Introduction

The reaction of epoxides and CO_2 to form cyclic carbonates have been of increasing interest in catalysis research. As discussed in Section 1.4.2, cyclic carbonates are very relevant compounds and have vast uses in industry. The reaction is 100% atom economical[148] but is not spontaneous, requiring a catalyst to activate CO_2, the epoxide or both. The reaction is also highly exothermic as ring strain of the epoxide is relieved when converting the three-membered epoxide ring to a five-membered ring of the cyclic carbonate.[149]
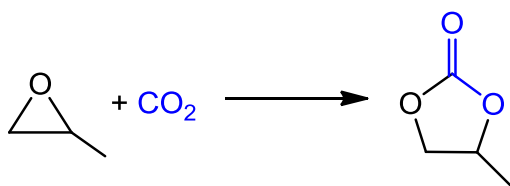
SCHEME 5.1: The reaction between propylene oxide and carbon dioxide to form propylene carbonate.

For the synthesis of propylene carbonate from propylene oxide and carbon dioxide, the ΔH was calculated to be -74.50 kJ mol^{-1} (Value calculated from standard ΔH_f values found in literature).[150–152] It is therefore crucial to understand and control the many parameters determining the selectivity of the reaction when designing a catalyst to efficiently produce cyclic carbonates.

Catalytic activities could also be improved from known, promising catalysts to reach higher turnover frequencies under mild temperature and pressure conditions.

5.1.1   Choice of Catalyst and Co-Catalyst for this Study

The different factors (metal centre, substrate, catalyst, co-catalyst) discussed in Section 1.4.2 have shown that many considerations have to be taken into account when selecting the different components of this reaction. There is a specific balance that has to be achieved between catalyst, co-catalyst and substrate to attain the desired selectivity. Table 5.1 summarizes some catalyst/co-catalysts systems with propylene oxide, showing the yield of propylene carbonate obtained and the different reaction conditions.

It is observed that high pressures and elevated temperatures are needed in these systems. The catalysts are also sophisticated, using salen ligands or substituted imidazolium rings. Some catalyst systems also combine metal halides with nucleophillic co-catalysts but only afforded moderate yields.

Through an initial screening of group 4-6 transition metal halides and oxychlorides with a standard nucleophile as co-catalyst, it was revealed that $NbCl_5$/DMAP and $NbCl_5$/TBAB pairs formed very efficient catalyst systems.[114] Not only are they inexpensive, the latter was also active at ambient conditions and was able to promote the formation of propylene carbonate in high yields with excellent TOFs when compared to catalyst systems with sophisticated organometallic complexes. It also performed well when the CO_2 concentration was low at 12% in a gas mixture, which is approximately the concentration of CO_2 in flue gas.[161]

Mechanistic studies on the fine dynamics of the catalyst/co-catalyst relationship are also few in literature and was therefore the driving force for this study.

For the cycloaddition of CO_2 and propylene oxide, a simplified mechanism has been proposed and can be represented by a succession of three steps. The epoxide ring is first opened by the nucleophillic attack of the co-catalyst (**A**), followed by CO_2 insertion (**B**) and finally the release of the carbonate product from the metal centre (**C**) (Scheme 5.2, right). An alternate mechanism that involves CO_2 activation by the nucleophillic species has also been proposed but at high CO_2 pressures (Scheme 5.2, left).

5.2   Results and Discussion

The detailed mechanism of the synthesis of propylene carbonate with $NbCl_5$ as catalyst and DMAP, TBAB and several ionic liquids as co-catalyst will be discussed in this section. The

TABLE 5.1: Different catalytic systems for the synthesis of propylene carbonates from CO_2 and propylene oxide.

Catalyst + Co-Catalyst	CO_2 Pressure (bar)	Temp. (°C)	Time (h)	TON	TOF (h^{-1})	Yield (%)
$Al(CH_2CH_3)_3 + H_2O +$ acac	50	20	18	-	-	10.57[153]
$Zn(CH_2CH_3)_2 + H_2O$ (1:1)	50	20	48	-	-	13.36[153]
Chiral(salen)Co + 1-ethyl-3-methyl imidazoliumbromide	5	25	3	-	144	43.2[154]
$Cr(III)(salen)azide +$ PCy_3	35	60	4	-	149	94[155]
$Cr(III)(salen)azide +$ $PPN^+N_3^-$	35	60	4	-	190	98[155]
$Cr(III)(salen)azide +$ PPN^+Cl^-	35	60	4	-	192	97[155]
$TiCl_4/n-Bu_4NOAc$	10-15	35	3	-	-	28[156]
$ZrCl_4/n-Bu_4NOAc$	10-15	35	3	-	-	8[156]
$NiCl_2/n-Bu_4NOAc$	10-15	35	3	-	-	3[156]
$NiBr_2/n-Bu_4NOAc$	10-15	35	3	-	-	11[156]
$CrCl_3/n-Bu_4NOAc$	10-15	35	3	-	-	30[156]
$FeCl_3/n-Bu_4NOAc$	10-15	35	3	-	-	39[156]
$AlCl_3/n-Bu_4NOAc$	10-15	35	3	-	-	53[156]
$VCl_3/n-Bu_4NOAc$	10-15	35	3	-	-	50[156]
$ZnBr_2/n-Bu_4NOAc$	10-15	35	3	-	-	19[156]
$MoCl_5/n-Bu_4NOAc$	10-15	35	3	-	-	4[156]
$Al(III)(salen)C_2H_5 +$ TBAB	6	35	-	-	84	72[157]
$Al(III)(salen)C_2H_5 +$ N-N'-disubstituted imidazol(in)ium carboxylates	20	100	-	-	50	65[158]
$Co(III)(salen)O_2CCCl_3$ + TBAB	15	25	-	-	245	56[159]
$Co(III)(salen)Cl +$ DMAP	10	100	-	-	1200	67[160]

reaction mechanism has been elucidated by a comprehensive approach through kinetic analysis and *in situ* IR spectroscopy. The studies show the synergistic relationship between catalyst and co-catalyst in promoting the cycloaddition of CO_2 to propylene oxide, forming propylene carbonate. The high Lewis acidity and oxophilicity of the niobium center have also been found to bring distinctive mechanistic features.
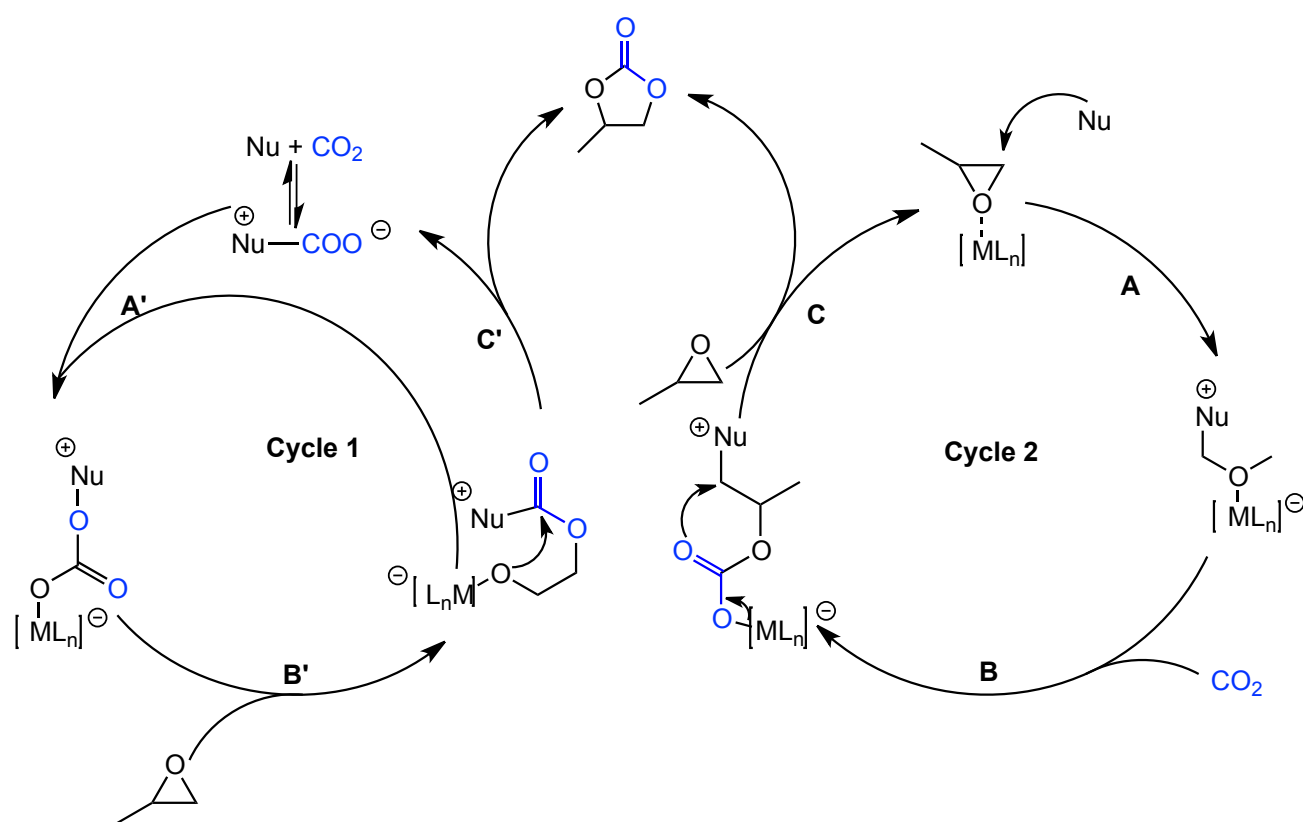
SCHEME 5.2: Simplified mechanism for the cycloaddition of CO_2 and propylene oxide. Cycloaddition occurs first by the coordination of CO_2 with the co-catalyst (Cycle 1) or the opening of the epoxide ring by the co-catalyst (Cycle 2).

N, N-dimethyl-4-aminopyridine (DMAP)

tetra-*n*-butylammonium bromide (TBAB)

17   **18**   **19**   **20**
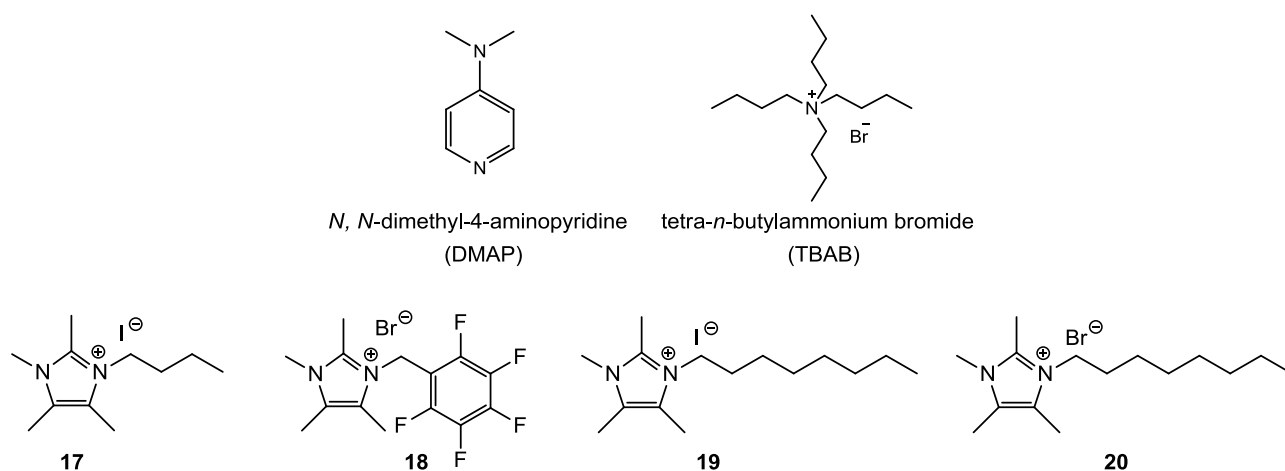
FIGURE 5.1: Co-catalysts used in this study: DMAP, TBAB and ionic liquids **17**-**20**.

5.2.1   Comparing Co-Catalysts

DMAP and TBAB can convert a variety of epoxides into their corresponding carbonates at room temperature and at low CO_2 pressure (0.15-1.00 bar) and concentration. The $NbCl_5$ and TBAB system was generally faster but $NbCl_5$ and DMAP were a convenient pair as they could be easily recovered at the end of the reaction by filtration to give pure propylene carbonate.

A notable difference between TBAB and DMAP as co-catalyst that has been previously found was that there is an induction time of 90 minutes before propylene carbonate is formed when DMAP was used. [114] The reaction with TBAB, however, proceeded almost immediately without an induction time. The induction time is attributed to the formation of an acid-base intermediate, **21** between $NbCl_5$ and DMAP that does not occur for TBAB (see Scheme 5.3). This could be due to the lower basicity of the bromide anion in TBAB which hinders the formation of such stable intermediates. The formation of **22** also shows that the mechanism of this reaction probably follows cycle 2 of Scheme 5.2.
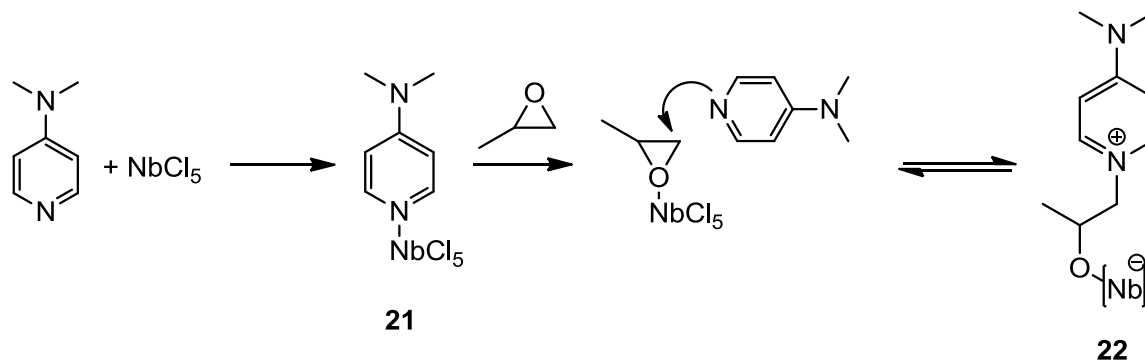
SCHEME 5.3: Intermediates formed upon mixing of $NbCl_5$ and DMAP. Both are observed in *in situ* IR, where only **22** and free DMAP are present after 90 minutes.

In addition to these co-catalysts, a series of ionic liquids were also used. The ionic liquids are methylated imidazolium salts with different alkyl groups substituted on the ring. The stabilizing anion used also varied from bromide to iodide.

A solution with a $NbCl_5$ to co-catalyst ratio of 0.5 was prepared in propylene oxide and 1 or 4 bar of CO_2 was introduced. The reaction was monitored by *in situ* IR spectroscopy and the evolution of the band at 1810 cm^{-1}, corresponding to propylene carbonate was followed. The reaction was carried out over 6 hours. The first 15 minutes of data was extrapolated and the gradient of the line was taken as the initial apparent rate, k_{obs}.

The initial rates and observed yields by NMR are tabulated in Table 5.2 and were compared to that of TBAB.

Ionic liquids **19** and **20** exhibited higher initial rates than **17** and **18** therefore the experiments were repeated over a shorter period of time (1 hour) at 4 bar CO_2 pressure for **19**, **20** and TBAB. The yields and TOFs were tabulated (Table 5.3). The IR spectrum measured *in situ* also seems to suggest that the solubility of CO_2 in propylene oxide decreases with increasing amounts of formed propylene carbonate.

TABLE 5.2: Rates and yields obtained for ionic liquids **17-20** and TBAB.

Co-Catalyst	1 bar CO$_2$		4 bar CO$_2$	
	Yield (obtained by NMR) (%)	k_{obs} ($mol \cdot L^{-1} \cdot min^{-1}$)	Yield (obtained by NMR) (%)	k_{obs} ($mol \cdot L^{-1} \cdot min^{-1}$)
17	14.6	0.0057	-	-
18	11.3	0.0044	18.2	0.0068
19	10.0	0.0059	84.0	0.0479
20	18.5	0.0174	67.6	0.0454
TBAB	21.4	0.0067	93.5	0.0266

TABLE 5.3: TOFs calculated for TBAB and ionic liquids **19** and **20**.

Co-Catalyst	Yield (obtained by NMR) (%)	TOF (h^{-1})
19	71.0	118.7
20	58.5	70.5
TBAB	47.6	62.1

5.2.2 Determining Order of Reaction with TBAB as Co-Catalyst

The order of reaction of NbCl$_5$ and TBAB was determined by kinetic analysis (method of initial rates). The initial rates were extrapolated from the profiles of propylene carbonate formation that was recorded by *in situ* IR measurements.

The concentration of TBAB was kept constant at 0.1425 M as the amount of NbCl$_5$ was varied. The mixture was stirred for 5 minutes to allow for proper mixing before 1 bar of CO$_2$ was introduced. The absorbance of the peak at 1810 cm^{-1} corresponding to the carbonyl moiety in propylene carbonate was monitored (Figure 5.2).
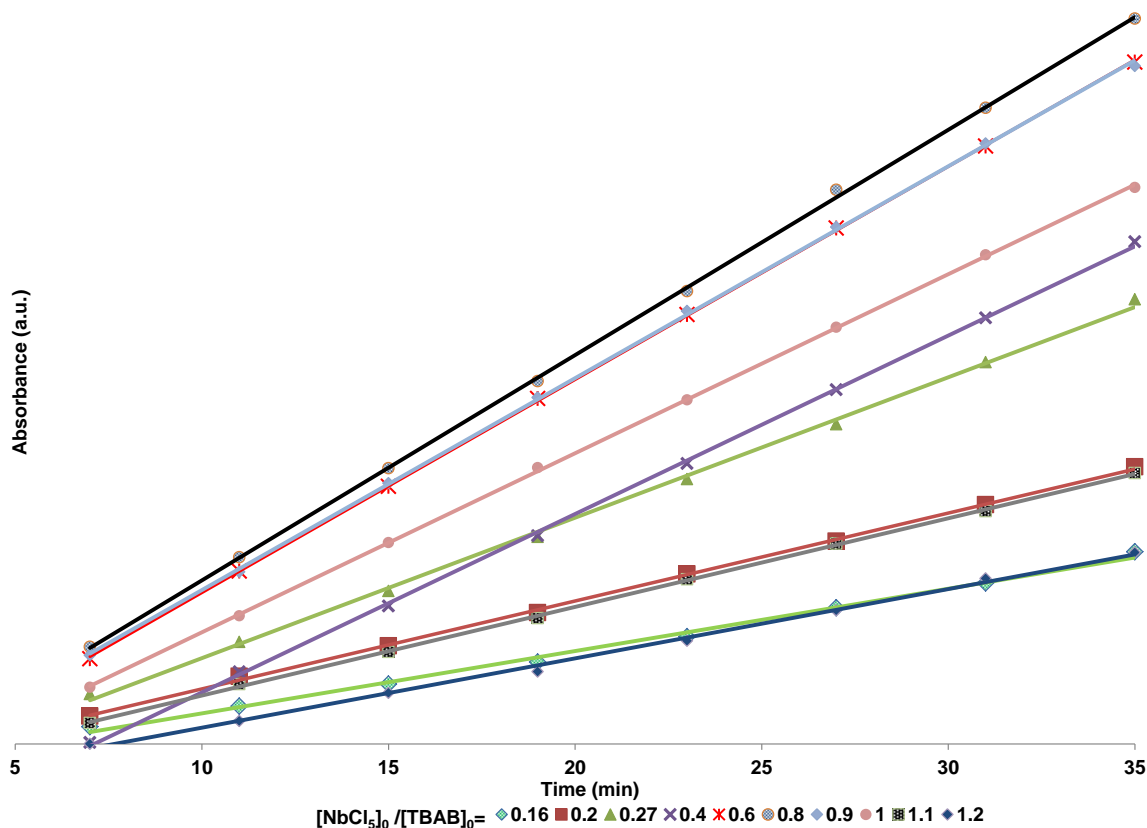
FIGURE 5.2: Plot of absorbances against time by varying [NbCl$_5$] and keeping [TBAB] constant; obtained from *in situ* IR spectroscopy.

The slope of each profile was then extrapolated in the first 15 minutes of reaction and taken as the apparent reaction rate (k_{obs}). The order of the reaction can then be determined by the slope of the logarithmic plot defined by the Equation 5.2.

$$k_{obs} = k[cat]^n = \left(\frac{d[PC]}{dt} \right)_{initial} \tag{5.1}$$

$$\Rightarrow \lg(k_{obs}) = n \cdot \lg[cat] + \lg k \tag{5.2}$$

The values and trend obtained for different $\frac{[NbCl_5]_0}{[TBAB]_0}$ ratios are shown in Table 5.4 and Figure 5.3 (left).

TABLE 5.4: Rates obtained for different $\frac{[\text{NbCl}_5]_0}{[\text{TBAB}]_0}$ ratios at 25°C.

Entry	$[\text{NbCl}_5]_0$ $(mol \cdot L^{-1})$	$[\text{TBAB}]_0$ $(mol \cdot L^{-1})$	$\frac{[\text{NbCl}_5]_0}{[\text{TBAB}]_0}$	k_{obs} $(mol \cdot L^{-1} \cdot min^{-1})$
1	0.0228	0.1425	0.16	0.0023
2	0.0285	0.1425	0.20	0.0029
3	0.0385	0.1425	0.27	0.0046
4	0.0570	0.1425	0.40	0.0058
5	0.0855	0.1425	0.60	0.0069
6	0.114	0.1425	0.80	0.0072
7	0.128	0.1425	0.90	0.0067
8	0.143	0.1425	1.00	0.0057
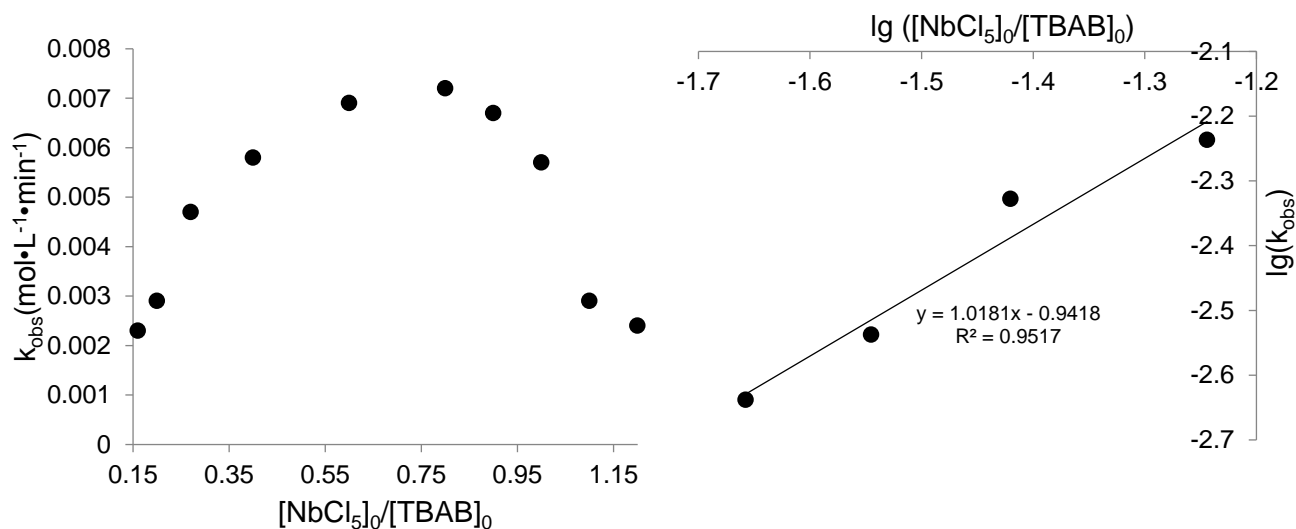
FIGURE 5.3: Initial rates of propylene carbonate formation, k_{obs} obtained through *in situ* IR for the NbCl$_5$/TBAB system plotted against the catalyst/co-catalyst ratio (left).Double logarithmic plot obtained for the reaction promoted by TBAB by varying $[\text{NbCl}_5]_0$ and for $[\text{NbCl}_5]_0 \leqslant 0.4$ (right).

The rate, k_{obs} appears to follow a linear profile only at low $[\text{NbCl}_5]_0$ values ($\frac{[\text{NbCl}_5]_0}{[\text{TBAB}]_0} \leqslant 0.4$). The logarithmic plot shown in Figure 5.3 (right) depicts first order kinetics for NbCl$_5$ through the gradient of the best fit line in this concentration range (gradient is 1.02).

The experiments were repeated with varying TBAB concentrations and constant NbCl$_5$ concentration (0.1425 M). The values and trend obtained for the different ratios of TBAB to NbCl$_5$ are shown in Table 5.5 and Figure 5.4 (left).

TABLE 5.5: Rates obtained for different $\frac{[\text{TBAB}]_0}{[\text{NbCl}_5]_0}$ ratios at 25°C.

Entry	$[\text{NbCl}_5]_0$ $(mol \cdot L^{-1})$	$[\text{TBAB}]_0$ $(mol \cdot L^{-1})$	$\frac{[\text{TBAB}]_0}{[\text{NbCl}_5]_0}$	k_{obs} $(mol \cdot L^{-1} \cdot min^{-1})$
1	0.1425	0.07120	0.50	0.000900
2	0.1425	0.1070	0.75	0.00144
3	0.1425	0.1425	1.00	0.00594
4	0.1425	0.1780	1.25	0.00810
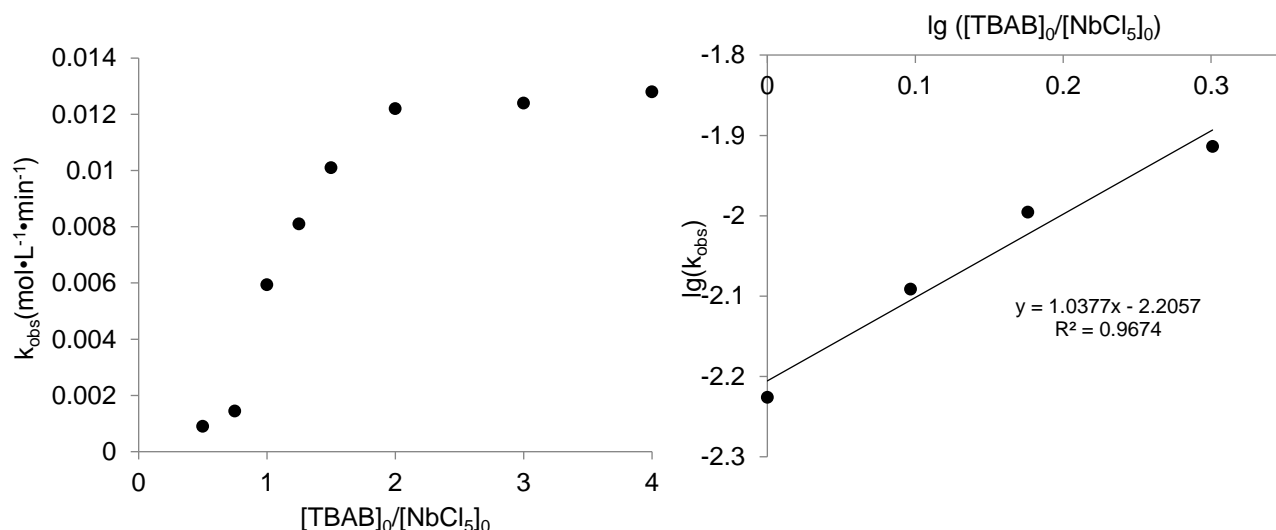
FIGURE 5.4: Initial rates of propylene carbonate formation, k_{obs} obtained through *in situ* IR for the NbCl$_5$/TBAB system plotted against the co-catalyst/catalyst ratio (left). Double logarithmic plot obtained for the reaction promoted by TBAB by varying [TBAB]$_0$ and for $1 \leqslant \frac{[\text{TBAB}]_0}{[\text{NbCl}_5]_0} \leqslant 2$. (right)

The rate, k_{obs} appears to follow a linear profile when $1 \leqslant \frac{[\text{NbCl}_5]_0}{[\text{TBAB}]_0} \leqslant 2$. The logarithmic plot shown in Figure 5.4 (right) depicts first order kinetics for TBAB through the gradient of the best fit line in this concentration range (gradient is 1.04).

5.2.3 Determining Order of Reaction of Catalyst with DMAP as Co-Catalyst

Graphs obtained through the same procedure described in Section 5.2.2 was plotted for the NbCl$_5$/DMAP system. NbCl$_5$ was varied while [DMAP] was kept constant at 0.1425 M. The

values and trend obtained for the different ratios of $NbCl_5$ to DMAP are shown in Table 5.6 and Figure 5.5 (left). Also for DMAP, the initial reaction rates were measured by introducing CO_2 90 minutes after the catalyst and co-catalyst have fully dissolved in propylene oxide to obtain induction-free, linear kinetic profiles.

TABLE 5.6: Rates obtained for different $\frac{[NbCl_5]_0}{[DMAP]_0}$ ratios at 25°C.

Entry	$[NbCl_5]_0$ $(mol \cdot L^{-1})$	$[DMAP]_0$ $(mol \cdot L^{-1})$	$\frac{[NbCl_5]_0}{[DMAP]_0}$	k_{obs} $(mol \cdot L^{-1} \cdot min^{-1})$
1	0.0178	0.1425	0.125	0.00025
2	0.0356	0.1425	0.250	0.00050
3	0.0570	0.1425	0.400	0.00075
4	0.0712	0.1425	0.500	0.00088
5	0.0855	0.1425	0.600	0.0010
6	0.107	0.1425	0.750	0.0011
7	0.143	0.1425	1.00	0.0013
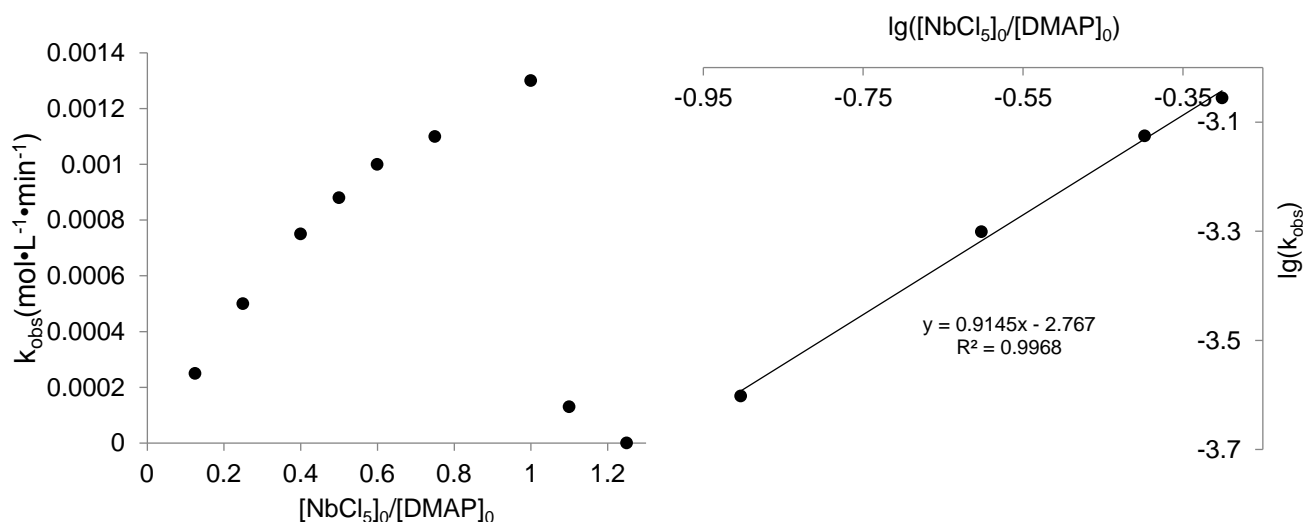
FIGURE 5.5: Initial rates of propylene carbonate formation, k_{obs} obtained through *in situ* IR for the $NbCl_5$/DMAP system plotted against the catalyst/co-catalyst ratio (left). Double logarithmic plot obtained for the reaction promoted by DMAP by varying $[NbCl_5]_0$ and for $\frac{[NbCl_5]_0}{[DMAP]_0} \leqslant 0.5$ (right).

The logarithmic plot shown in Figure 5.5 (right) depicts first order kinetics for $NbCl_5$ through the gradient of the best fit line in this concentration range (gradient is 0.915).

The experiments were repeated, now varying the concentration of DMAP and keeping the concentration of $NbCl_5$ constant at 0.1425 M. The values and trend obtained for the different $\frac{[DMAP]_0}{[NbCl_5]_0}$ ratios are shown in Table 5.7 and Figure 5.6 (left).

TABLE 5.7: Rates obtained for different $\frac{[DMAP]_0}{[NbCl_5]_0}$ ratios at 25°C.

Entry	$[NbCl_5]_0$ $(mol \cdot L^{-1})$	$[DMAP]_0$ $(mol \cdot L^{-1})$	$\frac{[DMAP]_0}{[NbCl_5]_0}$	k_{obs} $(mol \cdot L^{-1} \cdot min^{-1})$
1	0.1425	0.1140	0.80	0
2	0.1425	0.1425	1.00	0.00125
3	0.1425	0.1780	1.25	0.00172
4	0.1425	0.2140	1.50	0.00211
5	0.1425	0.2490	1.75	0.00242
6	0.1425	0.2850	2.00	0.00266
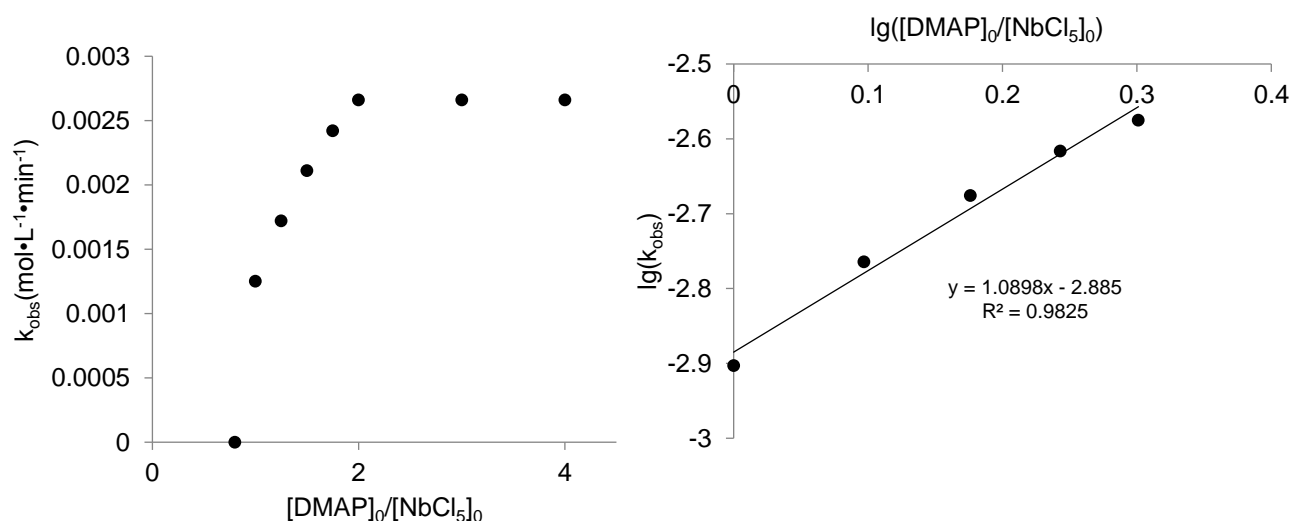
FIGURE 5.6: Initial rates of propylene carbonate formation, k_{obs} obtained through *in situ* IR for the $NbCl_5$/DMAP system plotted against the co-catalyst/catalyst ratio (left). Double logarithmic plot obtained for the reaction promoted by DMAP by varying $[DMAP]_0$ and for $1 \leqslant \frac{[DMAP]_0}{[NbCl_5]_0} \leqslant 2$ (right).

The rate, k_{obs} appears to follow a linear profile when $1 \leqslant \frac{[DMAP]_0}{[NbCl_5]_0} \leqslant 2$. The logarithmic plot shown in Figure 5.6 (right) depicts first order kinetics for DMAP through the gradient of the best fit line in this concentration range (gradient is 1.09).

Comparing the results obtained in this and the previous Section 5.2.2, $NbCl_5$ shows first order kinetics at lower concentrations ($\frac{[NbCl_5]_0}{[TBAB]_0} \leqslant 0.5$) for both co-catalysts. When the ratio between the catalyst and co-catalyst approaches 1, a progressive decrease in the reaction order was observed.

In both cases, inhibition is also observed as soon as the concentration of catalyst exceeds that of the co-catalyst. In the case of DMAP, a sharp drop in activity was noticed. Accordingly, when the concentration of the co-catalyst is varied, while the concentration of $NbCl_5$ is kept constant, no reaction was observed in the case of DMAP and sluggish reaction rates were observed for TBAB. Good reaction rates were only observed when the concentration of co-catalyst was at least equivalent to or higher than the concentration of $NbCl_5$. Both co-catalysts show first order reaction rates when their concentration matches or exceeds the the concentration of $NbCl_5$, but when more than 2 equivalents of co-catalyst was used, no further increase of reaction rate was observed (entries 6-8 in Table 5.5 and Table 5.7).

5.2.4   Identification and Characterization of Intermediates by NMR

To support the kinetic data obtained, NMR-scale experiments were conducted. An equimolar solution of $NbCl_5$ and DMAP was prepared and the signals relative to the protons of the pyridine ring (6.0-8.2 ppm) were monitored. Three species were initially detected (Figure 5.7) as two sets of three signals appeared, corresponding to the α (depicted in blue) and β (depicted in red) protons on the pyridine ring for 3 different species. The peaks at 6.07 ppm and 7.68 ppm can be assigned to free DMAP by comparison with the spectrum of pure DMAP in propylene oxide. The peaks at 6.18 ppm and 7.89 ppm were observed to have diminished within 90 minutes, independent of the $NbCl_5$/DMAP ratio and is therefore assigned to intermediate **21** (Figure 5.10). The peaks at 6.40 ppm and 8.10 ppm belong to **22** as assigned by bidimensional NMR experiments. The COSY and HMBC spectra are shown in Figure 5.8 and Figure 5.9 respectively.

The bidimensional NMR spectra of intermediate **22** were recorded from a solution of $NbCl_5$ to DMAP ratio of 1.5 at 90 min after the mixing of the reagents (after the induction time). At this catalyst/co-catalyst ratio, the solution only contains one DMAP derivative with H_α at 8.08 ppm and H_β at 6.37 ppm, propylene oxide and excess $NbCl_5$ (coordinated by PO). The correlation peaks shown in Table 5.8 were individuated through HMBC and COSY experiments that confirm that the DMAP-derivative present in solution under these conditions correspond to intermediate **22**.
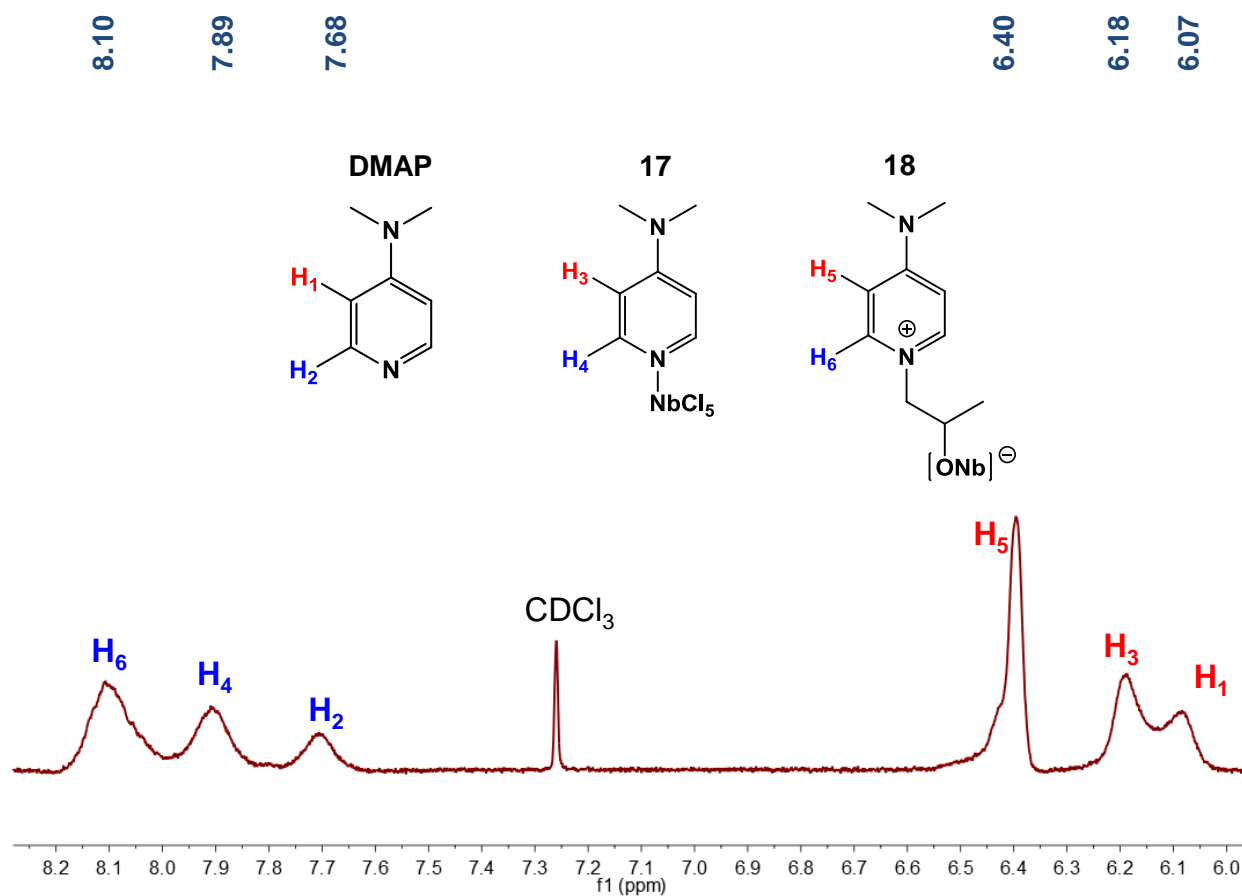
FIGURE 5.7: Proton NMR of an equimolar solution of DMAP and NbCl$_5$ in the region of 6.0-8.2 ppm. Spectrum was measured 5 minutes after mixing the catalysts. Three species are observed: free DMAP, intermediates **21** and **22**.
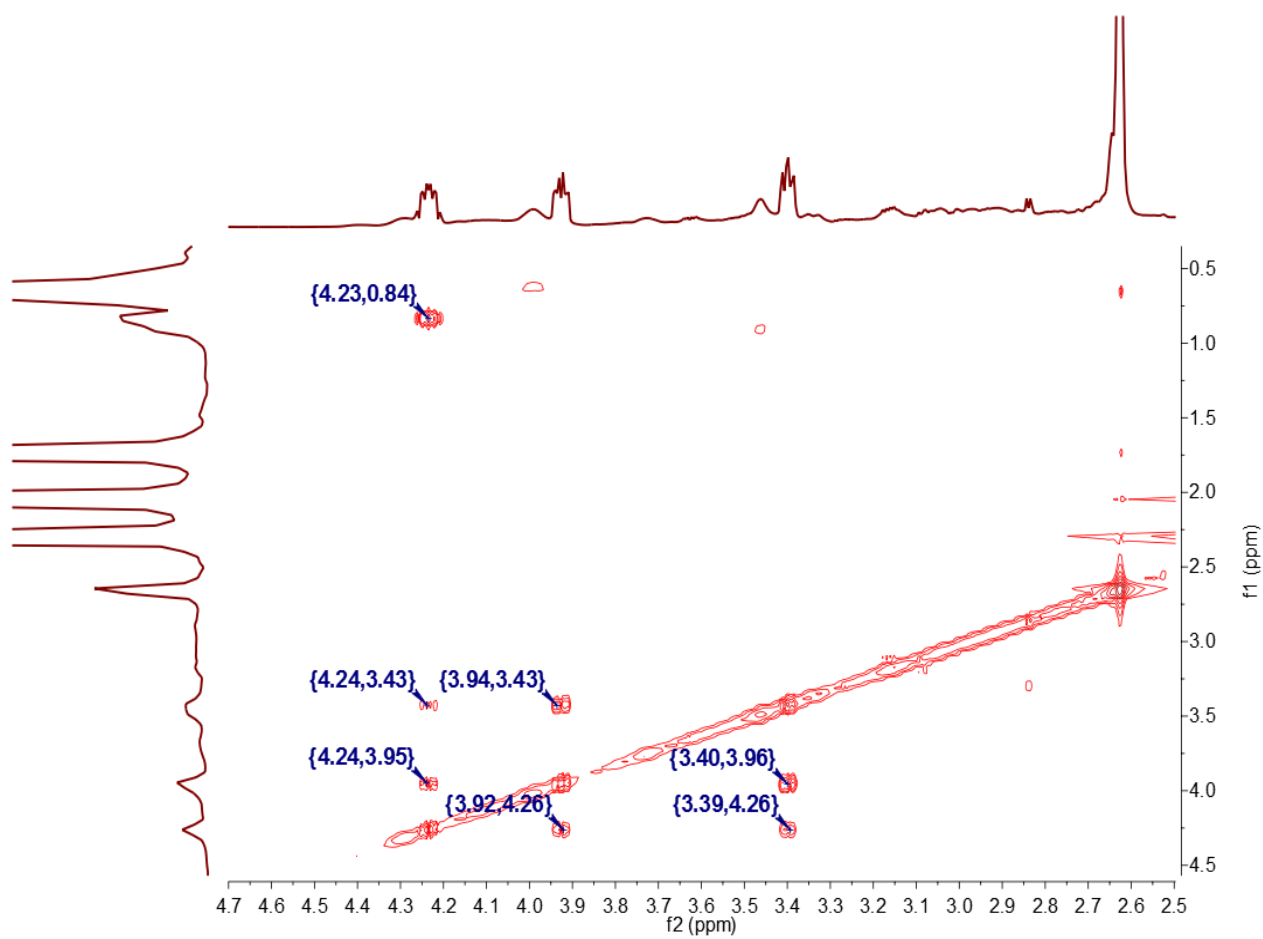
FIGURE 5.8: COSY spectrum of complex **22**.
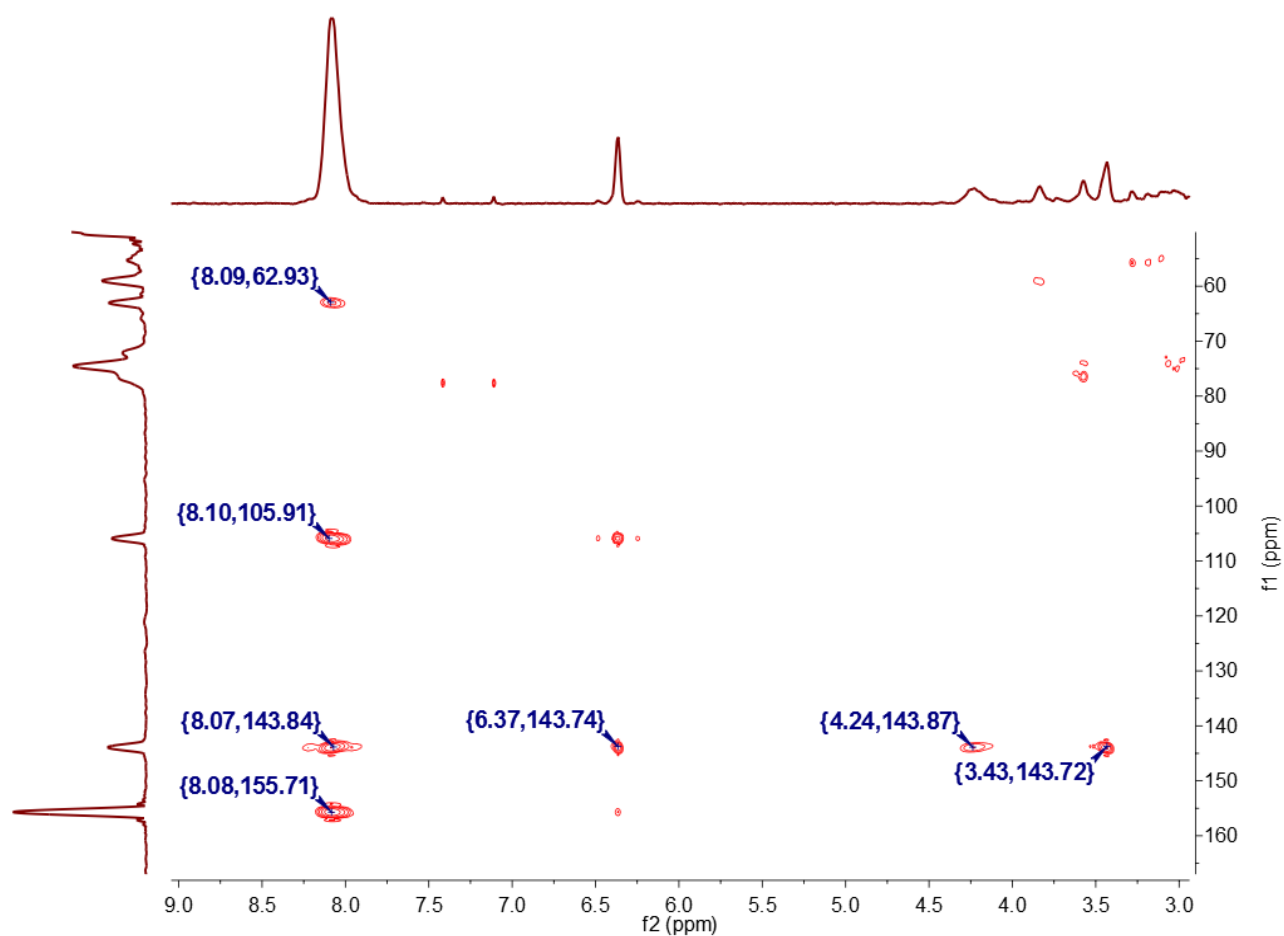
FIGURE 5.9: HMBC spectrum of complex **22**.

TABLE 5.8: ^{1}H$-^{13}$C and ^{1}H$-^1$H couplings identified for intermediate **22**.
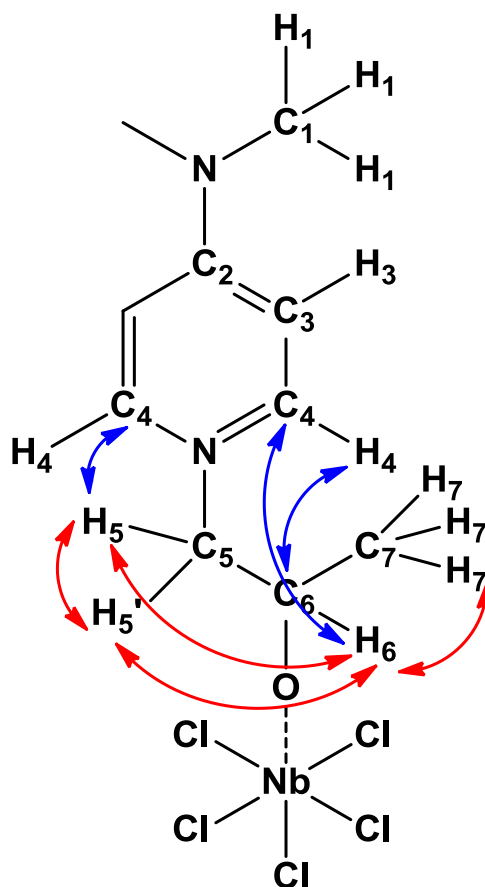
(Couplings within the pyridine ring have been omitted for clarity)

Entry	δ_H	δ_C	HMBC (blue) (^{1}H$-^{13}$C)	COSY (red) (^{1}H$-^1$H)
1	2.88	38.90	2	-
2	-	155.40	-	-
3	6.37	105.89	2, 4	4
4	8.08	143.80	2, 3, 6	3
5	3.40	76.29	4	5', 6
5'	3.92	76.29	-	5, 6
6	4.23	62.97	4	5, 5', 7
7	0.84	21.26	-	6

The COSY spectrum (Figure 5.8) shows the coupling between the three protons of the aliphatic chain in **22** (H$_5$ (3.40 ppm), H$_{5'}$ (3.92 ppm) and H$_6$ (4.23 ppm)) and the coupling between H$_6$ and the protons of the methyl group H$_7$ (0.84 ppm) which confirm the structure of the aliphatic chain.

The HMBC spectrum (Figure 5.9) shows the correlation between C$_4$ of the pyridine ring (143.9 ppm) and the protons of the aliphatic chain (H$_5$, H$_6$) and also H$_3$ (6.37 ppm). A coupling was

additionally identified between H_4 (8.08 ppm) of the pyridine ring and C_6 (62.97 ppm) of the aliphatic chain. The presence of these HMBC correlation peaks confirm the connectivity between the aliphatic fragment and the pyridine ring. Therefore the signals observed at 8.10 ppm and at 6.40 ppm in the ^{1}H NMR of the reaction mixture can be assigned to intermediate **22**.

The intensity of these signals corresponding to **22** grows to a maximum within 90 minutes from the time of mixing of the reagents, as expected. On the other hand, as previously mentioned, the peaks corresponding to **21** diminish over 90 minutes. This is shown in the time evolution profile (Figure 5.10).
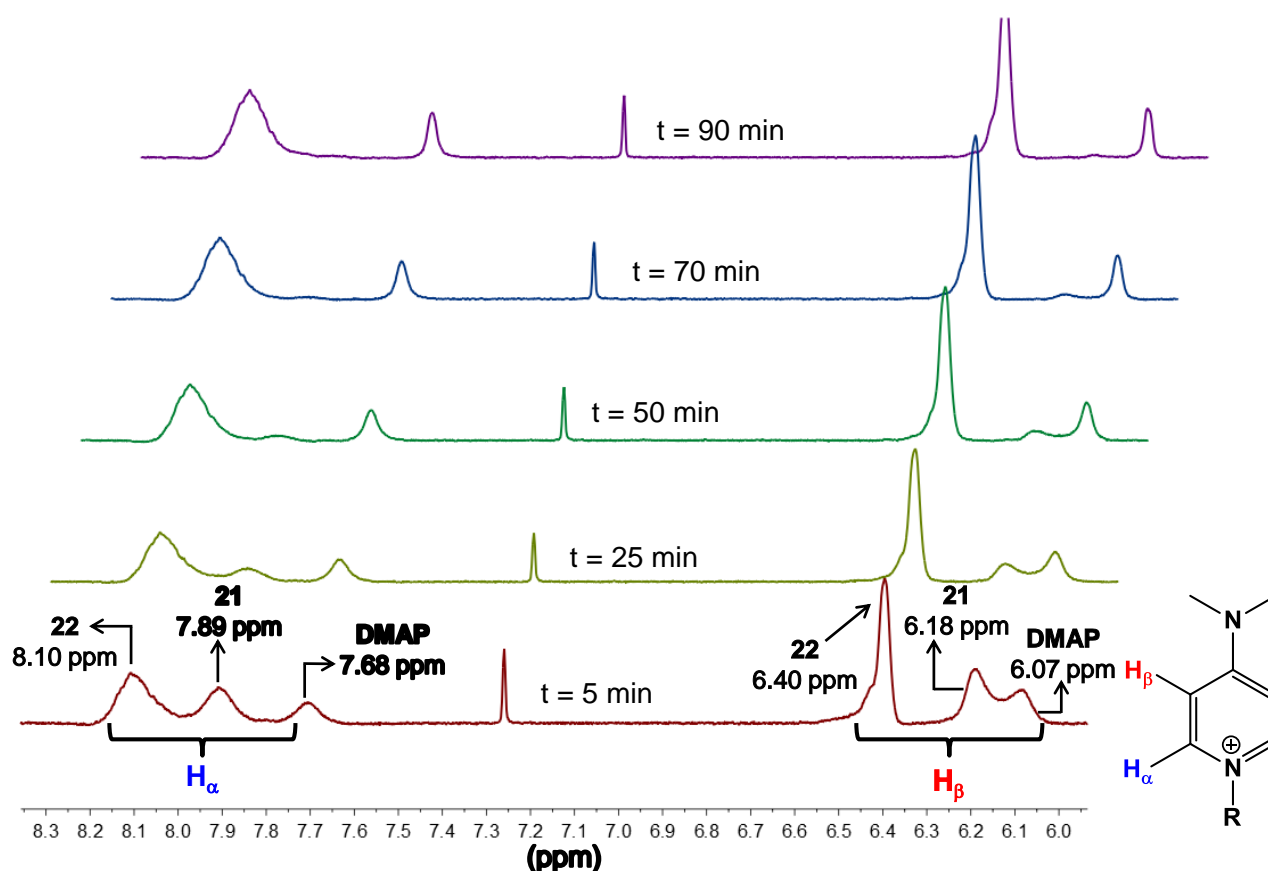
FIGURE 5.10: Time evolution profile of the protons on the pyridine ring in an equimolar solution of DMAP and NbCl$_5$ in propylene oxide.

5.2.5 Determining Amount of Free DMAP in Solution by NMR Studies

The amount of free DMAP in solution at the equilibrium shown in Scheme 5.3 with varying amounts of NbCl$_5$ was then quantified by NMR spectroscopy. NMR experiments with ratios of NbCl$_5$ to DMAP ranging from 1-1.5 were performed. The peaks corresponding to free DMAP, **21**

and **22** were then integrated with the residual CDCl$_3$ peak as reference. The relative abundances were calculated and plotted against time and the graphs are shown in Figure 5.11.
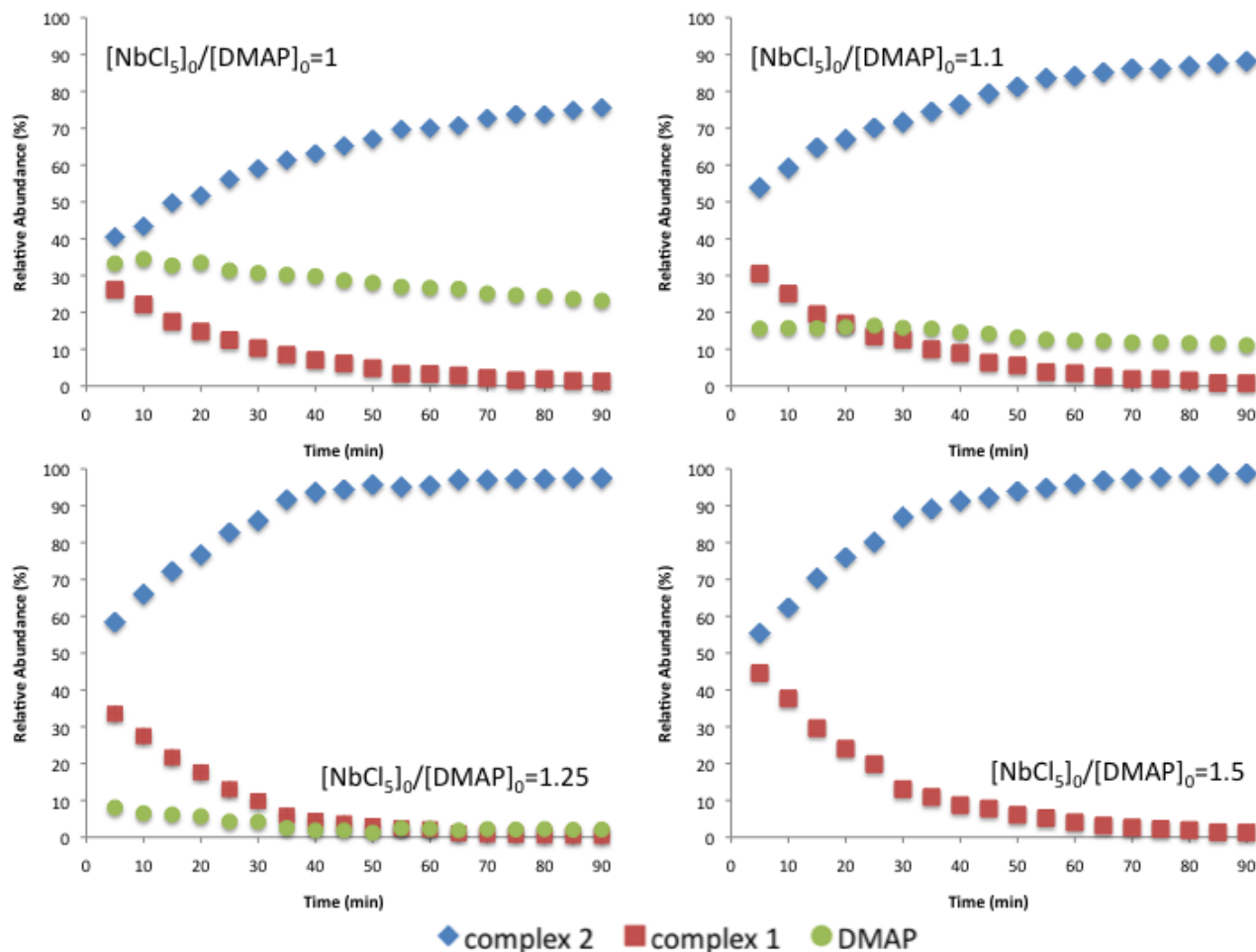
FIGURE 5.11: Relative abundances of the species in solution for different NbCl$_5$ to DMAP ratios calculated by the integration of proton NMR spectra collected.

By integrating the NMR resonances of DMAP and **22** at t = 90 minutes, it is observed that for equivalent initial concentrations of DMAP and NbCl$_5$, only about 25% of the initial DMAP amount is still free in solution when the equilibrium is reached. This number decreases to 11% when a small excess of NbCl$_5$ is added ($\frac{[\text{NbCl}_5]_0}{[\text{DMAP}]_0} = 1.1$). When the amount of excess NbCl$_5$ is further increased ($\frac{[\text{NbCl}_5]_0}{[\text{DMAP}]_0} \geqslant 1.25$), virtually no free DMAP is available in solution (Table 5.9).

TABLE 5.9: Relative abundance of free DMAP at equilibrium in relation to its initial concentration and to the concentration of intermediate **22**.

Entry	$\frac{[\text{NbCl}_5]_0}{[\text{DMAP}]_0}$	$\frac{[\text{DMAP}]}{[\textbf{22}]}$	$\frac{[\text{DMAP}]}{[\text{DMAP}]_0}$ (%)
1	1.00	0.333	25
2	1.10	0.125	11
3	1.25	0.0216	2
4	1.50	0	0

Based on these quantified results, the inhibition of the reaction observed with an excess of $NbCl_5$ can be correlated to the absence of free co-catalyst available. The NMR results, together with the kinetic data strongly suggest a bifunctional role for the co-catalytic moieties in the reaction mechanism, but with only one molecule of co-catalyst taking part in the rate determining step (reaction is first order with respect to co-catalyst). The absence of the co-catalyst in the presence of excess $NbCl_5$ seems to hinder the accomplishment of an additional role beyond ring opening within the catalytic cycle as the co-catalyst is fully consumed in forming intermediates such as **22**.

5.2.6   Dual Role of Co-Catalyst Supported by *in situ* IR Studies

In situ IR spectroscopy was used to prove the existence of a dual role for the co-catalyst. $\frac{[NbCl_5]_0}{[DMAP]_0}$ was set to 1.25, where nearly no free DMAP is available in solution (entry 3, Table 5.9). After the initial induction period of 90 minutes where **21** was entirely converted to **22** under an argon atmosphere, 1 bar of CO_2 was added (**A**, Figure 5.12). Consistent with the kinetic data, no propylene carbonate was observed to have formed under these conditions.

The only effects of CO_2 addition on the IR spectrum of the reaction were the appearance of the characteristic CO_2 stretching band at 2338 cm^{-1} and the appearance of a new signal at 1680-1690 cm^{-1}. The reactor was then depressurized (**B**, Figure 5.12) and a suitable amount of DMAP was added to the reaction mixture to set $\frac{[NbCl_5]_0}{[DMAP]_0} = 1$. During the depressurization, the intensity of the signal at 1680-1690 cm^{-1} was also diminished. The reactor was then re-pressurized with 1 bar of CO_2, which gave rise to the signal at 1680-1690 cm^{-1} again, indicating that the species being formed was dependent on CO_2 pressure (black line, Figure 5.12).

With the readdition of CO_2, intermediate **21** was also formed again by the reaction of the newly added base and the excess $NbCl_5$. After an induction period necessary to convert **21** into **22**, the formation of propylene carbonate was then observed (**D**, Figure 5.12). The reaction rate stabilizes when the concentration of **22** reaches its equilibrium value.

In a similar experiment, the additional amount of DMAP was replaced with an equivalent molar amount of TBAB. In this case, the formation of propylene carbonate started immediately without any induction time as expected (**C**, Figure 5.12).
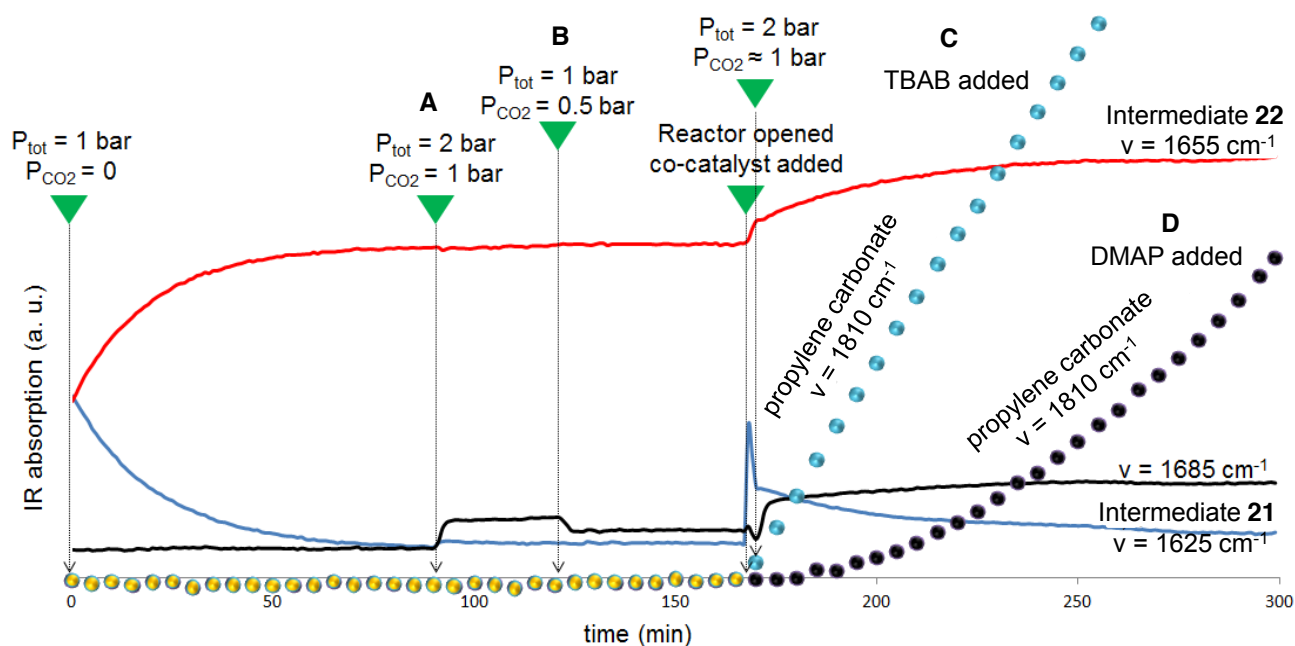
FIGURE 5.12: *In situ* IR study of $\frac{[NbCl_5]_0}{[DMAP]_0} = 1.25$ in propylene oxide where no propylene carbonate was formed due to lack of free co-catalyst. When $\frac{[NbCl_5]}{[DMAP]}$ was set to 1, propylene carbonate formation took off immediately with TBAB (C) and an induction period with DMAP (D) .

These series of experiments prove that even though the same type of intermediates are formed in solution independent of the $[NbCl_5]_0$ to $[DMAP]_0$ ratio, the formation of propylene carbonate is halted when there are no free co-catalyst molecules available to complete the catalytic cycle.

According to the proposed mechanism in Scheme 5.2 (cycle 2), with the first equivalent of co-catalyst being introduced in step A, the additional molecule of co-catalyst would be used to assist either step B (CO_2 insertion) or C (release of carbonate). For the former, DMAP could activate CO_2 by forming a DMAP-CO_2 adduct as observed for N-heterocyclic carbenes[162,163] or cyclic aminidines.[164]

Activation by the co-catalyst is also possible for TBAB only if part of the tetraalkylammonium salt decomposes to tributylamine, which would then act as the nucleophile. Such behaviour was indeed observed by North *et al.* for the synthesis of cyclic carbonates promoted by a bimetallic aluminum-salen complex and TBAB at ambient conditions. A dual role for the co-catalyst was also mentioned.[165,166]

For this experiment, the identification of the intermediate corresponding to the band at 1680-1690 cm^{-1} was the key to understanding the reaction mechanism as it was the only indication of an intermediate formed upon the addition of CO_2 when DMAP or TBAB was used. In a comparable *in situ* IR study by Darensbourg *et al.*, the co-polymerization of CO_2 (55 bar) and 2-(3,4-epoxycyclohexyl)trimethoxysilane by a DMAP/Cr-salen system at room temperature was investigated.[167] They observed the formation of two new bands in the ARS and C=O stretching

regions at 1650 cm^{-1} and 1680 cm^{-1} and assigned them to the formation of an adduct of Cr, DMAP and CO_2 (**23**, Figure 5.13), and the product of epoxide insertion between the metal and carboxylate (**5**, Figure 5.13) respectively.
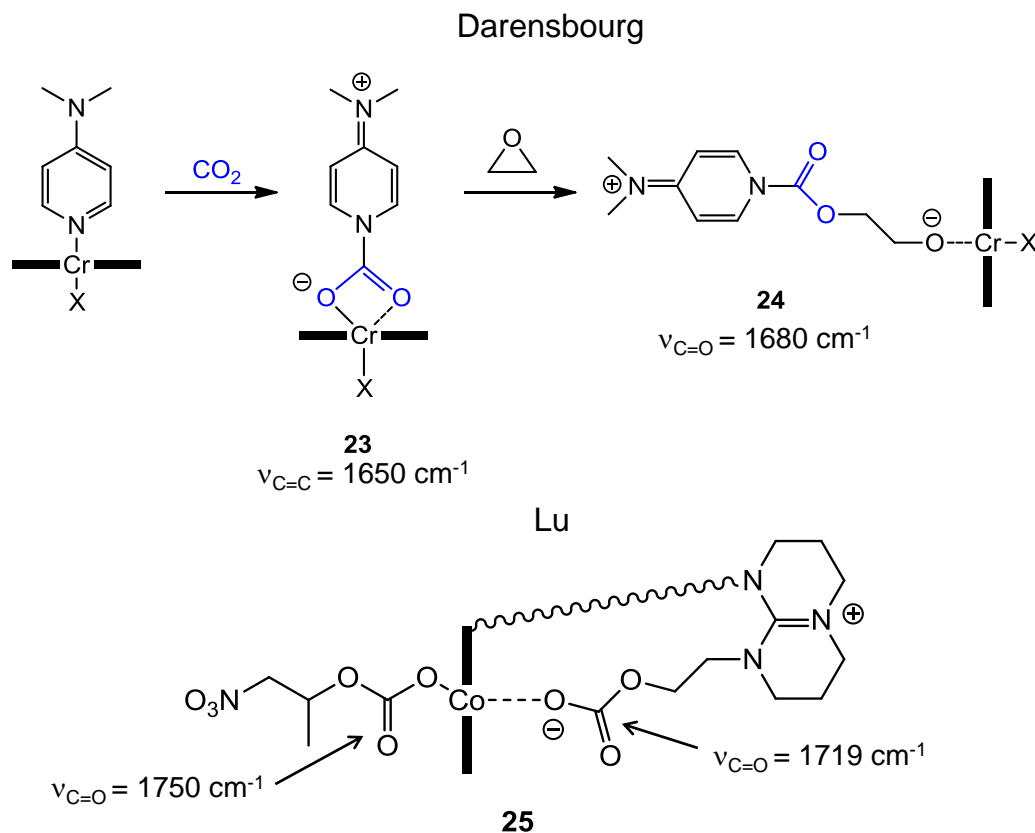
FIGURE 5.13: Proposed mechanism by Darensbourg for the insertion of CO_2 for a DMAP/CrN$_3$(Salen) system (top). C=O bands that were assigned to the formation of a bi-hemicarbonate species, **25** (bottom).

Another study by Lu *et al.* showed the formation of two bands at 1750 and 1719 cm^{-1} in the *in situ* IR spectrum of a CH_2Cl_2 solution of a triazabicyclodecene tethered Co(III) complex upon addition of CO_2. They assigned the bands to the C=O stretching of an intermediate similar to **25** upon CO_2 insertion. The insertion of CO_2 proved to be reversible upon exposure of the solution to N_2 (band at 1719 cm^{-1}) or by increasing the temperature to 60 °C (band at 1750 cm^{-1}).[168]

Considering both case studies, the nucleophile could be involved in CO_2 activation through different pathways as shown in Scheme 5.4. **P1** represents the activation of CO_2 by insertion into the metal-nucleophile adduct. **P2** represents a direct CO_2 activation by DMAP through the formation of a carbamate-like adduct. Lastly **P3** shows the "unassisted" insertion of CO_2 into the metal-alkoxide bond of **22**, forming hemicarbonate **26** without the involvement of the

Insertions following pathway **P3** are known to occur under mild conditions for a wide range of transition metals including Nb.[169–171]
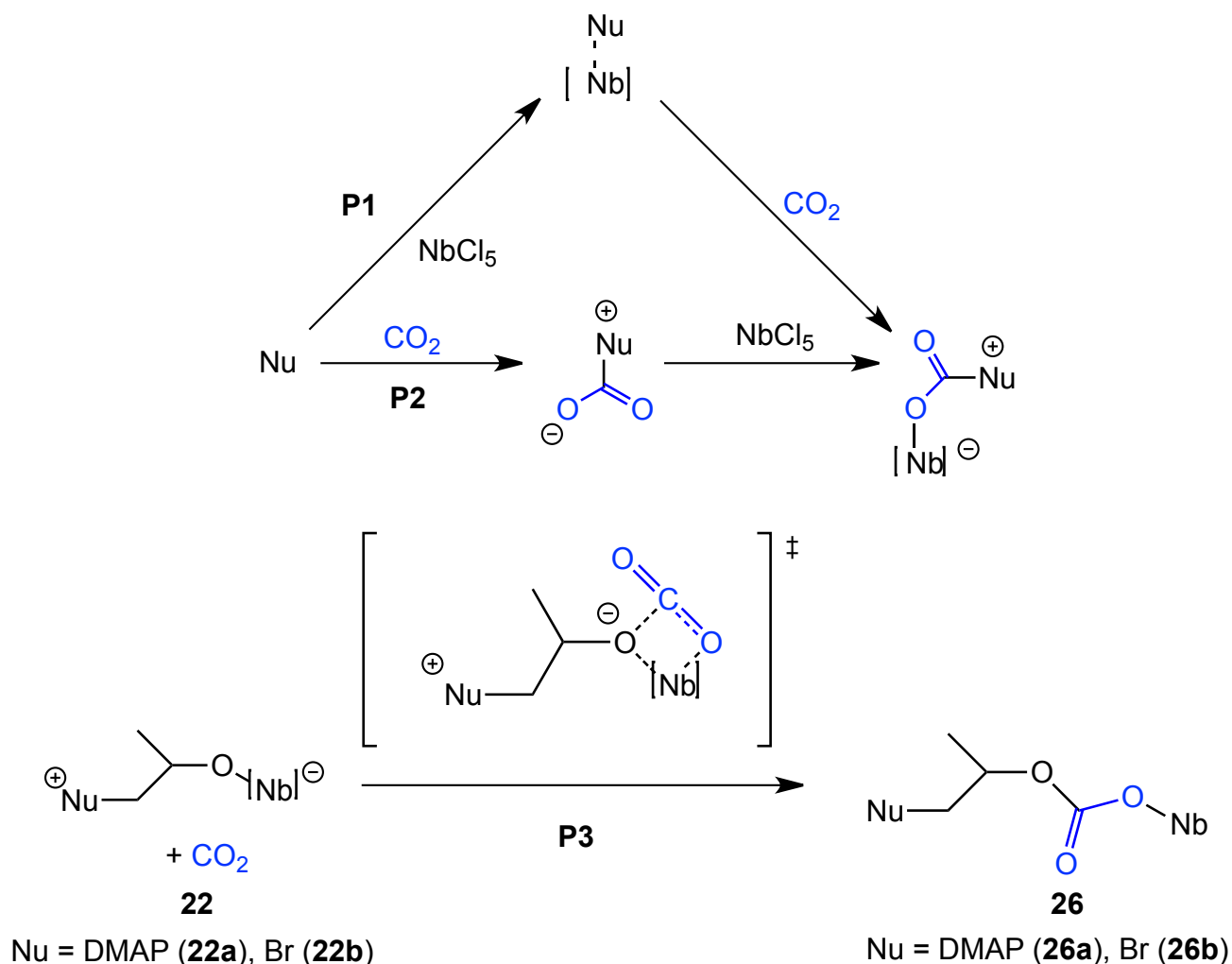
SCHEME 5.4: Possible pathways of CO_2 activation and insertion.

5.2.7 Intermediates of Carbon Dioxide Insertion

A careful search of the intermediates of CO_2 coordination and insertion was done through *in situ* IR experiments. The effect of stepwise variations of CO_2 pressure on the IR spectrum of propylene oxide solutions of $NbCl_5$ and DMAP or TBAB was studied.

For $NbCl_5$ and DMAP, the peaks corresponding to the intermediates could be isolated by setting $\frac{[NbCl_5]_0}{[DMAP]_0} = 1.5$ to suppress the formation of propylene carbonate. This way, all the peaks that evolve would correspond to the products of CO_2 insertion and can be easily identified.
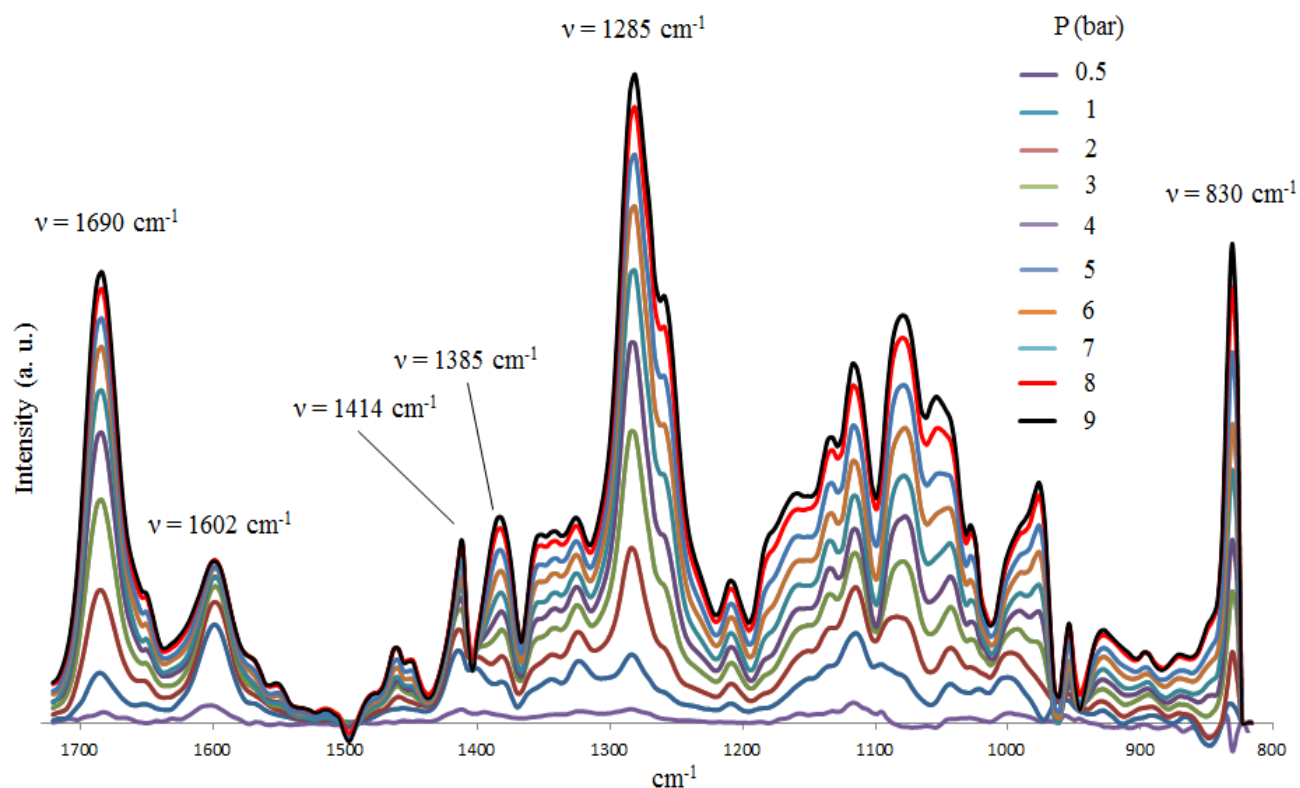
FIGURE 5.14: *In situ* IR profiles of various intermediates forming at varying CO_2 pressures.

Two main bands emerge at 1285 cm^{-1} and 830 cm^{-1} together with the peak at 1690 cm^{-1} (Figure 5.14). The evolution of the bands were monitored through time with the stepwise increase of CO_2 pressure. An instantaneous increase in their absorption intensities was observed with each step of CO_2 addition (Figure 5.15). The intensity at a given pressure does not change with time. When the pressure was released stepwise from the autoclave, the intensity of the bands decreased in a similar fashion, almost matching the trend of CO_2 depressurization. This reversibility of intermediate formation has been observed in literature for niobium and other transition metals.[60,168–172].
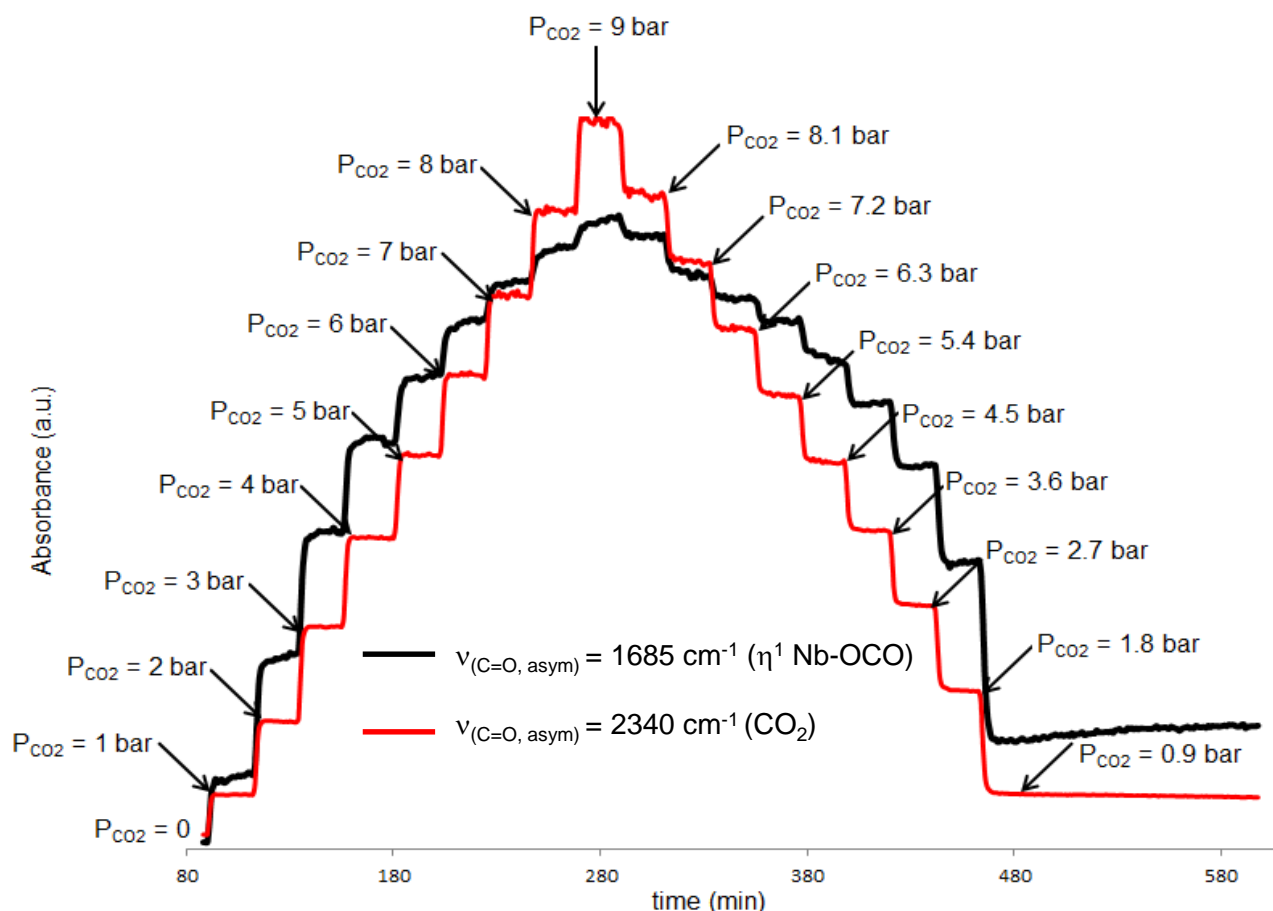
FIGURE 5.15: Evolution of the peak at 1685 cm^{-1} alongside variations in CO$_2$ pressure. The intensity of the signal at 2340 cm^{-1} (corresponding to CO$_2$) has been scaled down by a factor of 5 to fit in the graph.

The formation of these new signals also has no effect on the pre-existing band at 1655 cm^{-1} that corresponds to intermediate **22**. These observations seem to suggest that the bands at 1690 cm^{-1} and 1285 cm^{-1} correspond to the asymmetric and symmetric carbonyl stretching respectively of the hemicarbonate, **26**. The large difference of 405 cm^{-1} between the ν_{asym} and ν_{sym}, the high frequency of ν_{as} at 1690 cm^{-1} and the stronger intensity of ν_{sym} compared to ν_{asym} also suggest a monodentate η^1-coordination mode of CO$_2$ to the metal.[173] With reference to literature, the broad absorption band in the 1000-1200 cm^{-1} region and sharp band at 830 cm^{-1} (out of plane bending of OCOO group) can be assigned to the hemicarbonate **26**.

Characterization of hemicarbonate **26** was also attempted by NMR spectroscopy. However, due to the formation of trace amounts of propylene carbonate, the peaks corresponding to the hemicarbonate were overlapped by the peaks of propylene carbonate and the two sets of peaks could not be distinguished.

Other pressure-dependent bands also appear at 1602 cm^{-1}, 1414 cm^{-1} and 1385 cm^{-1}. These signals are consistent with the products of CO$_2$ insertion in niobium alkoxides.[174] They can be further correlated to a η^2 CO$_2$-coordinated complex (chelating carboxylate) where two oxygens

are coordinated to the same metal centre, based on the same considerations as the η^1 complex. With reference to Figure 5.14, it is also observed that the η^2 complex is favoured to form at low CO_2 pressures.
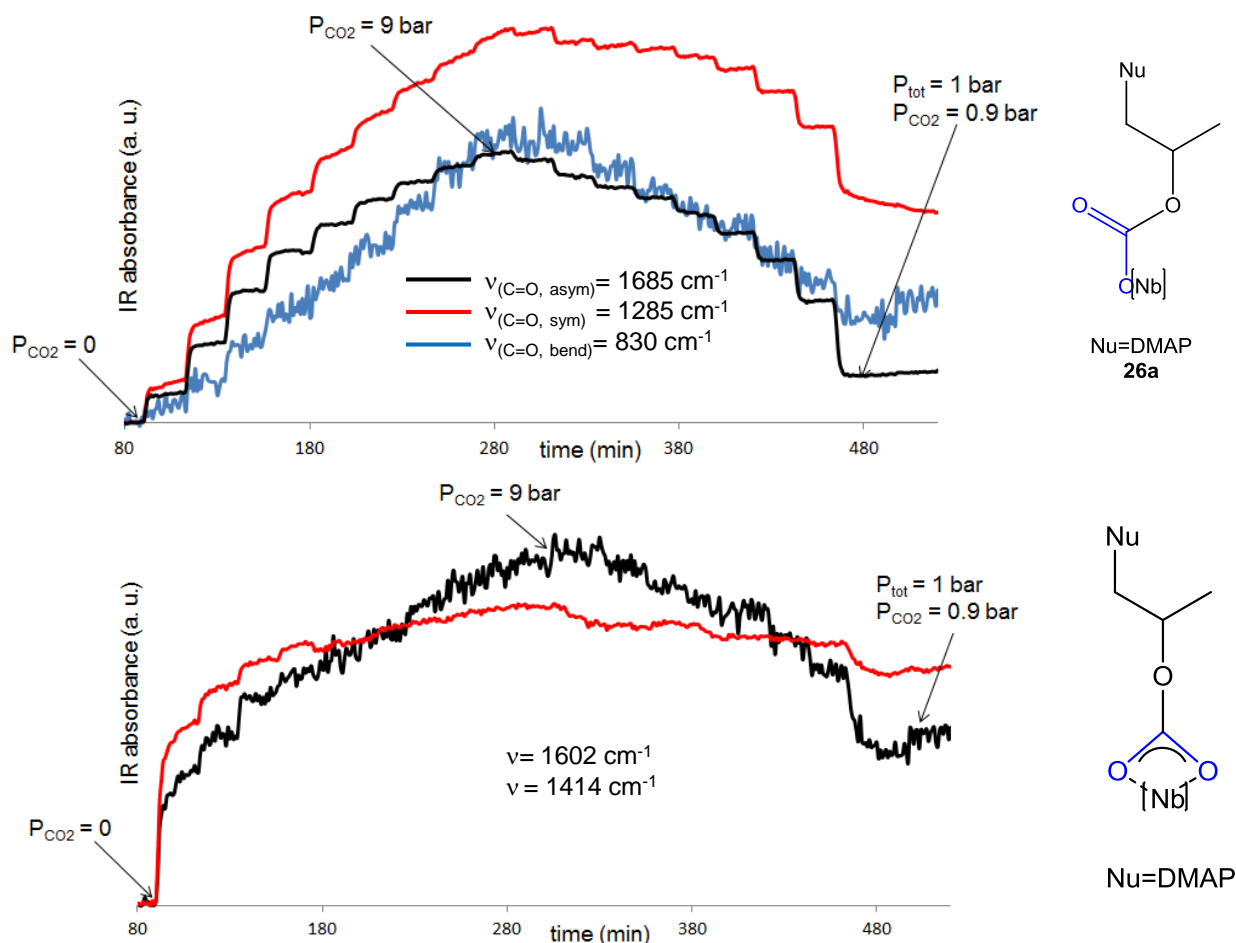
FIGURE 5.16: The CO_2 insertion in **26a** is reversible (top). Evolution of the peaks corresponding to the bidentate insertion with varying CO_2 pressure (bottom).

Peaks in the same regions were also observed with TBAB as co-catalyst. For TBAB, a short induction time would correspond to the formation of such intermediates before the formation of propylene carbonate starts. However, in the case of TBAB, small amounts of propylene carbonate still form even in the presence of excess $NbCl_5$. The absorption bands of propylene carbonate show at 1483, 1450, 1387 and 1352 cm^{-1} (in addition to the C=O peak at 1810 cm^{-1}) and therefore the bands of **26b** in these regions could not be isolated. In addition, traces of polymeric materials with $\nu_{C=O} = 1747$ cm^{-1} were also observed when the CO_2 pressure was increased. The IR spectra and the time evolution profile of the peaks are shown in Figure 5.17. From the time evolution profile it can also be seen that the signals at 1683 and 1281 cm^{-1} are reversible and dependent on CO_2 pressure, comparable with the results observed with **26b**. The absorption values of the bands and the correlated complexes are summarised in Table 5.10.
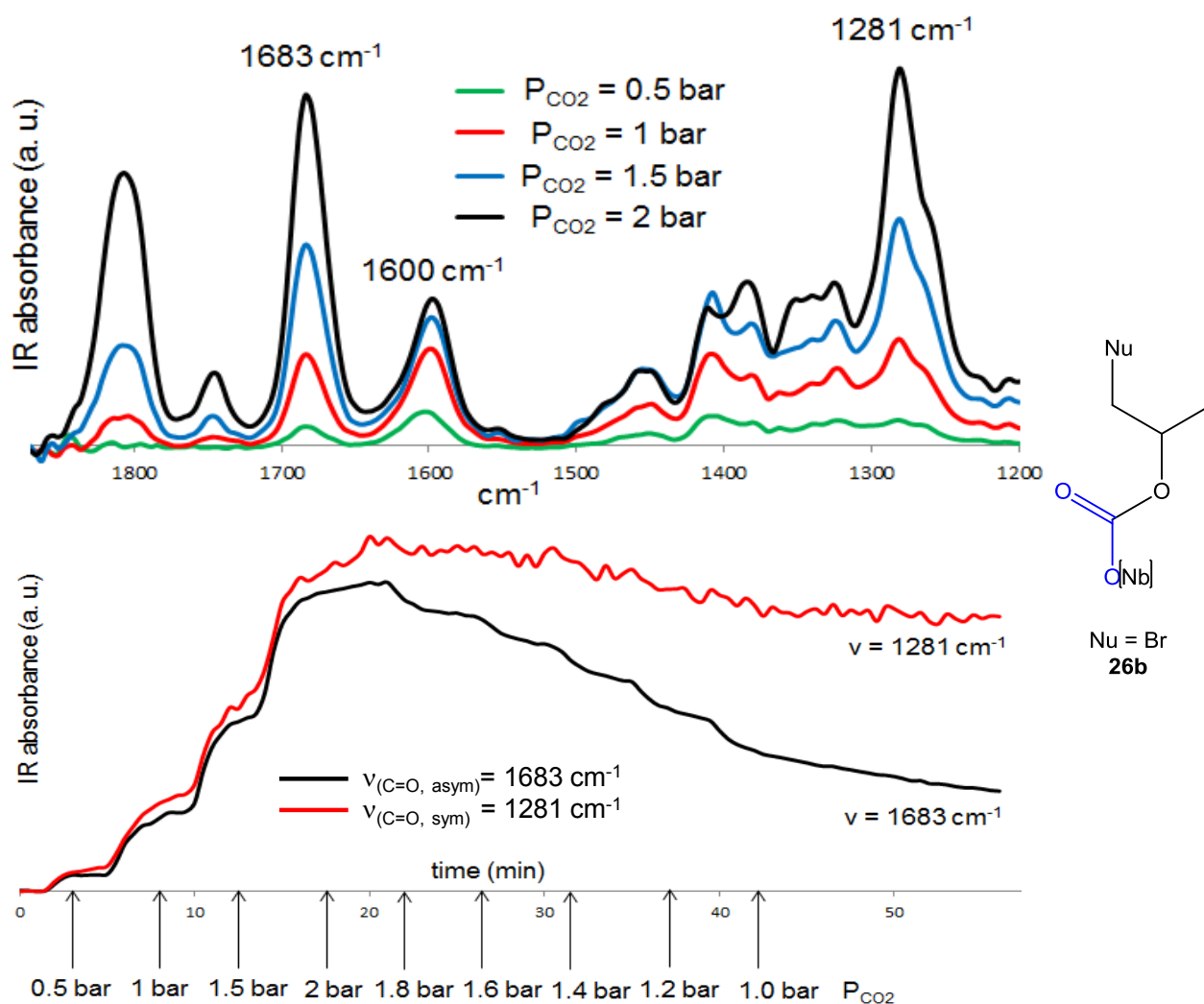
FIGURE 5.17: Formation of hemicarbonate **26b** bands obtained by *in situ* IR (top). Time evolution profile for the peaks at 1281 and 1683 cm^{-1} (bottom).

TABLE 5.10: Summary of IR bands and correlations.

ν (cm^{-1})	Correlation
830	Out of plane bending of -OCOO- group, intermediate **26a**
1000-1200	Intermediate **26a**
1285	Symmetric C=O stretching, intermediate **26a**
1690	Asymmetric C=O stretching, intermediate **26a**
1414, 1602, 1835	η^2 coordinated complex at low CO$_2$ pressures with DMAP as co-catalyst
1625	ARS, complex **21**
1655	ARS, complex **22**
1683	Asymmetric C=O stretching, intermediate **26b**
1281	Symmetric C=O stretching, intermediate **26b**
1598-1605	Asymmetric C=O stretching, η^2 coordinated complex with TBAB as co-catalyst

The IR data gives sufficient evidence to suggest that the hemicarbonate intermediate **26** is involved in a productive step in the catalytic cycle. Following the addition of CO_2, the catalytic components could be entirely explained by the hemicarbonate species that arise from the mono- and bidentate insertion of CO_2 in intermediate **22a**. The hemicarbonate also forms independently of the presence of free nucleophile in solution and would therefore exclude a role for DMAP or other nucleophiles in aiding the insertion of CO_2.

Subsequent experiments were performed to investigate the insertion of CO_2 in **21** with DMAP, TBAB and even tributylamine with CO_2 pressures up to 20 bar and no insertion was observed. This allows pathways **P1** and **P2** in Scheme 5.4 to be eliminated for consideration. It can therefore be concluded that the activation of CO_2 occurs through an unassisted insertion in the metal-alkoxy bond of **22**. At this point, the presence of free nucleophile in solution is not needed yet. Figure 5.15 also shows that the hemicarbonate concentration present at 1 bar CO_2 is only a small fraction of the concentration available at 9 bar CO_2.

5.2.8 Effects of Carbon Dioxide Pressure on the Formation of Propylene Carbonate

To complete the overall mechanistic picture, the effects of CO_2 pressure on the formation of propylene carbonate formation was studied. In the first series of experiments, the *in situ* IR profile of two different $NbCl_5$/DMAP solutions in propylene oxide was monitored while the CO_2 pressure was varied. Solution A had equimolar concentrations of $NbCl_5$ and DMAP and solution B had $\frac{[NbCl_5]_0}{[DMAP]_0} = 1.5$ (Figure 5.18).
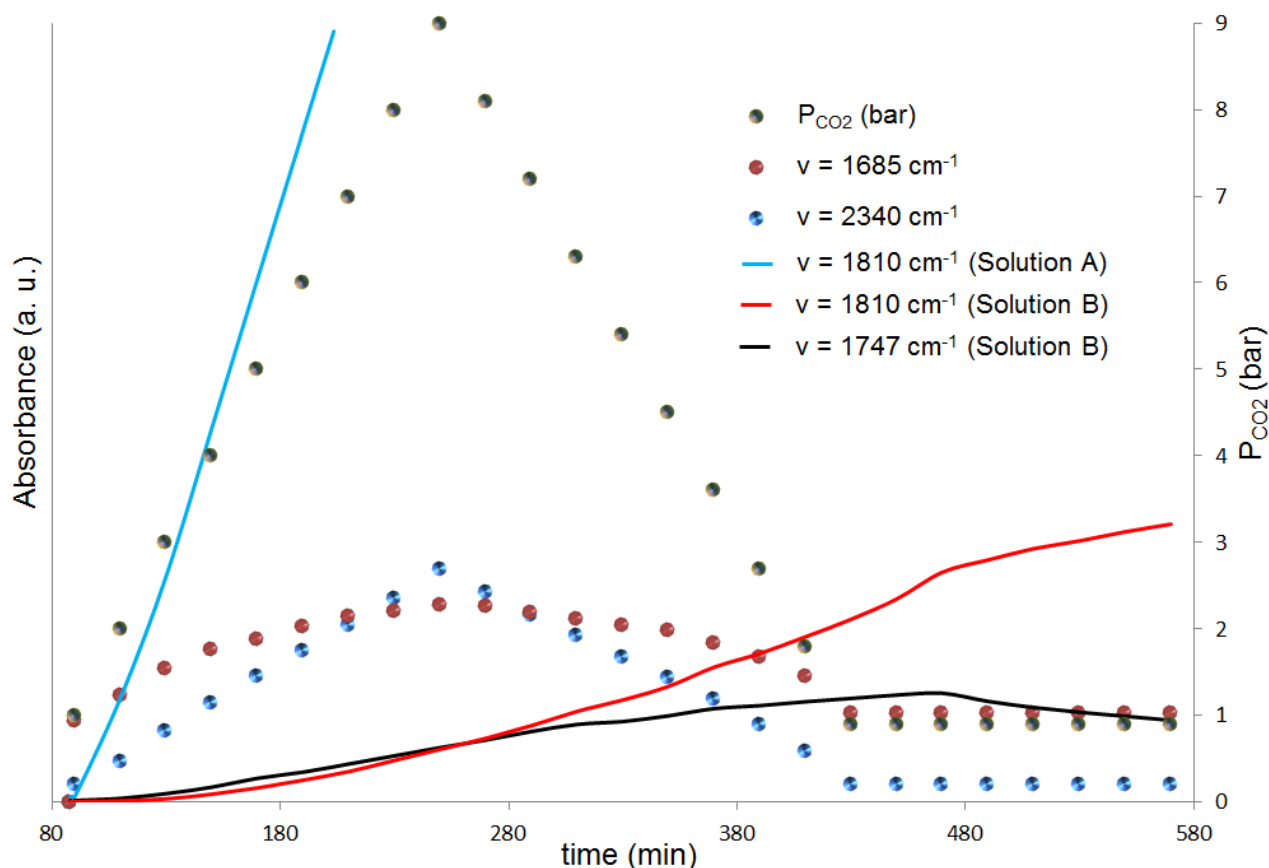
FIGURE 5.18: Time evolution of the signals at 1685 cm^{-1} for two different NbCl$_5$/DMAP solutions in propylene oxide. Solution A: $[DMAP]_0 = 0.1425$ M, $[NbCl_5]_0 = 0.1425$ M in propylene oxide; Solution B: $[DMAP]_0 = 0.1425$ M, $[NbCl_5]_0 = 0.21$ M in propylene oxide when CO$_2$ pressure is varied at regular intervals.

The IR spectra of the two solutions differ only for the profile of propylene carbonate formation and not the intermediates formed (**21**, **22a** and **26a**). For solution A, propylene carbonate forms immediately after the introduction of CO$_2$. As expected, no propylene carbonate is observed at 1 bar of CO$_2$ for solution B due to the lack of free co-catalyst. When the CO$_2$ pressure is higher than 3 bar, small amounts of propylene carbonate were observed in solution B with less than 3% conversion at the end of the reaction.

A peak at 1747 cm^{-1} was also observed and this was consistent with the carbonyl stretching in linear carbonates or polycarbonates. In this case, the formation of propylene carbonate seems to come from the back-biting of the linear polycarbonate to yield the thermodynamically favoured cyclic carbonate. This was confirmed by releasing the CO$_2$ pressure and observing the peak at 1747 cm^{-1} decrease in intensity while the peak at 1810 cm^{-1} (corresponding to propylene carbonate) grows. The formation of polymeric material at higher CO$_2$ pressures in solution B suggests that in the absence of free nucleophile, the hemicarbonate formed cannot be converted to propylene carbonate by ring closure (step C, Scheme 5.2). However, it allows for further

propylene oxide or CO_2 insertion into the M-O bond. This observation hints at the involvement of the co-catalyst in the ring closure step.

Based on all the mechanistic data compiled so far, a reaction sequence is presented as the sucession of three steps:

1. $\text{Nu} + \text{NbCl}_5 + \text{ propylene oxide } \rightleftharpoons \mathbf{22}$
2. $\mathbf{22} + CO_2 \rightleftharpoons \mathbf{26}$
3. $\mathbf{26} + \text{Nu} \longrightarrow \text{ propylene carbonate } + 2\,\text{Nu} + \text{NbCl}_5$
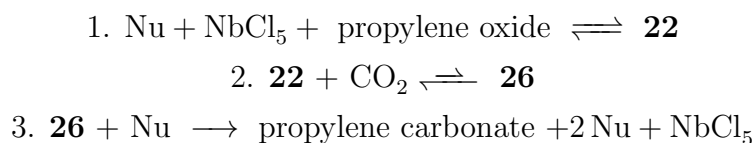
In the first step, **22** is first formed from the equilibrium shown in Scheme 5.2. A reversible CO_2 insertion occurs, giving **26**. At 1 bar of CO_2 the equilibrium is strongly shifted to the left side as seen in Figure 5.15. Finally, the nucleophile assists in the ring closure step leading to the formation of propylene carbonate.

This led to the hypothesis that the nucleophile-aided step of ring closure is the slow step of the catalytic cycle. The reaction rate would then depend on the concentration of free co-catalyst available and concentration of hemicarbonate **26**, and therefore, on CO_2 pressure. It was also shown earlier in Sections 5.2.2 and 5.2.3 that the reaction is first order with respect to the co-catalyst when $\frac{[\text{co}-\text{catalyst}]_0}{[\text{NbCl}_5]_0} \geqslant 1$. For higher concentrations of nucleophile, no further increase in the reaction rate is observed at 1 bar of CO_2. This may be because under such conditions, the concentration of the co-catalyst far exceeds the concentration of the hemicarbonate in solution at 1 bar CO_2, which becomes the only rate limiting factor.

5.2.9 Dependence of the Reaction on Hemicarbonate Concentration

A series of *in situ* IR experiments for both $NbCl_5$/TBAB and $NbCl_5$/DMAP systems were then conducted to determine the reaction dependence on the hemicarbonate concentration. Equimolar amounts of $NbCl_5$ and co-catalyst were used in this reaction. 0.5 or 1 bar of CO_2 was added every 5 minutes until the CO_2 pressure reached 5 bar and the IR spectrum was collected every 30 seconds. The values corresponding to the intensity of propylene carbonate at 1810 cm^{-1} measured at a given CO_2 pressure were plotted against time and fitted linearly as shown in Figure 5.19.
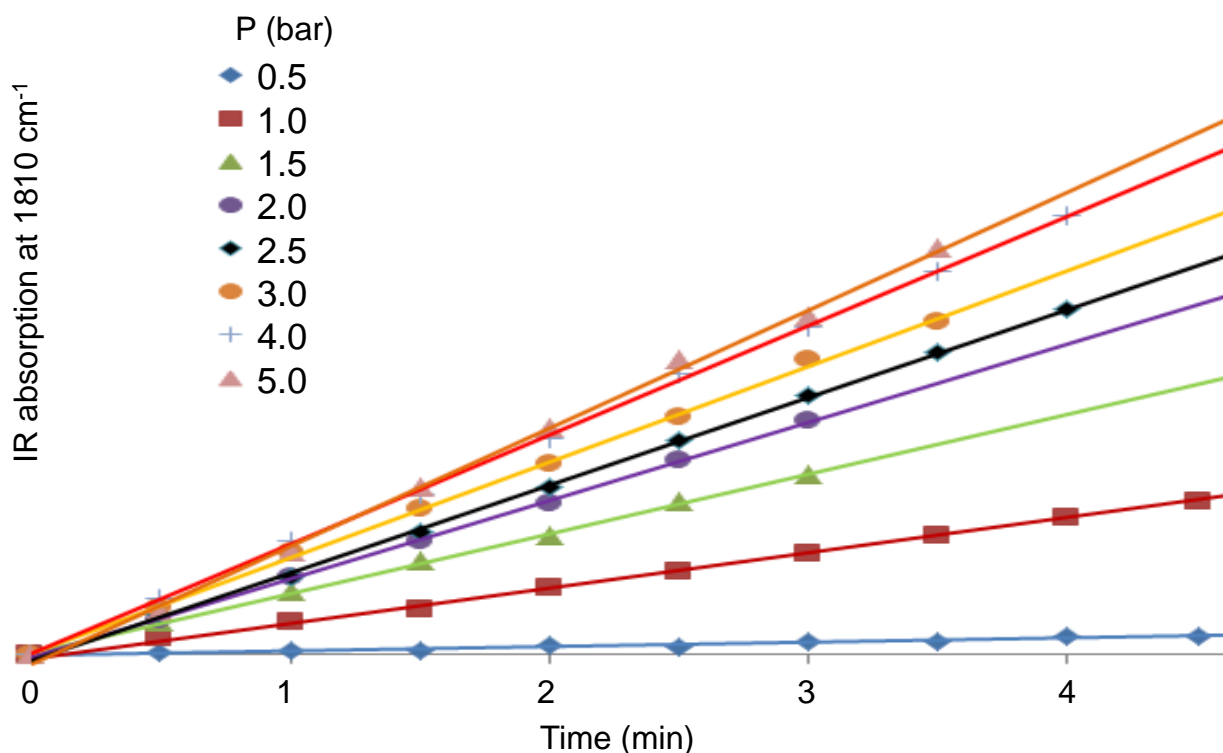
FIGURE 5.19: Profiles of propylene carbonate formation against time at different CO_2 pressures.

For both $NbCl_5$/DMAP and $NbCl_5$/TBAB systems, the intensity of the signals relative to the carbonyl stretching of CO_2 (2340 cm^{-1}), **26a** (1685 cm^{-1}) or **26b** (1683 cm^{-1}) were correlated with the initial rate of propylene carbonate formation (k_{obs}) at a given CO_2 pressure. A linear correlation between the concentration of each species and the intensity of the IR bands was assumed.

DMAP as Co-Catalyst

For a $NbCl_5$/DMAP system, CO_2 was introduced 90 minutes after the initial mixing of the reagents to account for the induction time needed to convert **21** to **22**. The CO_2 pressure was increased stepwise every ten minutes. The k_{obs} values obtained and the values relative to I_{26a} (intensity of the C=O absorption of **26a** at 1685 cm^{-1} and I_{CO_2} (intensity of C=O absorption for CO_2 at 2340 cm^{-1}) were used to determine the reaction order with respect to **26a** and CO_2. The kinetic data obtained at 25°C is summarised in Table 5.11. By plotting k_{obs} versus I_{26a}, a linear correlation between the reaction rate and the concentration of hemicarbonate **26a** in

solution is obtained (Figure 5.20, left). The corresponding logarithmic plot shows first order kinetics with respect to **26a** (Figure 5.20, right, gradient is 0.99).

TABLE 5.11: k_{obs}, I_{26a} and I_{CO_2} at different CO_2 pressures.

Entry	P_{CO2} (bar)	k_{obs} $(mol \cdot L^{-1} \cdot min^{-1})$	I_{26a}	I_{CO_2}
1	0.50	0.00015	0.0020	0.018
2	0.75	0.00064	0.0054	0.078
3	1.0	0.0010	0.0087	0.14
4	1.5	0.0016	0.014	0.26
5	2.0	0.0020	0.019	0.37
6	2.5	0.0023	0.024	0.48
7	3.0	0.0025	0.027	0.58
8	4.0	0.0029	0.033	0.76
9	5.0	0.0029	0.035	0.84

The plot of k_{obs} against I_{CO_2} does not depend linearly on the concentration of CO_2 in solution (and therefore pressure) as an effect of the progressive saturation of the equilibrium of formation
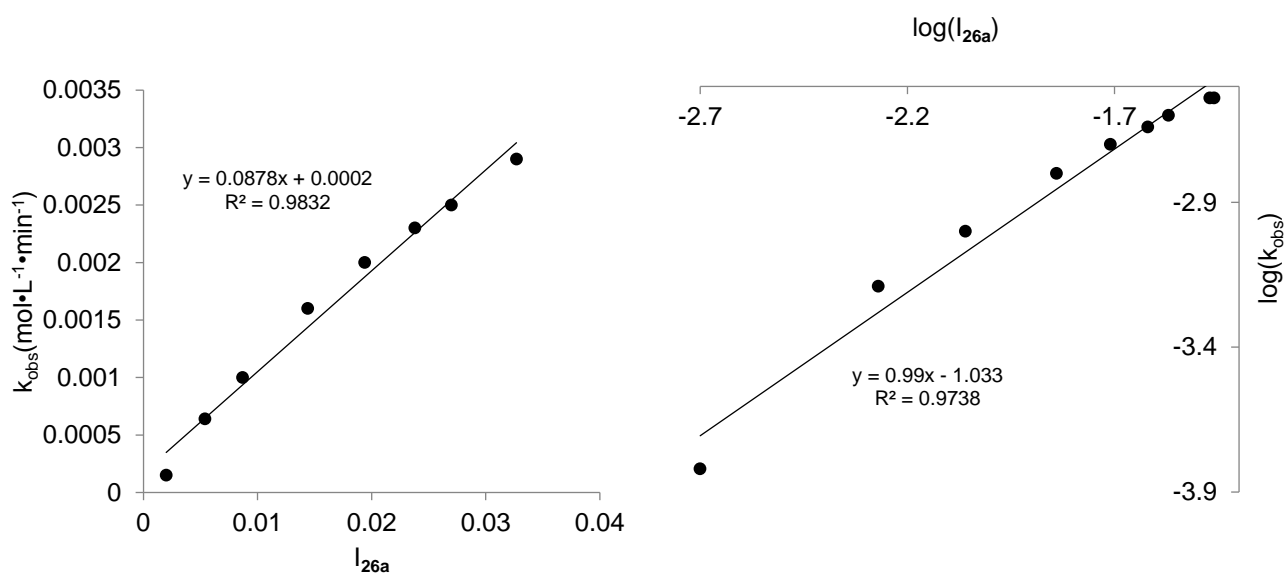
FIGURE 5.20: Dependence of reaction rate, (k_{obs}) on hemicarbonate concentration (I_{26a}) (left) and corresponding logarithmic plot (right).
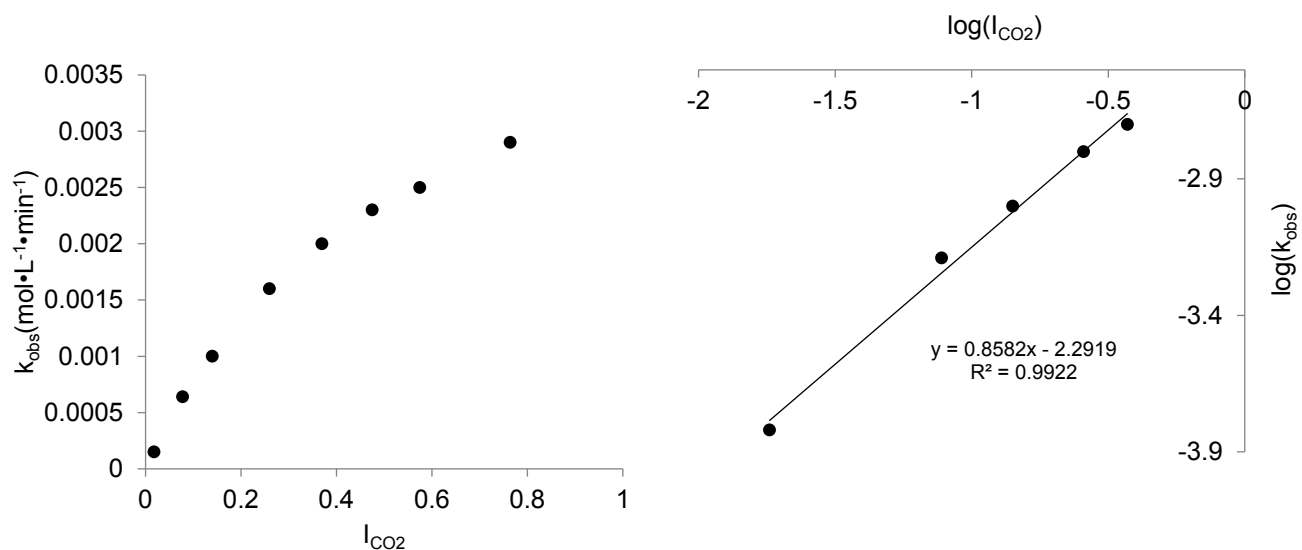
FIGURE 5.21: Dependence of reaction rate, (k_{obs}) on CO_2 concentration (I_{CO_2}) (left) and corresponding logarithmic plot for $P_{CO_2} \leqslant 2$ bar (right).

TBAB as Co-Catalyst

For the $NbCl_5$/TBAB system, CO_2 was introduced after 5 minutes of mixing, just enough to ensure complete dissolution of $NbCl_5$ and TBAB in propylene oxide due to the absence of an induction time for TBAB. The kinetic data obtained at 25°C is summarised in Table 5.12. By plotting k_{obs} versus I_{26b}, a linear correlation between the reaction rate and the concentration of hemicarbonate **26b** in solution is obtained (Figure 5.22, left). The corresponding logarithmic plot shows first order kinetics with respect to **26a** (Figure 5.22, right, gradient is 1.03).

TABLE 5.12: k_{obs}, I_{26b} and I_{CO_2} at different CO_2 pressures.

Entry	P_{CO2} (bar)	k_{obs} $(mol \cdot L^{-1} \cdot min^{-1})$	I_{26b}	I_{CO_2}
1	0.5	0.00080	0.0043	0.0040
2	1.0	0.0063	0.034	0.11
3	1.5	0.011	0.056	0.22
4	2.0	0.014	0.069	0.34
5	2.5	0.016	0.079	0.45
6	3.0	0.017	0.087	0.54
7	4.0	0.020	0.095	0.71
8	5.0	0.021	0.10	0.86
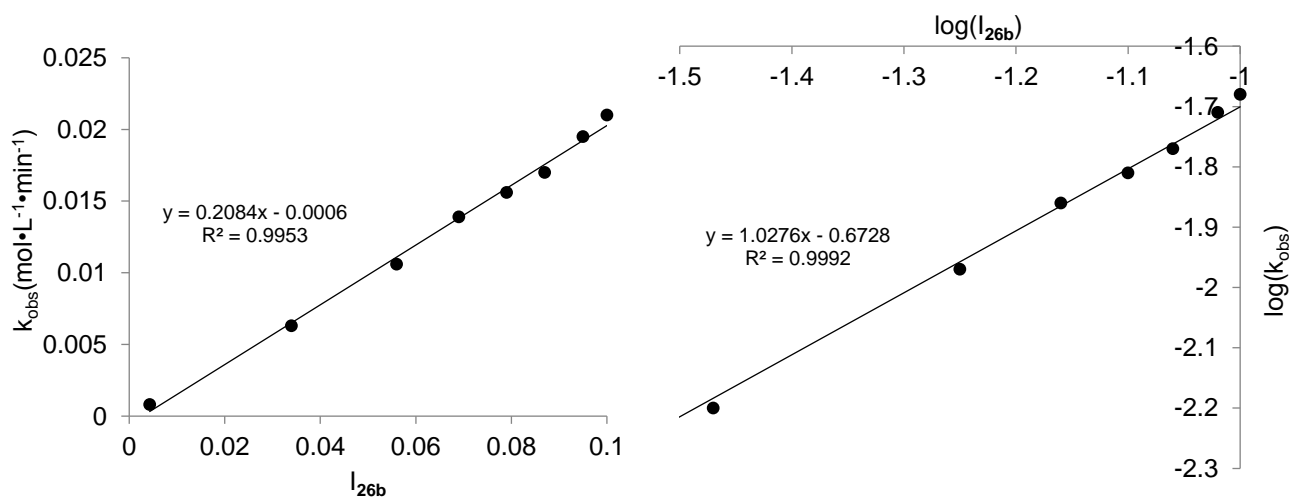
FIGURE 5.22: Dependence of reaction rate, (k_{obs}) on hemicarbonate concentration (I_{26b}) (left) and corresponding logarithmic plot (right).

The plot of k_{obs} against I_{CO_2} (Figure 5.23, left) shows that the reaction rate does not have a linear dependence on the CO_2 concentration (and therefore pressure) in solution as an effect of
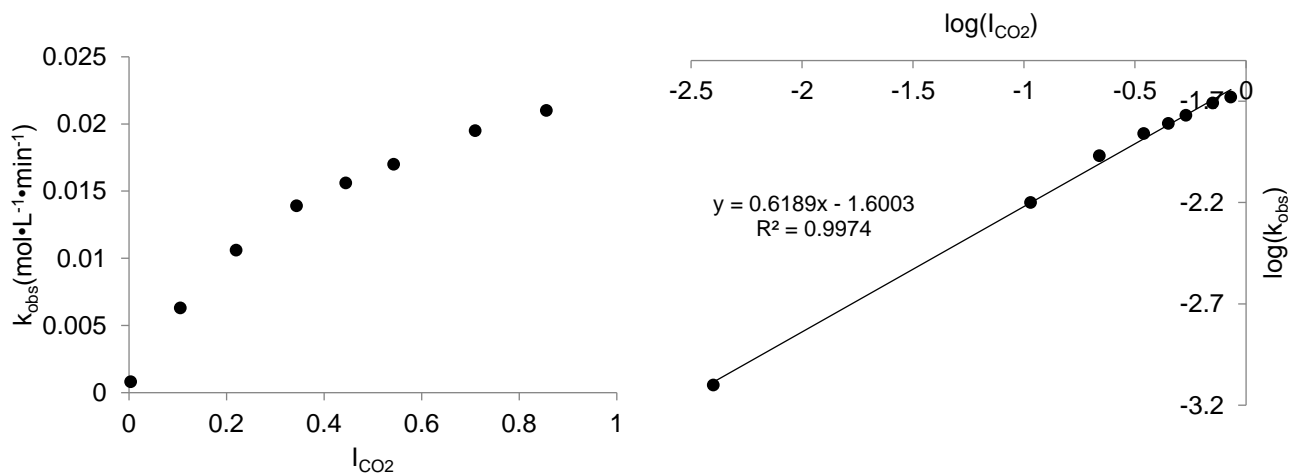
FIGURE 5.23: Dependence of reaction rate, (k_{obs}) on CO_2 concentration (I_{CO_2}) (left) and corresponding logarithmic plot for $P_{CO_2} \leqslant 2$ bar (right).

5.2.10 The Big Picture

The data collected in the previous Section 5.2.9 allowed for the correlation of the initial reaction rate of propylene carbonate formation with the concentration of hemicarbonate and CO_2 in solution at a given CO_2 pressure. The data is presented in Figure 5.24 and Figure 5.25.
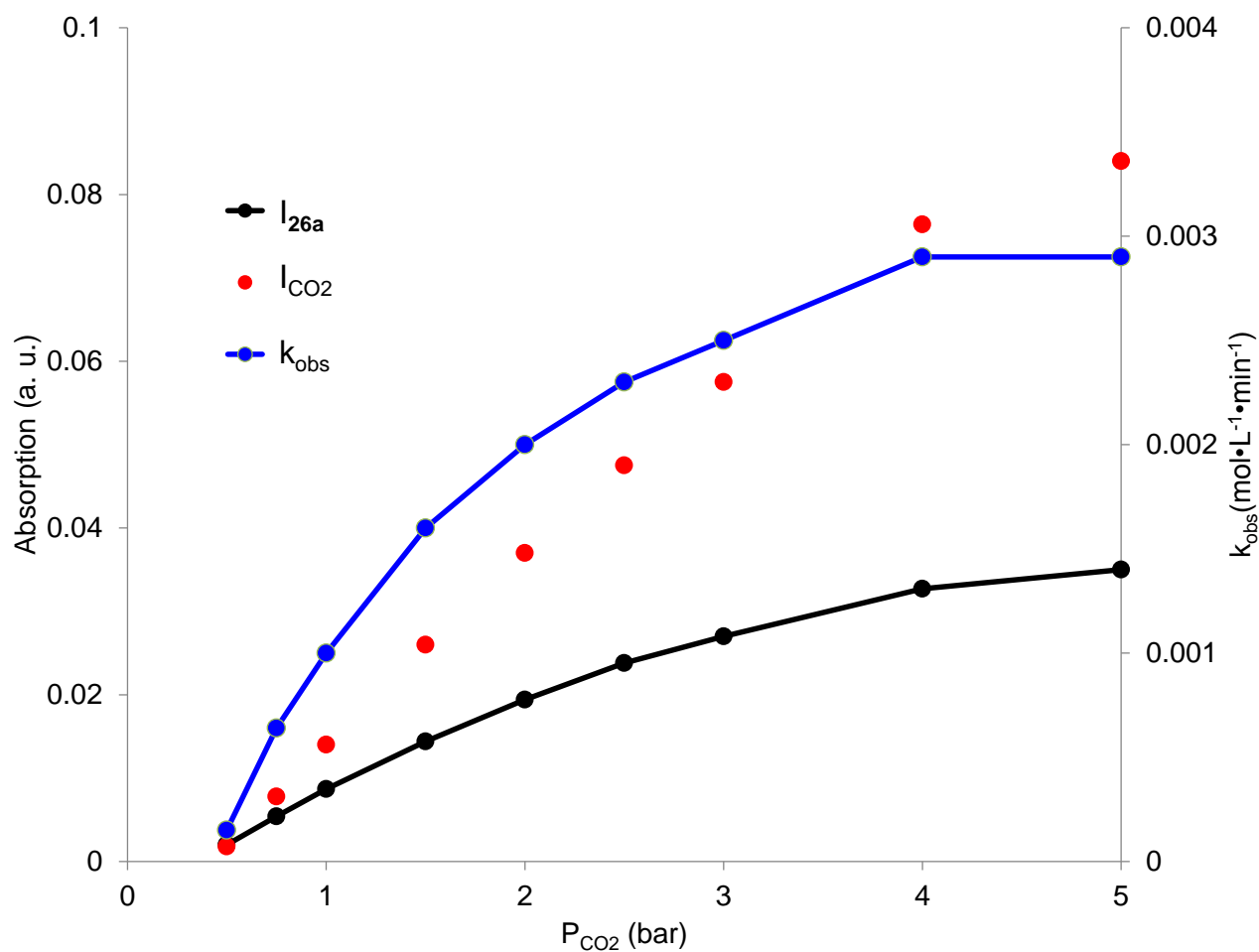
FIGURE 5.24: Pressure dependence of the initial rate of propylene carbonate formation, $k_{obs}(mol \cdot L^{-1} \cdot min^{-1})$, for NbCl$_5$/DMAP (blue line), IR absorbance of **26a** (black line), IR absorbance of CO$_2$ in solution (red) as functions of CO$_2$ pressure.
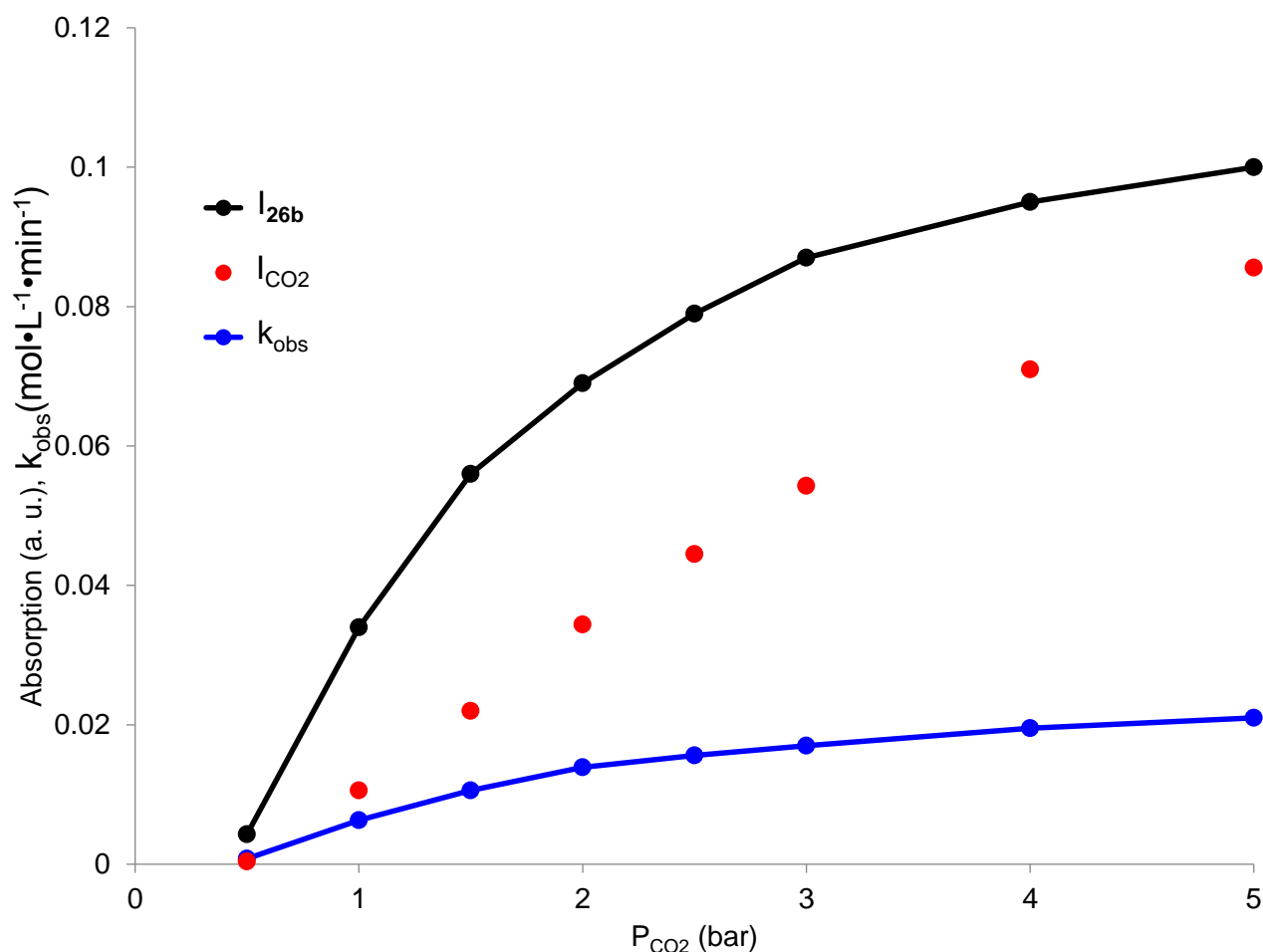
FIGURE 5.25: Pressure dependence of the initial rate of propylene carbonate formation, $k_{obs}(mol \cdot L^{-1} \cdot min^{-1})$, for $NbCl_5$/TBAB (blue line), IR absorbance of **26b** (black line), IR absorbance of CO_2 in solution (red) as functions of CO_2 pressure.

The results obtained are similar for both $NbCl_5$/DMAP and $NbCl_5$/TBAB systems. The concentration of CO_2 increases linearly with the CO_2 pressure, showing that no saturation of the solution by CO_2 is observed in this pressure range. In both cases, the reaction rate does not depend linearly on CO_2 pressure. The concentration of hemicarbonates **26a** and **26b** also does not increase linearly with CO_2 pressure and reaches a plateau because of the progressive saturation of the equilibrium between **22** and CO_2. As an effect, only a very limited pressure is observed for CO_2 pressures higher than 3 bar. At low CO_2 pressures ($\leqslant 2$ bar), the reaction order with respect to CO_2 is slightly lower than 1 (0.86 for DMAP and 0.64 for TBAB). However, in both systems, the reaction order with respect to hemicarbonates **26a** and **26b** is 1. This proves the assumption that the nucleophile assisted step of propylene carbonate liberation from the hemicarbonate is the rate limiting step of the reaction.

The overall mechanism showing the bifunctional role of the co-catalyst is proposed in Scheme 5.5.
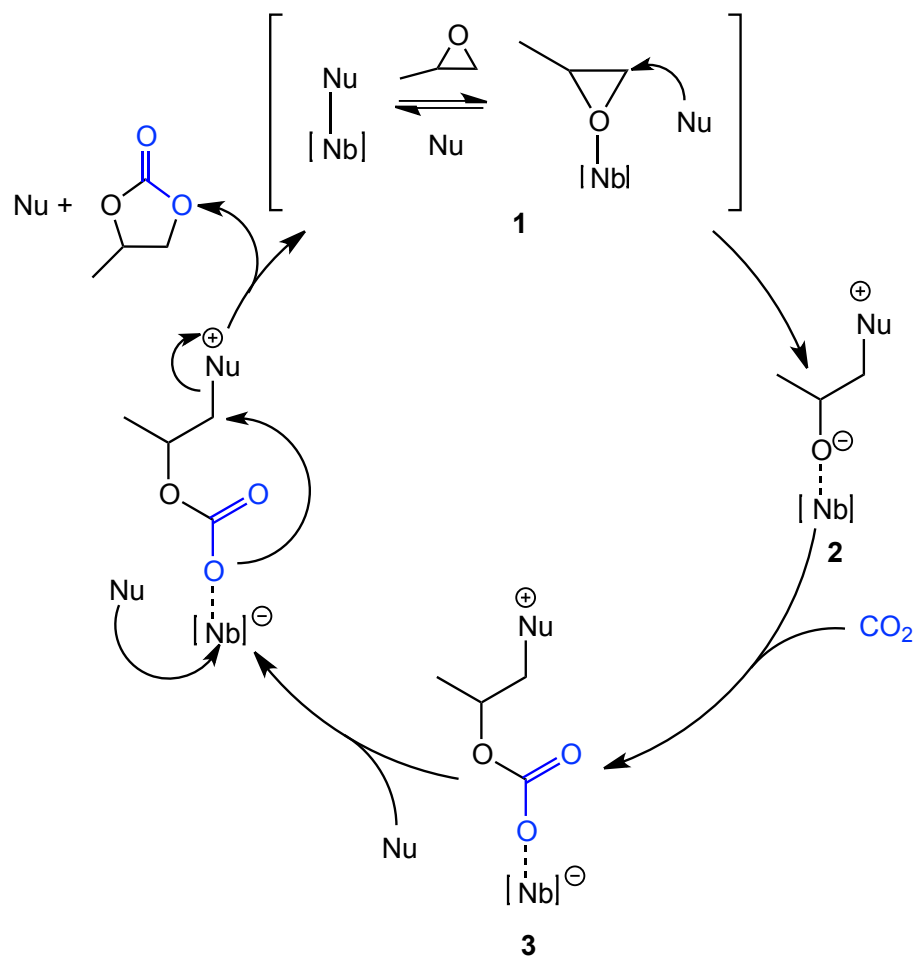
SCHEME 5.5: The overall proposed catalytic cycle showing the bifunctional role of the co-catalytic nucleophile.

The nucleophile first takes part in the ring opening of the epoxide, forming the [Nb]-[propylene oxide]-[nucleophile] adduct **2** which then undergoes CO_2 insertion to form the hemicarbonate **3**. Another nucleophile molecule then enters the catalytic cycle and helps to liberate the hemicarbonate by closing the ring.

5.3 Experimental

5.3.1 General Information and Materials

All air sensitive manipulations were performed in an inert argon atmosphere using Schlenk techniques or a glovebox.

Chemicals

Propylene oxide was purchased from Sigma Aldrich and refluxed over CaH_2 for at least 6 hours before distillation and degassed by the freeze-pump-thaw method. Tetra-n-butylammonium bromide (TBAB) was molten at 100-150 °C in a Schlenk tube, stirred under vacuum for 6 hours and stored in a glovebox. N,N-dimethyl-4-aminopyridine (DMAP, 99%) and $NbCl_5$ (99.9%) were purchased from Acros Organics and Sigma Aldrich respectively and used as received.

Solvents

$CDCl_3$ was dried in the usual method, degassed and stored in the glovebox over molecular sieves.

5.3.2 Instruments

Both 1D and 2D NMR experiments were recorded on 500 or 600 MHz Bruker Advance instruments. Chemical shifts are reported in ppm (δ, relative to TMS) using the solvent residual peak as an internal standard.

In situ infrared spectroscopy was performed on a Mettler Toledo ReactIR 45/Multimax RB 04-50 station equipped with 50 mL stainless steel autoclaves with DiComp diamond probes at the bottom as multiple reflection ATR element. The autoclaves were connected to a CO_2 cylinder by a Mettler Toledo LMPress60 pressure controller to provide gas dosage and constant pressure throughout the reaction.

The set-up in Figure 5.26 was used for all the reactions in this study. The stainless steel autoclave was heated for at least 4 hours at 130 °C under vacuum before each experiment. For each experiment, suitable amounts of the catalytic components ($NbCl_5$ and DMAP or TBAB) were added to the reaction autoclave under a stream of argon. Subsequently, propylene oxide was added through a syringe and the mixture was stirred at 500 r.p.m. through a mechanical stirrer. CO_2 was dosed and kept at the desired pressure during the whole course of the experiment by the automated pressure controller. The ATR-IR spectrum of the reaction was collected every 30, 45 or 60 seconds through the window at the bottom of the reaction vessel. For all reactions in this study the temperature was kept constant at 25 °C through a thermostat.
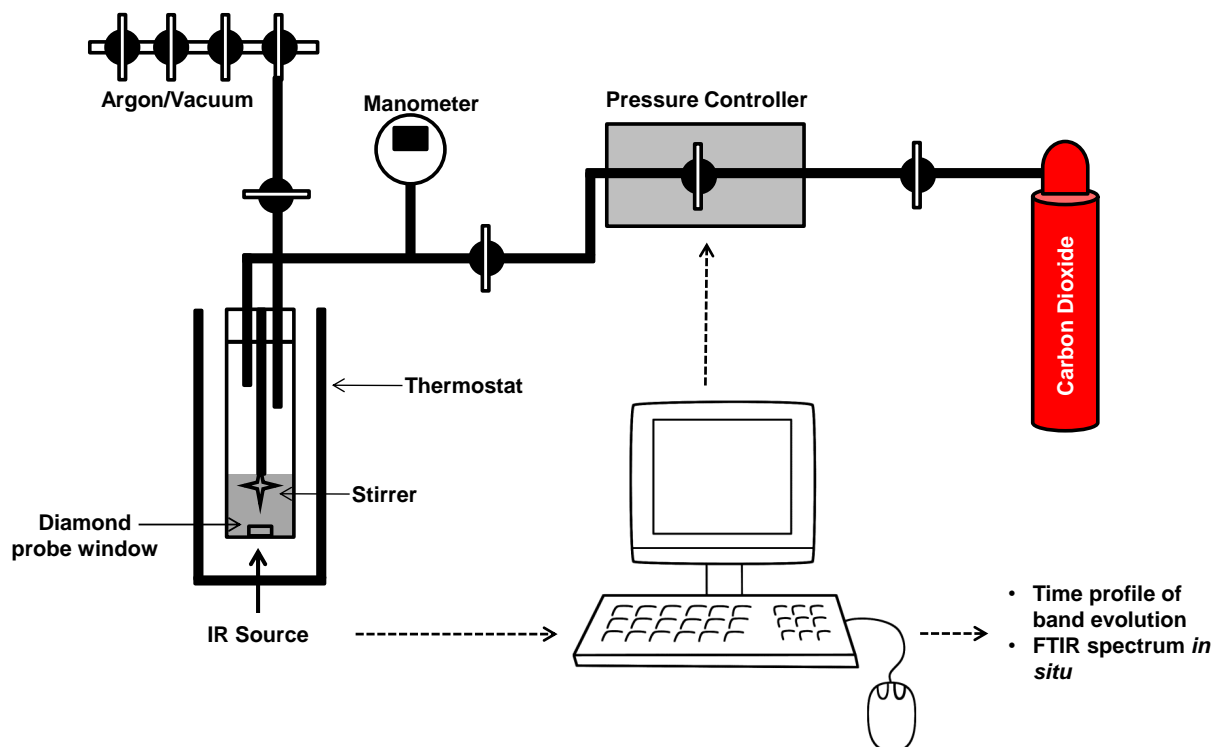
FIGURE 5.26: Experimental reaction setup: The *in situ* IR spectra collected periodically can be compiled by a software to give the time-evolution profile of a particular band over time.

5.3.3 Kinetic Experiments

Determining reaction order of $NbCl_5$ in the $NbCl_5$/TBAB catalysed synthesis of propylene carbonate

TBAB (367 mg, 1.14 mmol, 1 mol %) and the corresponding amount of $NbCl_5$ were added to the reaction vessel under a stream of argon. Propylene oxide was added through a syringe (8 mL, 114 mmol) at 25 °C. The mixture was stirred mechanically for 5 minutes at 500 r.p.m. to allow for proper mixing. The stirring rate was kept constant throughout the whole course of the experiment. After this period, 1 bar of CO_2 was introduced. The CO_2 pressure was kept constant throughout the experiment with the losses in CO_2 pressure due to conversion to propylene carbonate being immediately compensated by the automated pressure regulator. The ATR-IR spectrum of the reaction was collected every 60 s through the window at the bottom of the reaction vessel. The evolution of the carbonyl signal of PC at 1810 cm^{-1} was monitored.

Determining reaction order of $NbCl_5$ in the $NbCl_5$/DMAP catalysed synthesis of propylene carbonate

The procedures were repeated with DMAP (139 mg, 1.14 mmol, 1 mol%).

Determining reaction order of co-catalyst in the NbCl$_5$-Co-catalyst catalysed synthesis of propylene carbonate

The procedures were repeated with NbCl$_5$ (307 mg, 1.14 mmol, 1 mol%) and the appropriate amount of co-catalyst was added.

5.3.4   NMR Experiments with DMAP as co-catalyst

***In situ* NMR studies**

DMAP (16.6 mg, 0.136 mmol) was dissolved in propylene oxide (2 mL) in a glovebox. The clear solution was slowly added by syringe to an appropriate amount of NbCl$_5$ in a vial. An aliquot of the clear solution (0.4 mL) was then transferred into a J. Young tube and CDCl$_3$ (0.1 mL) was added to the sample to allow locking of the magnetic field and as an internal standard for signal integration. ^{1}H NMR was measured every 2.5 minutes for 90 minutes. The peaks were integrated with reference to the residual CDCl$_3$ peak and the relative abundances were calculated to obtain the graphs in Figure 5.11.

5.3.5   *In situ* IR Experiments and Investigation on the Reaction Intermediates

Reaction initiation by addition of co-catalyst

DMAP (111.4 mg, 0.912 mmol, 0.8 mol%, 0.114M) and NbCl$_5$ (308 mg, 1.14 mmol, 1 mol%, 0.143M, $\frac{[NbCl_5]_0}{[DMAP]_0} = 1.25$) were added to the *in situ* IR autoclave under a stream of argon. Propylene oxide (8 mL) was then added by syringe and the solution was stirred for 90 minutes at 25°C under argon. After the induction period, CO$_2$ (1 bar) was added. No propylene carbonate formation was observed by IR in the next 30 minutes. The reactor was then depressurised by the automated pressure regulator. After a period of stabilization, the reactor was opened under a stream of argon and DMAP (27.9 mg, 0.228 mmol, 0.2 mol%) was added to set $\frac{[NbCl_5]}{[DMAP]} = 1$. Under these conditions, following the re-addition of CO$_2$ (1 bar), the formation of propylene carbonate began after an induction time of about 15 minutes.

In a separate experiment, TBAB (73.5 mg, 0.228 mmol, 0.2 mol%) was added in the place of DMAP.

Identification of hemicarbonates 26a and 26b

For **26a**: DMAP (122.2 mg, 1 mmol) and NbCl$_5$ (405.3 mg, 1.5 mmol, $\frac{[NbCl_5]_0}{[DMAP]_0} = 1.5$) were

added to the *in situ* IR autoclave under a stream of argon. Propylene oxide (8 mL) was then added by syringe. After the 90 minute induction period, the IR spectrum was measured and used as a background for all successive measurements. As no propylene carbonate forms at this $NbCl_5$/DMAP ratio, the only signals that appear should belong to CO_2 ($\nu_{C=O} = 2340$ cm^{-1}) and its products of insertion and coordination. Initially 0.5 bar of CO_2 was added by the automated pressure controller, after which each step of CO_2 addition was carried out in 1 minute intervals for 20 minutes to raise the pressure to 1 bar. Subsequently, 1 bar of CO_2 was added to the system every 20 minutes up to 9 bar of CO_2. By subtraction of the last spectrum recorded before CO_2 addition, the signals belonging to the products of CO_2 were revealed (Figure 5.14).

The pressure controller was then programmed to release 1 bar of CO_2 from the reaction vessel every 20 minutes. Plotting the intensity of the signals relative to the hemicarbonate at 1690 cm^{-1} and CO_2 at 2340 cm^{-1} against time, Figure 5.15 was obtained.

For **26b**: The same method was used with TBAB (322.4 mg, 1 mmol, 0.14 M) and $NbCl_5$ (405.3 mg, 1.5 mmol, 0.21 M) in propylene oxide (8 mL) The ratio of $\frac{[NbCl_5]_0}{[TBAB]_0} = 1.5$ to identify the signals corresponding to **26b**.

Determination of reaction order according to hemicarbonates 26a, 26b and CO_2
For $NbCl_5$/DMAP: $NbCl_5$ (270.2 mg, 1 mmol) and DMAP (122.2 mg, 1 mmol) were dissolved in propylene oxide (7 mL, 100 mmol) in the autoclave. The solution was stirred mechanically at 500 r.p.m. CO_2 was added 90 minutes after initial mixing and pressure was increased stepwise every 10 minutes, with *in situ* IR measurements being collected every 45 seconds. Given the low absolute reaction rates, the propylene carbonate formation data at 0.5 and 0.75 bar were collected over a 20 minute period.

For $NbCl_5$/TBAB: $NbCl_5$ (270.2 mg, 1 mol) and TBAB (322.4 mg, 1 mmol) were dissolved in propylene oxide (7 mL, 100 mmol) and stirred mechanically at 500 r.p.m. for 5 minutes to allow complete dissolution of all solids. 0.5 bar CO_2 was added every 5 minutes until CO_2 pressure reached 5 bar. *In situ* IR spectrum was collected every 30 seconds.

5.4   Conclusion

The fine dynamics of catalyst and co-catalyst cooperation in the $NbCl_5$ catalysted synthesis of propylene carbonate from CO_2 and propylene oxide has been thoroughly studied. It has been established that the $NbCl_5$/DMAP or $NbCl_5$/TBAB pair showed the most promise in screening studies to convert propylene oxide into propylene carbonate. The catalyst pair is simple and inexpensive and works well at ambient temperature and low pressure. In addition to these co-catalysts, ionic liquids were also used. A notable difference between DMAP and TBAB as

co-catalyst is the presence of an induction time for DMAP, as the acid-base adduct is converted into a metal-alkoxide species.

The reaction order with respect to the catalyst and co-catalysts has been determined by kinetic analysis. It was found that $NbCl_5$ shows first order kinetics with both co-catalysts at lower concentrations ($\frac{[NbCl_5]_0}{[co-catalyst]_0} \leqslant 0.5$). When this ratio approaches 1, a decrease in reaction order was found. Accordingly, both co-catalysts also show first order kinetics when $1 \leqslant \frac{[co-catalyst]_0}{[NbCl_5]_0} \leqslant 2$.

An inhibition in the reaction rates was observed when the concentration of catalyst exceeds that of co-catalyst. NMR studies showed that this was due to the lack of free co-catalyst available in the case of DMAP. This finding indicated that there might be an additional role of the co-catalyst but with only one molecule being involved in the rate determining step (reaction order with respect to co-catalyst is 1).

By identifying the intermediates of CO_2 insertion by supressing the formation of propylene carbonate and literature, it was found that the activation of CO_2 inserts in the Nb-O bond unassisted and that free co-catalyst molecules are not required at this point. Upon studying the effects of CO_2 pressure on propylene carbonate formation, it was discovered that polymeric material was formed at higher CO_2 pressures in a solution without free co-catalyst. This suggests that the co-catalyst is involved in a ring closing step as the ring cannot be closed in the absence of co-catalyst.

Further investigations of the reaction dependence on the CO_2 intermediates (hemicarbonates) showed first order kinetics with respect to the hemicarbonates **26a** and **26b**. At low CO_2 pressures, the reaction order with respect to CO_2 was calculated to be slightly lower than 1 for both co-catalysts. This ultimately showed that the co-catalyst again assists in the liberation of propylene carbonate from the hemicarbonate, explaining the bifunctional role of the co-catalyst.

This mechanistic study contributes to the articles:

1. Amylia Abdul Ghani, Antoine Monassier, Julien Sofack-Kreutzer, Valerio D'Elia, Jeremie D. A. Pelletier, Markus Drees, Mirza Cokoja, Jean-Marie Basset and Fritz E. Kühn, "The fine dynamics of catalyst and co-catalyst cooperation in the $NbCl_5$ catalysed synthesis of cyclic carbonates from CO_2 and epoxides" *in preparation*

2. Michael E. Wilhelm, Michael H. Anthofer, Amylia Abdul Ghani, Robert M. Reich, Valerio D'Elia, Jean-Marie Basset, Mirza Cokoja and Fritz E. Kühn, "Niobium (V) chloride and imidazolium bromides as efficient dual catalyst system for the cycloaddition of carbon dioxide and propylene oxide" *in preparation*

Investigations were also performed with $Nb(OEt)_5$ as a side project but were not discussed as the focus of the study was on $NbCl_5$. The work with $Nb(OEt)_5$ contributes to part of the article:

B. Dutta, J. Sofack-Kreutzer, A. Abdul Ghani, V. D'Elia, J. D. A. Pelletier, M. Cokoja, F. E. Kühn and J. M. Basset, "Nucleophile directed selectivity towards linear carbonates in the $Nb(OEt)_5$ catalysed cycloaddition of CO_2 and propylene oxide" *submitted*

Chapter 6

Summary and Outlook

The oxidative coupling of ethylene or styrene and CO_2 on palladium complexes to form palladalactones was carried out. While most of the palladium complexes coupled to the alkene with ease, under the working conditions (4-10 bar CO_2, 2-8 hours, 0 °C), the palladium-alkene complexes were inactive towards CO_2. Instead, a peroxocarbonate was formed by the oxidative coupling of CO_2 and O_2 with $Pd(PCy_3)_2$.

Palladalactones were also synthesized by "bench" methods to study their ability to undergo β-hydride elimination by methyl iodide and methyl triflate. It was found that methyl triflate was the best methylating agent based on atom economy, reaction rates and selectivity. Palladalactones were also more susceptible to ring opening as compared to nickelalactones. This would be of particular future interest if the palladalactone could be obtained by the oxidative coupling of ethylene and CO_2 as the catalytic cycle shown in Scheme 4.6 could be further studied. In addition, a method to convert the palladium-hydride formed back to the palladium (0) species (therefore closing the cycle) is needed.

The mechanism of the $NbCl_5$/DMAP and $NbCl_5$/TBAB mediated synthesis of propylene carbonate from propylene oxide was studied. It was found that the co-catalyst served a bifunctional role in the catalytic cycle and a final reaction mechanism was proposed in Scheme 5.5. The co-catalyst is first involved in opening the epoxide ring, preparing it for CO_2 insertion. The resulting hemicarbonate then needs a second molecule of co-catalyst to aid in closing the carbonate ring, forming propylene carbonate. This mechanistic study gives a clear picture of the relationship between catalyst and co-catalyst for this reaction and would be useful for further optimization studies.

Bibliography

[1] Mikkelsen, M.; Jorgensen, M.; Krebs, F. C. *Energy & Environmental Science* **2010**, *3*, 43–81.

[2] Wojtowicz, M. A.; Pels, J. R.; Moulijn, J. A. *Fuel Processing Technology* **1993**, *34*, 1–71.

[3] Aresta, M.; Dibenedetto, A. *Dalton Transactions* **2007**, 2975.

[4] Boot-Handford, M. E. *et al. Energy Environ. Sci.* **2013**, –.

[5] Yang, H.; Xu, Z.; Fan, M.; Gupta, R.; Slimane, R. B.; Bland, A. E.; Wright, I. *Journal of Environmental Sciences* **2008**, *20*, 14–27.

[6] Song, C. *Catalysis Today* **2006**, *115*, 2–32.

[7] McLinden, M. O.; Lemmon, E. W.; Jacobsen, R. T. *Int. J. Refrig.* **1998**, *21*, 322–338.

[8] de Ven, M. V. *Cerevisia* **2011**, *36*, 103–105.

[9] Godec, M. L.; Kuuskraa, V. A.; Dipietro, P. *Energy & Fuels* **2013**, *27*, 4183–4189.

[10] Jessop, P. G.; Ikariya, T.; Noyori, R. *Nature* **1994**, *368*, 231–233.

[11] Ouyang, X.; Chen, J. W.; Zhang, X. G. *Geological Bulletin of China* **2010**, *29*, 1655–1661.

[12] North, M.; Pasquale, R.; Young, C. *Green Chemistry* **2010**, *12*, 1514–1539.

[13] Behr, A. *Carbon Dioxide Activation by Metal Complexes*; VCH Verlagsgesellschaft, Weinheim, Germany, 1988.

[14] Cokoja, M.; Bruckmeier, C.; Rieger, B.; Herrmann, W. A.; Kuehn, F. E. *Angewandte Chemie, International Edition* **2011**, *50*, 8510–8537.

[15] Atkins, P.; Overton, T.; Rourke, J.; Weller, M.; Armstrong, F. *Shriver and Atkins' Inorganic Chemistry*; Oxford University Press, Fifth Edition.

[16] Aresta., M.; Nobile, C. F.; Albano, V. G.; Forni, E.; Manassero, M. *J. Chem. Soc. Chem. Commun.* **1975**, 636.

[17] Aresta, M.; Nobile, C. F. *J. Chem. Soc. Dalton Trans* **1977**, 708.

[18] Dohring, A.; Jolly, P. W.; Krueger, C.; Romao, M. J. *Z. Naturforsch* **1985**, *40b*, 484.

[19] Sakaki, S.; Dedieu, A. *Inorg. Chem* **1987**, *26*, 3278.

[20] Bristow, G. S.; Hitchcock, P. B.; Lappert, M. F. *J. Chem. Soc. Chem. Commun.* **1981**, 1145.

[21] Fu, P. F.; Khan, M. A.; Nicholas, K. M. *J. Am. Chem. Soc.* **1992**, *114*, 6579.

[22] Fu, P. F.; Khan, M. A.; Nicholas, K. M. *J. Organomet. Chem.* **1996**, *506*, 49.

[23] Sakamoto, M.; Shimizu, I.; Yamamoto, A. *Organometallics* **1994**, *13*, 407.

[24] Alvarez, R.; Carmona, E.; Gutierrez-Puebla, E.; Marin, J. M.; Monge, A.; Poveda, M. L. *J. Chem. Soc. Chem. Commun.* **1984**, 1326.

[25] Gambarotta, S.; Floriani, C.; Chiesi-Villa, A.; Guastini, C. *J. Am. Chem. Soc.* **1985**, *107*, 2985.

[26] Alvarez, R.; Carmona, E.; Marin, J. M.; Poveda, M. L.; Gutierrez-Puebla, E.; Monge, A. *J. Am. Chem. Soc.* **1986**, *108*, 2286.

[27] Hirano, M.; Akita, M.; Tani, K.; Kumagai, K.; Kasuga, N. C.; Fukuoka, A.; Komiya, S. *Organometallics* **1997**, *16*, 4206.

[28] Karsch, H. H. *Chem. Ber.* **1997**, *110*, 2213.

[29] Komiya, S.; Akita, M.; Kasuga, N. C.; Hirano, M.; Fukuoka, A. *J. Chem. Soc. Chem. Commun.* **1994**, 1115.

[30] Floriani, C.; Fachninetti, G. *J. Chem. Soc. Chem. Commun.* **1974**, 615.

[31] Ishida, T.; Hayashi, T.; Mizobe, Y.; Hidai, M. *Inorg. Chem* **1992**, *31*, 4481.

[32] Gibson, D. H. *Chem. Rev.* **1996**, *96*, 2063–2095.

[33] Herskovitz, T. *J. Am. Chem. Soc.* **1977**, *99*, 2391–2392.

[34] Calabrese, J. C.; Herskovitz, T.; Kinney, J. B. *J. Am. Chem. Soc.* **1983**, *105*, 5914–5915.

[35] Fachninetti, G.; Floriani, C.; Zanazzi, P. F. *J. Am. Chem. Soc.* **1978**, *100*, 7405.

[36] Gambarotta, S.; Arena, F.; Floriani, C.; Zanazzi, P. F. *J. Am. Chem. Soc.* **1982**, *104*, 5082.

[37] Tanaka, K.; Ooyama, D. *Coordination Chemistry Reviews* **2002**, *226*, 211.

[38] Tanaka, H.; Nagao, H.; Peng, S. M.; Tanaka, K. *Organometallics* **1992**, *11*, 1450.

[39] Castro-Rodriguez, I.; Nakai, H.; Zakharov, L. N.; Rheingold, A. L.; Meyer, K. *Science* **2004**, *305*, 1757.

[40] Lundquist, E. G.; Huffmann, J. C.; Folting, K.; Mann, B. E.; Caulton, K. G. *Inorg. Chem.* **1990**, *29*, 128.

[41] Field, J. S.; Haines, R. J.; Sundermayer, J.; Woollam, S. F. *J. Chem. Soc. Dalton Trans.* **1993**, 2735.

[42] Litz, K. E.; Henderson, K.; Gourley, R. W.; Holl, M. M. B. *Organometallics* **1995**, *14*, 5008.

[43] Seechurn, C. C. C. J.; Kitching, M. O.; Colacot, T. J.; Snieckus, V. *Angew. Chem. Int. Ed.* **2012**, *51*, 5062.

[44] Heck, R. F. *Palladium Reagents in Organic Synthesis*; Academic, New York, 1985.

[45] Miyaura, N.; Suzuki, A. *Chem. Rev.* **1995**, *95*, 2457.

[46] Fulmer, G. R.; Miller, A. J. M.; Sherden, N. H.; Gottlieb, H. E.; Nudelmann, A.; Stoltz, B. M.; Bercaw, J. E.; Goldberg, K. I. *Organometallics* **2010**, *29*, 2176–2179.

[47] Shao, Y.; Paul, J.; Axelsson, O.; Hoffmann, F. M. *J. Phys. Chem.* **1993**, *97*, 7652.

[48] Leitner, W. *Coordination Chemistry Reviews* **1996**, *153*, 257–284.

[49] Hoberg, H.; Schaefer, D. *J. Organomet. Chem* **1982**, *236*, C28.

[50] Hoberg, H.; Oster, B. W. *J. Organomet. Chem* **1984**, *266*, 321.

[51] Hoberg, H.; Baerhausen, D. *J. Organomet. Chem* **1989**, *379*, C7.

[52] Hoberg, H.; Schaefer, S.; Burkhart, G.; Krueger, C.; Romao, M. J. *J. Organomet. Chem* **1984**, *266*, 203.

[53] Fischer, K.; Jonas, K.; Misbach, P.; Stabba, R.; Wilke, G. *Angewandte Chemie, International Edition* **1973**, *12*, 943.

[54] Wilke, G. *Angew. Chem.* **1960**, *72*, 581.

[55] Bernskoetter, W. H.; Tyler, B. T. *Organometallics* **2011**, *30*, 520.

[56] Omae, I. *Coord. Chem. Rev.* **2012**, *256*, 1384.

[57] Yin, X.; Moss, J. R. *Coord. Chem. Rev.* **1999**, *181*, 27.

[58] Darensbourg, D. J.; Mueller, B. L.; Bischoff, C. J.; Chojnacki, S. S.; Reibenspies, J. H. *Inorg. Chem.* **1991**, *30*, 2418.

[59] Simpson, R. D.; Bergman, R. G. *Organometallics* **1992**, *11*, 4306.

[60] Mandal, S. K.; Ho, D. M.; Orchin, M. *Organometallics* **1993**, *12*, 1714.

[61] Buffin, B. P.; Arif, A. M.; Richmond, T. G. *J. Chem. Soc. Chem. Commun.* **1993**, 1432.

[62] Mastroilli, P.; Moro, G.; Nobile, C. F.; Latronico, M. *Inorg. Chim. Acta* **1992**, *192*, 189.

[63] Hayward, P. J.; Blake, D. M.; Wilkinson, G.; Nyman, C. J. *J. Am. Chem. Soc.* **1970**, *92*, 5873.

[64] Wakatsuki, Y.; Maniwa, M.; Yamazaki, H. *Inorg. Chem* **1990**, *29*, 4204.

[65] Yang, Z. Z.; He, L. N.; Gao, J.; Liu, A. H.; Yu, B. *Energy & Environmental Science* **2012**, *5*, 6602.

[66] Behr, A. *Angewandte Chemie, International Edition* **1988**, *27*, 661.

[67] Walther, D. *Coord. Chem. Rev.* **1987**, *79*, 135.

[68] Park, S.; Rheingold, A. L.; Roundhill, D. M. *Organometallics* **1991**, *10*, 615.

[69] Chisholm, M. H.; Extine, M. W. *J. Am. Chem. Soc.* **1977**, *99*, 782.

[70] Chisholm, M. H.; Extine, M. W. *J. Am. Chem. Soc.* **1977**, *99*, 792.

[71] Weissermel, K.; Arpe, H. J. *Industrial Organic Chemistry*; VCH Verlagsgesellschaft, Weinheim, Germany, 1997.

[72] Shaikh, A. A. G.; Sivaram, S. *Chem. Rev.* **1996**, *96*, 951.

[73] Sakakura, T.; Kohno, K. *Chem. Commun.* **2009**, 1312.

[74] Haworth, W. N.; Machemer, H. *J. Chem. Soc* **1932**, 2270.

[75] 1991.

[76] Darensbourg, D. J.; Holtcamp, M. W. *Coord. Chem. Rev.* **1996**, *153*, 155.

[77] Baba, A.; Kashiwagi, H.; Matsuda, H. *Organometallics* **1987**, *6*, 137.

[78] Baba, A.; Kashiwagi, H.; Matsuda, H. *Tetrahedron Letters* **1985**, *26*, 1323.

[79] Arakawa, H. *et al. Chem. Rev.* **2001**, *101*, 953.

[80] Jessop, P.; Ikariya, T.; Noyori, R. *Chem. Rev.* **1995**, *95*, 259.

[81] Fukuoka, S.; Kawamura, M.; Komiya, K.; Tojo, M.; Hachiya, H.; Hasegawa, K.; Aminaka, M.; Okamoto, H.; Fukawa, I.; Konno, S. *Green Chemistry* **2003**, *5*, 497.

[82] Clements, J. H. *Ind. Eng. Chem. Res.* **2003**, *42*, 663.

[83] Calo, V.; Nacci, A.; Monopoli, A.; Fanizzi, A. *Org. Lett.* **2002**, *4*, 2561.

[84] Kihara, N.; Hara, N.; Endo, T. *J. Org. Chem* **1993**, *58*, 6198.

[85] Lu, X.; Zhang, Y. J.; Jin, K.; Luo, L. M.; Wang, H. *J. Catal.* **2004**, *227*, 537.

[86] Lu, X.; Zhang., Y. J.; Liang, B.; Li, X.; Wang, H. *J. Mol. Catal. A: Chem.* **2004**, *210*, 31.

[87] Lu, X.; Feng, X. J.; He, R. *Appl. Catal. A.* **2002**, *234*, 25.

[88] Lu, X.; He, R.; Bai, C. X. *J. Mol. Catal. A: Chem.* **2002**, *186*, 1.

[89] Paddock, R. L.; Nguyen, S. T. *J. Am. Chem. Soc.* **2001**, *123*, 11498.

[90] Darensbourg, D. J.; Fang, C. C.; Rodgers, J. L. *Organometallics* **2004**, *23*, 924.

[91] Shen, Y. M.; Duan, W. L.; Shi, M. *J. Org. Chem* **2003**, *68*, 1559.

[92] Kasuga, K.; Kabata, N. *Inorg. Chim. Acta* **1997**, *257*, 277.

[93] Huang, J. W.; Shi, M. *J. Org. Chem* **2003**, *68*, 6705.

[94] Sun, J. M.; Fujita, S. I.; Zhao, F. Y.; Arai, M. *Appl. Catal. A.* **2005**, *287*, 221.

[95] Kossev, K.; Koseva, N.; Troev, K. *J. Mol. Catal. A: Chem.* **2003**, *194*, 29.

[96] Baba, A.; Nozaki, T.; Matsuda, H. *Bull. Chem. Soc. Jpn.* **1987**, *60*, 1552.

[97] Peng, J.; Deng, Y. *New. J. Chem.* **2001**, *25*, 639.

[98] Kim, H. S.; Kim, J. J.; Kim, H.; Hang, H. G. *J. Catal.* **2003**, *220*, 44.

[99] Li, F.; Xiao, L.; Xia, C.; Hu, B. *Tetrahedron Letters* **2004**, *45*, 8307.

[100] Xiao, L. F.; Li, F. W.; Peng, J. J.; Xia, C. G. *J. Mol. Catal. A: Chem.* **2006**, *253*, 265.

[101] Zhang, S.; Chen, Y.; Li, F.; Lu, W.; Dai, W.; Mori, R. *Catal. Today* **2006**, *115*, 61.

[102] Sun, J.; Fujita, S. I.; Arai, M. *J. Organomet. Chem* **2005**, *690*, 3490.

[103] Coates, G. W.; Moore, D. R. *Angew. Chem. Int. Ed.* **2004**, *43*, 6618.

[104] Kember, M. R.; Buchard, A.; Williams, C. K. *Chem. Commun.* **2011**, *47*, 141.

[105] Pescarmona, P. P.; Taherimehr, M. *Catal. Sci. Technol.* **2012**, *2*, 2169.

[106] Klaus, S.; Lehenmeier, M. W.; Anderson, C. E.; Rieger, B. *Coord. Chem. Rev.* **2011**, *255*, 1460.

[107] Shen, Y. M.; Duan, W. L.; Shi, M. *J. Org. Chem.* **2003**, *68*, 1559.

[108] Jutz, F.; Andanson, J. M.; Baiker, A. *Chem. Rev.* **2011**, *111*, 322.

[109] Lu, X. B.; Shi, L.; Wang, Y. M.; Zhang, R.; Zhang, Y. J.; Peng, X. J.; Zhang, Z. C.; Li, B. *J. Am. Chem. Soc.* **2006**, *128*, 1664.

[110] Darensbourg, D. J. *Chem. Rev.* **2007**, *107*, 2388.

[111] Buchard, A.; Kember, M. R.; Sandemann, K. G.; Williams, C. K. *Chem. Commun.* **2011**, *47*, 212.

[112] Chisholm, M. H.; Zhou, Z. *J. Am. Chem. Soc.* **2004**, *126*, 11030.

[113] Clementi, E.; Raimondi, D. L.; Reinhardt, W. P. *J. Chem. Phys.* **1967**, *47*, 1300.

[114] Monassier, A.; D'Elia, V.; Cokoja, M.; Dong, H.; Pelletier, J. D. A.; Basset, J. M.; Kuehn, F. E. *ChemCatChem* **2013**, *5*, 1321.

[115] Alt, H. G.; Denner, C. E. *J. Organomet. Chem* **1990**, *390*, 53.

[116] Cohen, S. A.; Bercaw, J. E. *Organometallics* **1985**, *4*, 1006.

[117] Aresta, M.; Quaranta, E. *J. Organomet. Chem* **1993**, *463*, 215.

[118] Hoberg, H.; Jenni, K. *J. Organomet. Chem* **1987**, *322*, 193.

[119] Aresta, M.; Pastore, C.; Giannoccaro, P.; Kovacs, G.; Dibenedetto, A.; Papai, I. *Chem. Eur. J.* **2007**, *13*, 9028.

[120] Carter, E. A.; Goddard, W. A. *J. Phys. Chem.* **1988**, *92*, 5679.

[121] Herberhold, M. *Metal Pi Complexes*; Elsevier, 1972.

[122] Maitlis, P. M. *The Organic Chemistry of Palladium*; Academic, New York, 1971.

[123] Ozawa, F.; Ito, T.; Nakamura, Y.; Yamamoto, A. *J. Organomet. Chem* **1979**, *168*, 375.

[124] Ito, T.; Tsuchiya, H.; Yamamoto, A. *Bull. Chem. Soc. Jpn.* **1977**, *50*, 1319.

[125] Ozawa, F.; Ito, T.; Yamamoto, A. *J. Am. Chem. Soc.* **1980**, *102*, 6457.

[126] Duong, H. A.; Tekavec, T. N.; Arif., A. M.; Louie, J. *Chem. Commun.* **2004**, *40*, 112.

[127] Dibugno, C.; Pasquali, M.; Leoni, P. *Inorg. Chim. Acta.* **1988**, *149*, 19.

[128] Pushkar, J.; Wendt, O. F. *Inorg. Chim. Acta.* **2004**, *357*, 1295.

[129] Li, H.; Grasa, G. A.; Colacot, T. J. *Org. Lett.* **2010**, *12*, 3332.

[130] Boehm, V. P. W.; Gstoettmayr, C. W. K.; Weskamp, T.; Herrmann, W. A. *J. Organomet. Chem* **2000**, *595*, 186.

[131] Hoberg, H.; Schaefer, D. *J. Organomet. Chem* **1983**, *251*, C51.

[132] Fischer, R.; Langer, J.; Malassa, A.; Walther, D.; Goerlsa, H. *Chem. Commun.* **2006**, 2510.

[133] Graham, D. C.; Mitchell, C.; Bruce, M. I.; Metha, G. F.; Bowie, J. H.; Buntine, M. A. *Organometallics* **2007**, *26*, 6784.

[134] Hoberg, H.; Peres, Y.; Milchereit, A. *J. Organomet. Chem* **1986**, *307*, C38.

[135] Bruckmeier, C.; Lehenmeier, M. W.; Reichardt, R.; Vagin, S.; Rieger, B. *Organometallics* **2010**, *29*, 2199.

[136] Lejkowski, M. L.; Lindner, R.; Kageyama, T.; Bodizs, G. E.; Plessow, P. N.; Mueller, I. B.; Schaefer, A.; Rominger, F.; Hofmann, P.; Futter, C.; Schunk, S. A.; Limbach, M. *Chem. Eur. J.* **2012**, *18*, 14017.

[137] Plessow, P. N.; Weigel, L.; Lindner, R.; Schaefer, A.; Rominger, F.; Limbach, M.; Hofmann, P. *Organometallics* **2013**, *32*, 3327.

[138] Lee, S. Y. T.; Cokoja, M.; Drees, M.; Li, Y.; Mink, J.; Herrmann, W. A.; Kuehn, F. E. *Chemsuschem* **2011**, *4*, 1275.

[139] Kakino, R.; Nagayama, K.; Kayaki, Y.; Shimizu, I.; Yamamoto, A. *Chem. Lett.* **1999**, 685.

[140] Nagayama, K.; Kawataka, F.; Sakamoto, M.; Shimizu, I.; Yamamoto, A. *Bull. Chem. Soc. Jpn.* **1999**, *72*, 573.

[141] Doh, M.; Jung, M.; Lee, D.; Osakada, K.; Yamamoto, A. *J. Korean. Chem. Soc.* **1993**, *37*, 423.

[142] Osakada, K.; Ozawa, M. D. D.; Yamamoto, A. *Organometallics* **1990**, *9*, 2197.

[143] Bar, A. K.; Chakrabarty, R.; Mukherjee, P. S. *Organometallics* **2008**, *27*, 3806.

[144] Lee, S. Y. T. Synthesis of Acrylic Acid Derivatives from Carbon Dioxide and Ethylene, Mediated by Molecular Nickel Complexes. Ph.D. thesis, Technische Universitaet Muenchen, 2012.

[145] Iverson, C. N.; Lachicotte, R. J.; Mueller, C.; Jones, W. D. *Organometallics* **2002**, *21*, 5320.

[146] Hayashi, T.; Konishi, M.; Kobori, Y.; Kumada, M.; Higuchi, T.; Hirotsu, K. *J. Am. Chem. Soc.* **1984**, *106*, 158.

[147] Stang, P. J.; Olenyuk, B.; Fan, J.; Arif, A. M. *Organometallics* **1996**, *15*, 904.

[148] Trost, B. M. *Acc. Chem. Res.* **2002**, *35*, 695.

[149] North, M. In *New and Future Developments in Catalysis: Activation of Carbon Dioxide*; Suib, S. L., Ed.; Newnes, 2013.

[150] Mourea, H.; Dode, M. *Bull. Soc. Chim. France* **1937**, *4*, 637.

[151] Vasileva, T. F.; Zhiltosova, E. N.; Vvedenski, A. A. *Russ. J. Phys. Chem. (Engl. Transl.)* **1972**, *46*, 316.

[152] Cox, J. D.; Wagman, D. D.; Medvedev, V. A. *CODATA Key Values for Thermodynamics*; Hemisphere Publishing Corp, New York, 1984.

[153] Inoue, S.; Koinuma, H.; Tsuruta, T. *Makromol. Chem.* **1969**, *130*, 210.

[154] Chen, S. W.; Kawthekar, R. B.; Kim, G. J. *Tetrahedron Letters* **2007**, *48*, 297.

[155] Darensbourg, D. J.; Mackiewicz, R. M.; Phelps, A. L.; Billodeaux, D. R. *Acc. Chem. Res.* **2004**, *37*, 836.

[156] Bok, T.; Noh, E. K.; Lee, B. Y. *Bull. Korean. Chem. Soc.* **2006**, *27*, 1171.

[157] Lu, X. B.; Zhang, Y. J.; Liang, B.; Li, X.; Wang, H. *J. Mol. Catal. A: Chem.* **2004**, *210*, 31.

[158] Zhou, H.; Zhang, W. Z.; Liu, C. H.; Qu, J. P.; Lu, X. B. *J. Org. Chem.* **2008**, *73*, 8039.

[159] Lu, X. B.; Liang, B.; Zhang, Y. J.; Tian, Y. Z.; Wang, Y. M.; Bai, C. X.; Wang, H.; Zhang, R. *J. Am. Chem. Soc.* **2004**, *126*, 3732.

[160] Paddock, R. L.; Nguyen, S. T. *Chem. Commun.* **2004**, 1622.

[161] Veersteg, P.; Rubin, E. S. *Intl. J. Greenhouse Gas Control* **2011**, *5*, 1596.

[162] Gu, L.; Zhang, Y. *J. Am. Chem. Soc.* **2010**, *132*, 914.

[163] Riduan, S. N.; Zhang, Y.; Ying, J. Y. *Angew. Chem. Int. Ed.* **2009**, *48*, 3322.

[164] Perez, E. R.; Santos, R. H. A.; Gambardella, M. T. P.; de Macedo, L. G. M.; Rodrigues-Filho, U. P.; Launay, J.-C.; Franco, D. W. *J. Org. Chem.* **2004**, *69*, 8005.

[165] North, M.; Pasquale, R. *Angew. Chem. Int. Ed.* **2009**, *48*, 2946.

[166] Clegg, W.; Harrington, R. W.; North, M.; Pasquale, R. *Chem. Eur. J.* **2010**, *16*, 6828.

[167] Darensbourg, D. J.; Mackiewicz, R. M. *J. Am. Chem. Soc.* **2005**, *127*, 14026.

[168] Ren, W. M.; Liu, Z. W.; Wen, Y. Q.; Zhang, R.; Lu, X. B. *J. Am. Chem. Soc.* **2009**, *131*, 11509.

[169] Aresta, M.; Dibenedetto, A.; Pastore, C. *Inorg. Chem.* **2003**, *42*, 3256.

[170] Dibenedetto, A.; Pastore, C.; Aresta, M. *Catal. Today* **2006**, *115*, 88.

[171] Hidai, M.; Hikita, T.; Uchida, Y. *Chem. Lett.* **1972**, 521.

[172] Darensbourg, D. J.; Mueller, B. L.; Reibenspies, J. H.; Bischoff, C. J. *Inorg. Chem.* **1990**, *29*, 1791.

[173] Kato, M.; Ito, T. *Inorg. Chem* **1985**, *24*, 504.

[174] Secondo, P. M.; Land, J. M.; Baughman, R. G.; Collier, H. L. *Inorg. Chim. Acta.* **2000**, *309*, 13.

List of Figures

List of Schemes

List of Tables